2022

# Geological Survey Paper 9:

# Structure of the southwest high-grade coastal belt, southern Tyennan domain, Tasmania


Authors: D. R. Gray
M. J. Vicary
Date: 06/07/2022
Email: info@mrt.tas.gov.au
Website: www.mrt.tas.gov.au


REPORT No: GSP9

View of the northern coastline of Mulcahy Bay. The Mulcahy River mouth is the cleft in the coastal peneplain (middle right of photo). The photo is looking southwest along the southwest- striking high strain zone or pelite "mylonite" exposed in the beach (photo lower left). The Davey Metamorphic Complex high-grade pelitic rocks occur in the coastal outcrops from the river mouth (photo centre middle-ground) to the high-strain zone. The high-strain, mylonitic foliation truncates the north-south trending foliation of the high-grade rocks.


Tasmanian Government
Mineral Resources Tasmania
mrt

CONTENTS

## *Abstract*

*The Southwest High-grade Coastal Belt of the Southern Tyennan domain appears to consist of a simple, overall west-dipping sequence of fault-bounded and structurally intercalated high-grade albite and garnet bearing schists and gneiss, low-grade quartzite, phyllite and graphitic phyllite. The high-grade belt forms a structural carapace to the underlying quartzite-dominated Propsting-De Witt mega-sheath fold. This however, belies the structural complexity of the high-grade belt.*

*In the northern part, the regional structure of the Southwest Coastal Belt is dominated by a major south-closing, west-plunging, reclined to recumbent macro-isoclinal fold (Nye Bay fold-nappe) cored by high-grade schist and flanked by phyllite and low-grade quartzite. The upper, overturned western limb has a map width of ~7km and extends from Top Rocks to Nye Bay. The lower eastern limb of the fold-nappe from Mulcahy Bay southwards is transitional into a series of second-order, structurally lower, isoclinal macro-folds defined by alternating high-grade and low-grade layers. These have axial trace length of ~26 km and extend from Mulcahy Bay to Port Davey. In the southern part, from Alfhild Bay to Port Davey the map pattern is dominated by a complex "mushroom" fold interference pattern where early, northwest-trending, reclined isoclinal macro-folds are refolded by younger, open Devonian north-east-trending, southwest-plunging folds changing to open, more north-south trending, south-plunging folds at Port Davey.*

*Due to the overall west-dip of the West Coast succession the northern and most western part at Top Rocks is structurally higher than the macro-fold sets at Port Davey. The fold-nappe in the north is therefore at the highest structural level. It has an overturned western limb, is south-closing, west-plunging and approaching reclined geometry, and has a high-grade schist core (hinge zone). All these relationships are identical to those of the Franklin Fold-nappe that dominates the structurally highest part of the Central Tyennan domain to the north. The Franklin fold-nappe has been mapped to Mt McCall, some 75 km to the north (Gray & Vicary, 2021b), and now with potential continuation beneath the Cambro-Ordovician of the Elliot Range suggests that the highest levels of the Tyennan structural unit has an markedly asymmetric over-fold (fold-nappe) that extends the entire western margin of the Tyennan massif on the order of 200 km.*

*The current macro-structure and regional structural geometry was established from formlines in the dominant foliation Sm and So/Sm, the mapped distribution of lithologies, and early isocline (F1/F2) fold axis and lineation Lm attitude data. Changes from clockwise to counter-clockwise rotation of early isocline axes towards the mineral lineation Lm occur at Nye Bay, Mulcahy Bay, Brier Holme Head-Svenor Point, and Sandblow Bay. These define the axial surface trace positions of major folds and match the positions of the axial surface traces of the inferred macro-folds.*

*This part of the Southern Tyennan consists of a high-grade metamorphic sheet overlying a composite low-grade sheet of phyllite overlying quartzite. Contacts between the high-grade and low-grade units are high-strain, mylonitic zones (HSZ) that in many cases have brittle/cataclastic overprints from Devonian and younger deformations. Shear sense indicators suggest a complex movement picture with the overall emplacement shear sense towards the southwest (~250°).*

*A tenet of the structural interpretation for the Southwest High-grade coastal belt is that the high strain to mylonitic contacts between the high-grade schists and low-grade phyllite-quartzite sequence are folded with the litho-tectonic sequence during fold-nappe and isoclinal macro-fold evolution.*

Tasmanian Government

Mineral Resources Tasmania

Department of State Growth
www.mrt.tas.gov.au

# Structure of the southwest high-grade coastal belt, southern Tyennan domain, Tasmania

David R. Gray[1], Michael J. Vicary[2], and Andrew W. McNeill[3]
[1] *Consultant Structural Geologist to Mineral Resources Tasmania*
[2] *Geological Survey Branch - Mineral Resources Tasmania*
[3] *Chief Government Geologist, Mineral Resources Tasmania*

ARTICLE INFO

Published: 6 July 2022
Publisher: Mineral Resources Tasmania
Report No.: GSP9

KEYWORDS

Structural Geology
Davey Metamorphic Complex
Southern Tyennan

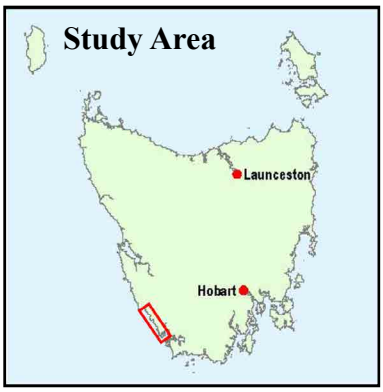


## 1.0 INTRODUCTION

The southwest coastal belt of high-grade metamorphic rocks includes the coastal exposures of medium to high-grade rocks extending from Top Rocks in the north to Port Davey in the south (Figure 1). It includes some of the highest structural units in the Southern Tyennan domain with structurally interleaved quartzite, phyllite and high-grade schist and garnet bearing quartzite. It has been previously designated the Davey Metamorphic Complex by Meffre et al. (2000).

### 1.1 Lithological Assemblages

Three broad lithologic assemblages have been recognised (Hall, 1966; Williams and Corbett, 1977) including:

1. quartzite;
2. quartz schist with phyllite;
3. phyllite with garnet-albite- quartz-mica schist.

Lithologies of the high-grade coastal belt (Davey Metamorphic Complex) are described and discussed in Williams (1982), McNeill (1985), and Meffre et al. (2000, 2001).

The **low-grade sequence** (McNeill, 1985) consists of:

- quartzite with minor interlayered phyllite;
- quartz-rich phyllites;
- black graphitic phyllite with minor interlayered quartz-rich phyllites.

The **high-grade amphibolite facies metamorphic rock-sequence** (McNeill, 1985; Meffre et al., 2001) consists of:

- albite schist with minor thin quartzite bands;
- garnet schist and feldspathic gneiss ± amphibolie boudins;
- massive quartz-feldspar rocks;
- feldspar-rich rocks with garnet amphibolite bands.

Rounded to lenticular bodies of amphibole-rich rocks are a minor component of the high-grade complex, but are common at certain structural levels. Three types have been identified on the basis of modal mineralogy. Porphyroblastic garnet amphibolite occurs as 1 to 3m long boudins. Hornblende-plagioclase-quartz amphibolite occurs as boudins up 10 m in length and show dimensional preferred orientation of hornblende. Garnet-hornblende amphibolite occurs occasionally as small boudins.

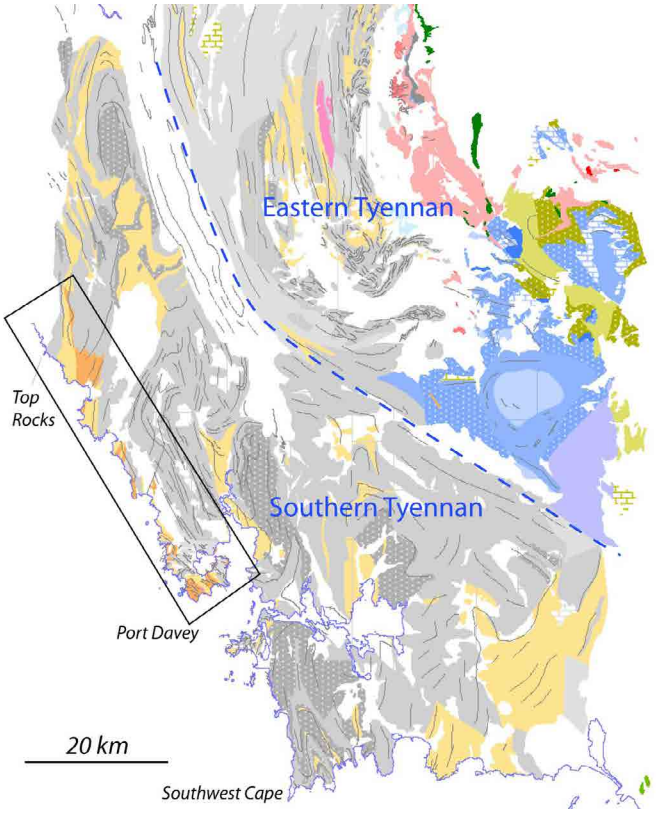


*Figure 1: Litho-tectonic 1:250000 scale map of southwest Tasmania showing the position and distribution of the high-grade coastal belt of metamorphic rocks (black rectangle) in the Southern Tyennan domain. Map base is from Mineral Resources Tasmania 1:25000 and 1:250000 digital geological atlas.*

*Dark orange: H-G metamorphic rocks; light orange: L-G dominant pelitic sequence; light grey: L-G quartzite dominant sequence; white stipple-darker grey: L-G platy schistose quartzite*

### 1.2 Map Distribution of Litho-tectonic Units

The broad distribution of the high-grade schists with the low-grade phyllites and quartzites are shown in the earliest unpublished maps produced during BHP mapping of Exploration Leases in the early 1960's (Hall, 1966, Hall et al., 1969) (Figure 2). The mapping shows the high-grade schist coastal belt as a fault-bounded intercalated package of quartz schist (qs), pelitic and semi-pelitic schist (ps), and coarse schist, gneiss and amphibolite (cs) separated from the inland belt of massive quartzite (q) by a major northwest-trending fault.

Geological Survey mapping by Williams (1978) and Hall (2005, 2006, 2008) (see Hall & Vicary, 2010a, b, c and d), as well as mapping of the high-grade belt in 1997 by Berry, Meffre and Hall (Meffre et al., 2000, 2001) showed an apparent complex distribution of alternating low-grade and high-grade rocks (Figure 3). Most of the observed contacts between the high-grade rocks and the low-grade rocks were shown to be high-strain zones defined by mylonitic L-S tectonites, but many of the zones have been reactivated and overprinted by late-stage brittle faulting (Meffre et al., 2001).

### 1.3 Structural Elements

Structural elements in the Southwest High-grade Coastal belt were originally defined in the Port Davey area by Williams and Corbett (1977) and Williams (1978, 1982). These included:

1. Transposed dominant So/Sm layering in the quartz schist, phyllite and garnet bearing schists and gneissic rocks.
2. F1 isoclines with a penetrative axial surface cleavage are commonly preserved as small-scale, isolated and boudinaged fold cores within and bounded by the transposed layering.
3. F2 isoclinal folds that fold an early lineation and have crenulation cleavage in the fold cores. The F2 folds vary from large F2 over-folds with 0.5 km half-wavelengths to small mesoscopic isoclines, but large-scale stratigraphic reversals with fold hinges unrecognised suggest the presence of larger F2 folds (Williams and Corbett, 1977; Williams, 1978).
4. Open to tight, upright F3 folds with an axial surface crenulation cleavage. These are generally north-south-trending with variably plunging hingelines.

McNeill (1985) describes similar elements and relationships in the Nye Bay area in the northern part of the complex, but showed many of the lithological contacts were mylonitic high-strain zones with extensional-stretching lineations, L-S tectonite fabrics and S-C' fabrics (shear bands and/or extensional crenulation cleavages). Porphyroblast tails and shear bands (S-C' surfaces) in the more strongly deformed parts all showed sinistral top-to-the south shear sense indicators (Meffre et al, 2001).

As a consequence, McNeill (1985) and Meffre et al. (2001) suggest that the sequence of transposition of sedimentary layering to So/Sm, accompanied by boudinage of all metabasic lithologies to lenticular blocks, and isoclinal intrafolial F1/F2 folding parallel to the dominant lineation was the product of continuous deformation involving increasing shear. This implied that:

1. The F1 and F2 folds were not produced during separate events in a polyphase deformation sequence.
2. The distinction of S1 and S2 may be arbitrary as this style of deformation is likely to lead to strong rotational strain violating the assumptions of the classical structural interpretation (based on Turner & Weiss, 1963).
3. The parallelism of fold axes and stretching lineations are a function of the rotation of fold hingelines towards the bulk stretch direction. (cf. Quinquis et al. 1978).

### 1.4 Metamorphic Petrology and Metamorphism

Spry and Baker (1965), Williams (1982), McNeill (1985), Meffre et al. (2000) and Chmielowski (2009) have investigated the metamorphism of the West Coast High-grade Coastal belt (Figure 4a). Mulder (2013) and Mulder et al. (2015) investigated the Red Point Metamorphic Complex but this will be dealt with in another paper (Gray & Vicary, 2022b).

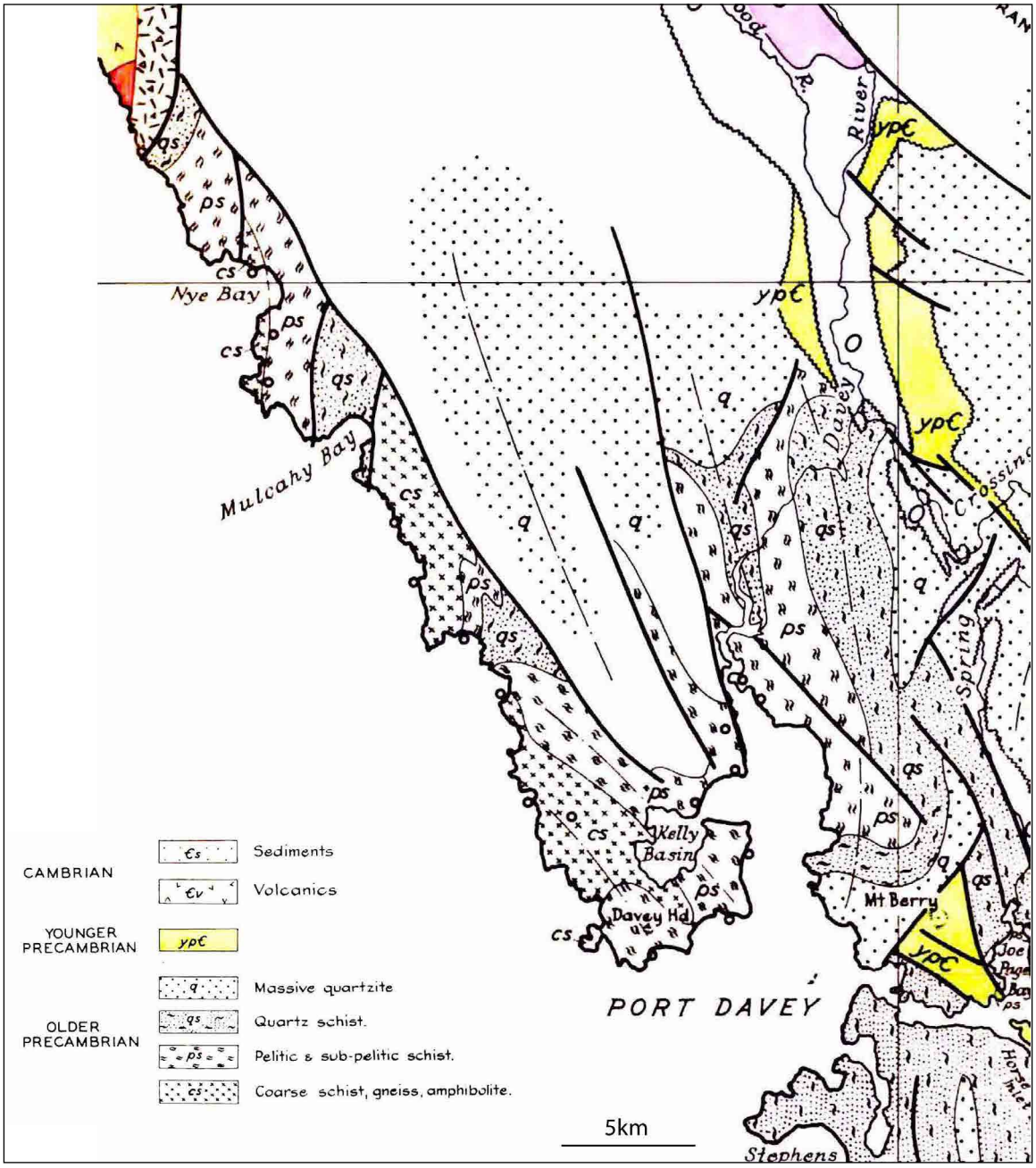


Figure 2 (above). Part of the South West Tasmania Geological Map for the South-west portion of BHP Exploration Lease E.L.13/65. Compiled May 1966 by W.D.M. Hall from field surveys by M.Edyvean, C. Gee, M. Hall and H. McIntyre. G4970A. Mineral Resources Tasmania Company Report 66-424.

*Purple: Silurian sedimentary succession.*

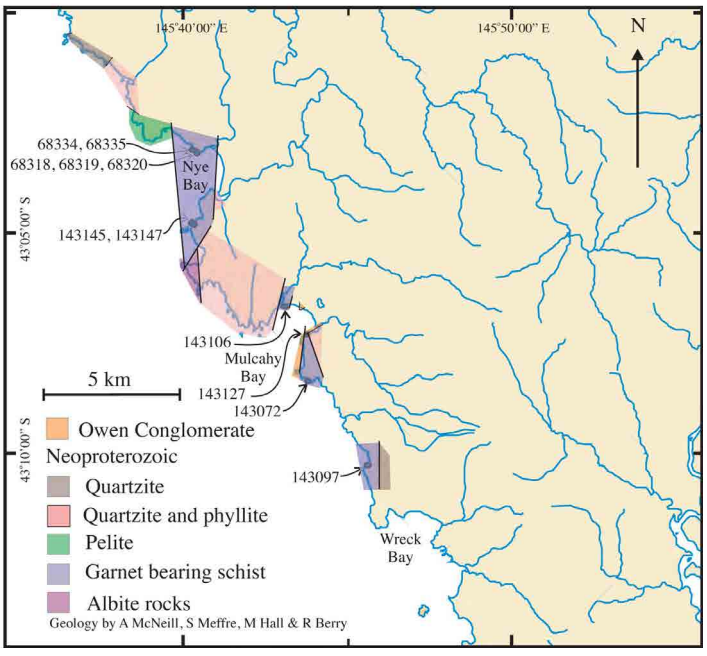


Figure 3 (right). Lithological map of the coastal belt from Top Rocks to Wreck Bay showing the metamorphic sequence as a series of fault-bounded slices. The heavy black lines are fault/mylonite zones separating the different metamorphic blocks or slices. The diagram is Figure 2.1 from Chmielowski (2009) based on Meffre et al. (2001).

The chronology of crystallisation and deformation in the Nye Bay schists indicates the metamorphic maxima, based on the formation of sillimanite, occurred late syn- to early post formation of the dominant cleavage (McNeill, 1985).

*Estimated PT Conditions*

The composite assemblage biotite-garnet-kyanite-muscovite¬-albite-quartz-sillimanite may be used to characterise the metamorphic maximum. The PT conditions of the metamorphic maximum fall in the stability fields of quartz-muscovite and sillimanite, and above the granite-melting curve. Conditions are therefore in the range 6kb and 630°C to approximately 9kb and 730°C (Figures 4a and 4b). Temperatures are above the kyanite-sillimanite boundary, and close to, or above the melting curve; that is, approximately 650°C. The combined results from geobarometry and geothermometry, including all data from the garnet-biotite thermometer, indicate temperatures of 635 ±500c and pressures of 7.5 ±1 kb. Garnet zoning may indicate retrograde re-equilibration, resulting in lower temperature estimates.

Garnets from Nye Bay are large (~2cm) with two distinct habits: 1) euhedral shape with inclusion free cores and rims dusty with fine grained inclusions, and 2) patchy shape with abundant quartz inclusions that show a marked density change across the core-rim boundary (Chmielowski & Berry, 2012) Geothermobaromnetric calculations using THERMOCALC (Chmielowski & Berry, 2012) give:

- Garnet cores: initial garnet growth at 560°C and ~0.56GPa.
- Garnet rim: late growth with a slight increase in both temperature (<100°C) and pressure (~0.04GPa), with conditions changing from the kyanite field into the sillimanite field (Figure 4b), consistent with the observations of sillimanite-rimming kyanite (McNeill, 1985).

Metabasites with hornblende-plagioclase (An40) -garnet assemblage support amphibolite facies conditions (McNeill, 1985), but the metamorphism involves a transition from the kyanite field to the sillimanite field by increasing P+T (Figure 4b). Possible retrogression in the pelitic lithologies suggests that the mafic/amphibolitic lithologies may provide the best estimate of the metamorphic maximum (McNeill, pers. com., 2022). Subsequent Gt-cpx geothermometry (Ellis and Green, 1979) and Ab-Jd+Q thermobarometry (Holland, 1980) on Nye Bay garnet amphibolites gave 745°C and 10.6 kb (McNeill, unpublished data).

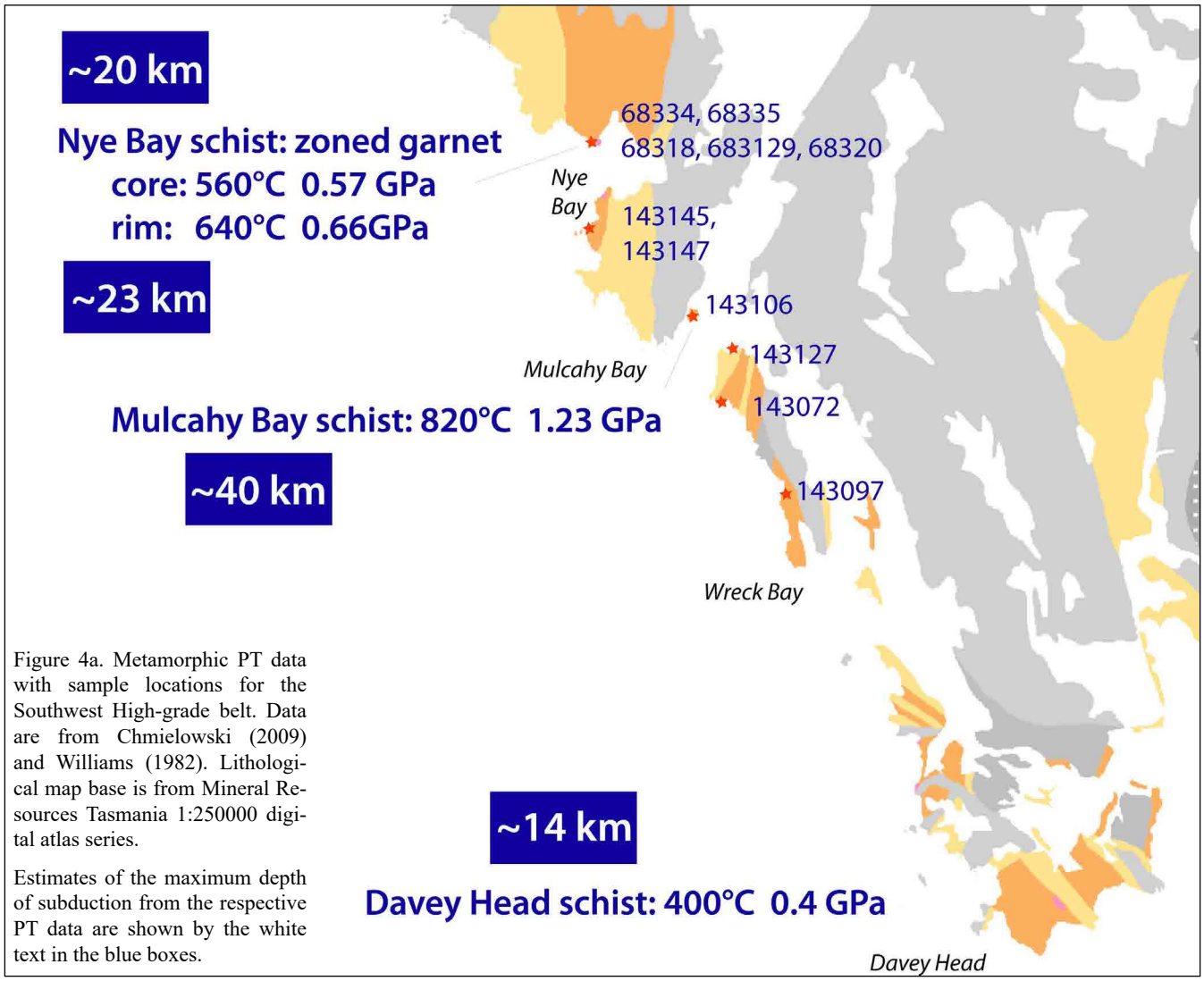


Figure 4a. Metamorphic PT data with sample locations for the Southwest High-grade belt. Data are from Chmielowski (2009) and Williams (1982). Lithological map base is from Mineral Resources Tasmania 1:250000 digital atlas series.

Estimates of the maximum depth of subduction from the respective PT data are shown by the white text in the blue boxes.

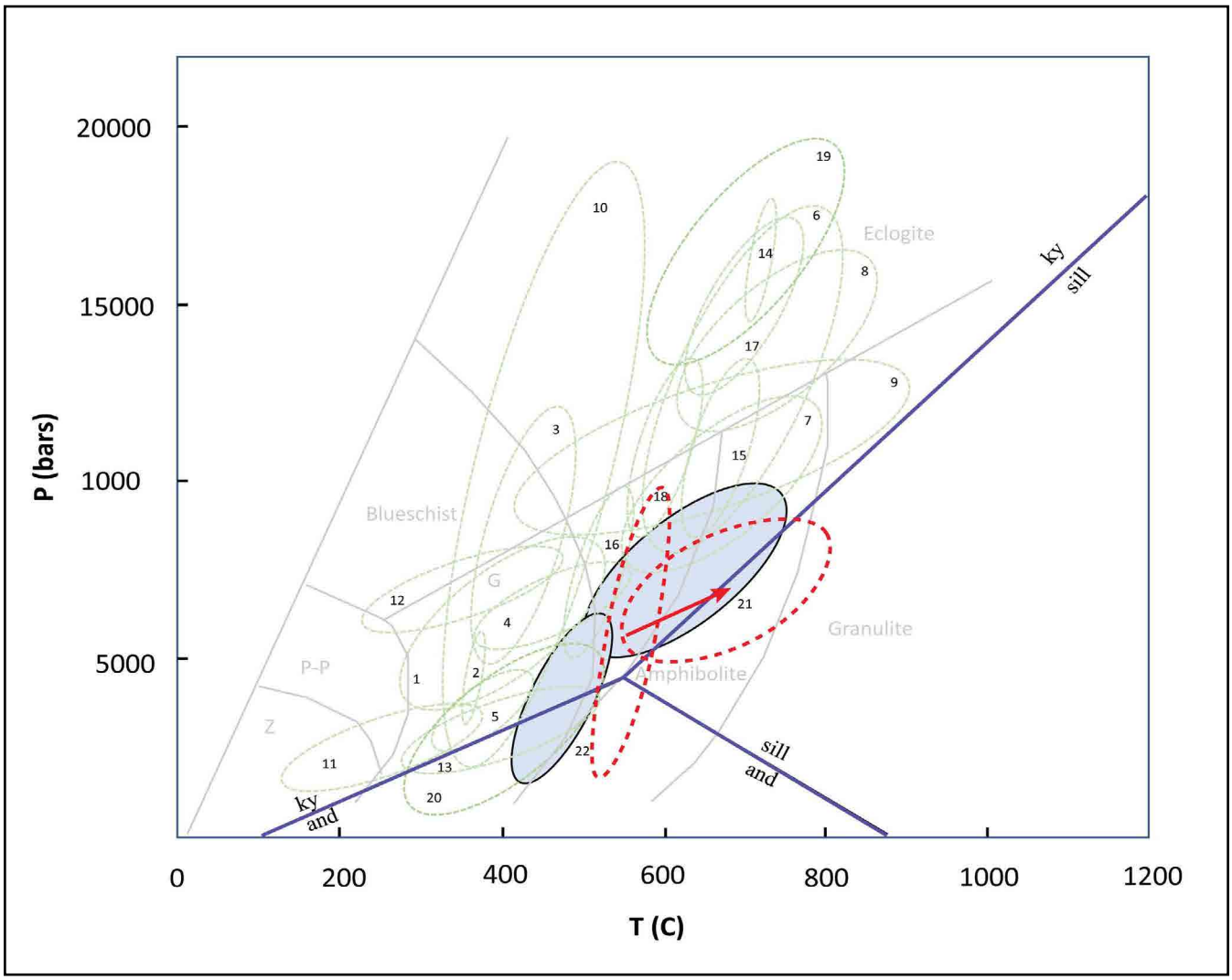


Figure 4b. Metamorphic PT determinations for the Tasmanian Proterozoic rocks. (Diagram modified from Chmielowski & Berry, 2012, fig. 2). The blue ellipses represent the Southwest high-grade coastal belt PT determinations with ellipse 21 based on data from Nye Bay (McNeill, 1985) and Ellipse 22 based on data from Port Davey (Turner, 1989). The red dashed ellipses are THERMOCALC determined max P/T conditions from garnet cores to garnet rims from Nye Bay with the arrow showing increasing P and T from the kyanite field towards the sillimanite field (Chmielowski & Berry, 2012, fig.9).

### 1.5 Age Dating/ Geochronology

Chemical U-Th-Pb Monazite dating of samples from Nye and Mulcahy Bay areas provide a range of ages for the high-grade metamorphic rocks from 511 Ma - 505 Ma (Figure 5) with a Mean Standard Weighted Deviation (MSWD) of up to ±12Ma (Chmielowski & Berry, 2012).

### 1.6 Previous Work

The lithological distribution, structure and metamorphism of rocks from Top Rocks to Nye Bay were mapped and analysed by Andrew McNeill as part of a University of Tasmania Honours thesis (McNeill, 1985). Further structural and lithological mapping from the Giblin River mouth south to Wreck Bay was undertaken by Ron Berry, Sebastian Meffre and Mike Hall in 1997 (Berry, 1997*). This work resulted in a lithological map (Figure 3) and discussion on the nature of the contacts between the various metamorphic units (Meffre et al., 2000, 2001). Mike Hall and John Miller undertook mapping in 2004 from Top Rocks to Towterer Beach (Hall, 2005* and Miller, 2004*). Mike Hall and Michael Vicary undertook mapping in 2006 with resultant 1:25000 digital map compilations (Hall, 2006; Hall & Vicary, 2010a, b, c and d), and Mike Hall subsequently from Wreck Bay to Sandblow Bay (Hall 2008).

### 1.7 Current Compilation

The current compilation utilises field notebooks and field maps from Williams (1976), 1978, McNeill (1985), Hall (2005, 2006, 2008), Berry (1997) and Miller (2004), as well as the Mineral Resources Tasmania 1:25000 digital atlas maps of Mulcahy (Hall & Vicary 2010a), Elliott (Hall & Vicary 2010b), Propsting (Hall & Vicary, 2010c) and Rookery (Hall & Vicary, 2010d). The synthesis would not have been possible without these sources.

The structural synthesis of the West Coast high-grade coastal belt has involved production of 5 detailed structural maps incorporating areas from 1) Top Rocks to Nye Bay, 2) Nye Bay to Mulcahy Bay, 3) Mulcahy Bay to Wreck Bay, 4) Wreck Bay to Sandblow Bay, and 5)

*unpublished field note books

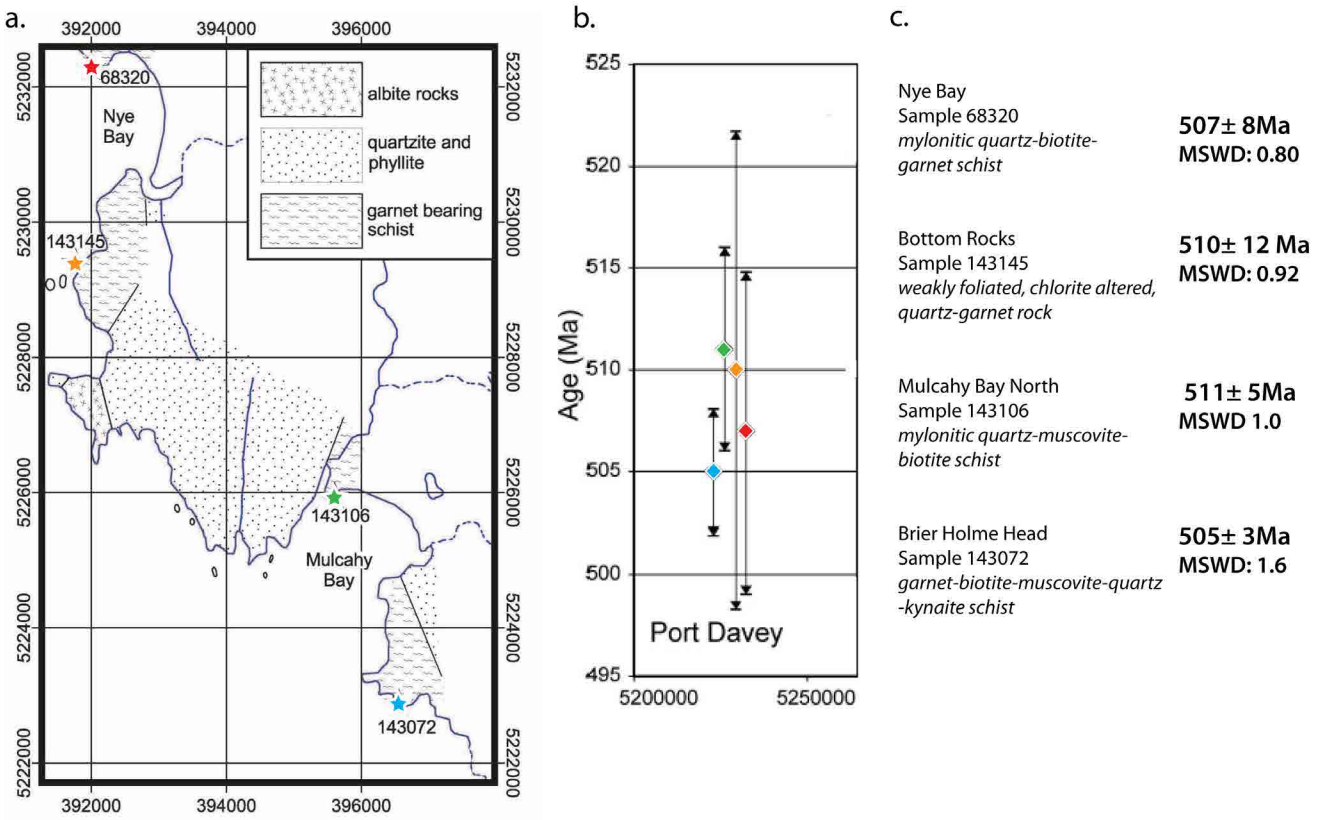


Figure 5. Chemical U-Th-Pb Monazite age data from the northern part of the Southwest High-grade Coastal belt. a) Sample location map for (Berry et al., 2007, fig.8). b) Summary of metamorphic age data with ages plotted against AMG Northing. Error bars shown are 95% confidence (Berry et al., 2007, fig. 10), and c) with rock descriptions and determined ages.

Sandblow Bay to Davey Head (Figure 6). Each of these regions is treated separately below and the contained structural elements and structural relationships are presented and discussed in relation to the larger scale structure.

Structural data from the above sources is tabulated in Appendix 1.

The following structural terminology is used:

| | |
|---|---|
| So/Sm | metamorphic foliation parallel to bed ding (commonly a transposition layering) |
| So/Sm env | enveloping surface to folded So/Sm |
| Sm | dominant or main metamorphic foliation |
| Sb | shear band (S-C' structure) |
| AST | fold axial surface trace |
| AS/Sm | dominant foliation sub-parallel to fold axial surfaces |
| Sm/Sb | dominant foliation developing from Sb, shear band foliation |
| Scc: | crenulation cleavage |
| Scl | Devonian overprinting low-grade cleavage |
| S1 | early slaty cleavage |
| Lm | dominant lineation |
| Lstretch | stretching lineation |
| Lelongation | mineral elongation lineation |
| TD | transport direction |
| Lint | intersection lineation |
| Lrod | rodding lineation developed from de forming Lint |
| FA | fold axis |
| F1, F2, F3 | local age of fold axes (oldest to youngest) |
| Lm^FA | angle between Lm and FA |
| Sm^Sb | angle between Sm and Sb |

## 2.0 STRUCTURE AND METAMORPHIC CHARACTER OF WEST COAST BELT ROCKS

### 2.1 The Low-Grade Sequence

The low-grade sequence consists of quartzite, quartz-rich phyllites with minor graphitic phyllite, and black graphitic phyllite with minor interlayered quartz phyllite. The quartzites generally lack sedimentary structures, although ripple marks occur at one locality (see Section 2.1.3). Much of the description and photographs following are from McNeill (1985) and are from the coastal section from Top Rocks to the north end of Nye Bay.

#### *2.1.1 Nature of the Layering*

The layering is a bedding-parallel foliation So/Sm (Figures 7 and 8) that ranges from an intense foliation with boudinaged layering (Figure 7) to a strong foliation with pressure shadows (Figure 9), to an intense transposition fabric with isoclinal folds and coarsely spaced "ropy"-like crenulation cleavage (Figure 10). This foliation is bedding parallel along isocline fold limbs to a spaced cleavage in fold hinges (Figure 11).

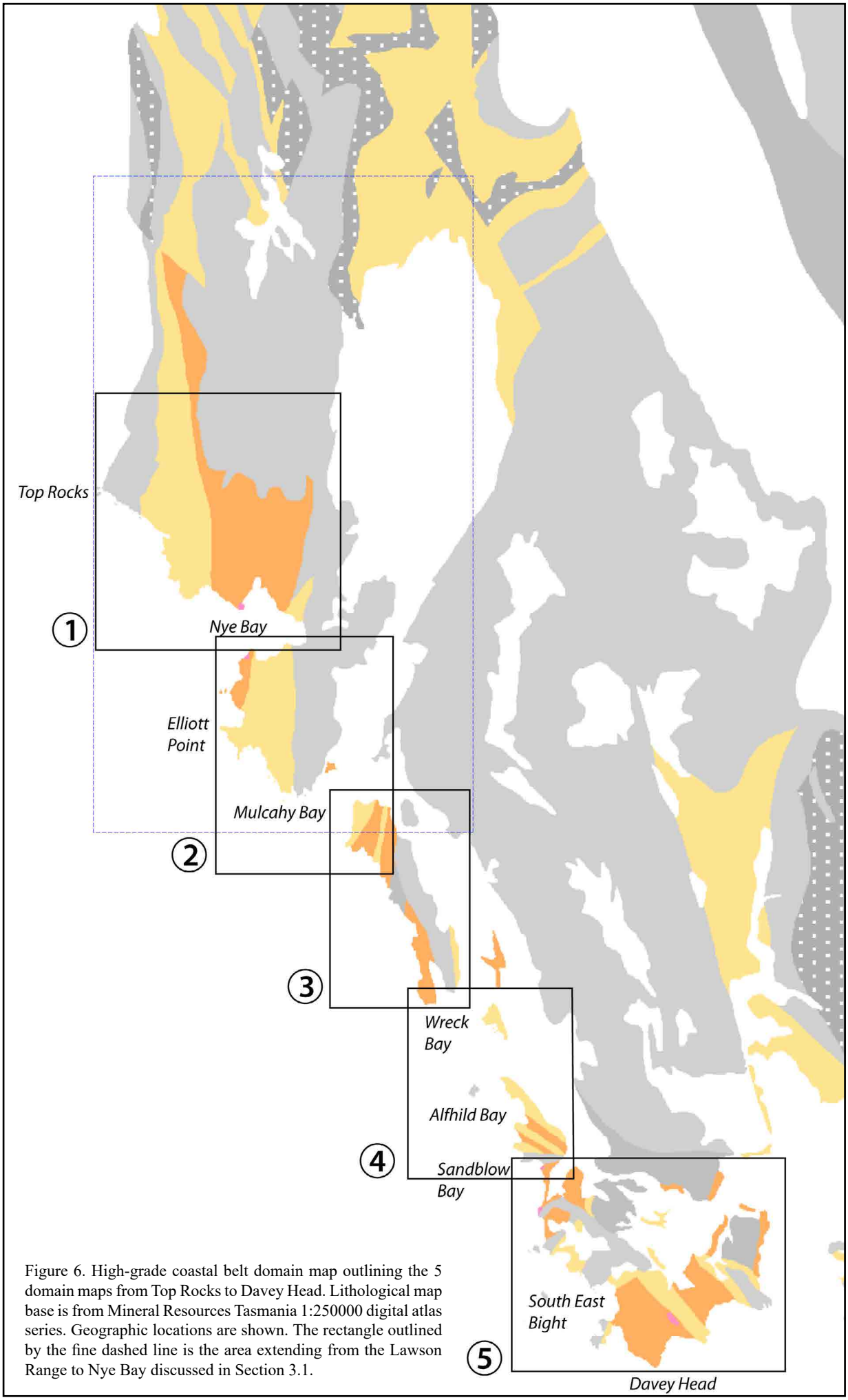


Figure 6. High-grade coastal belt domain map outlining the 5 domain maps from Top Rocks to Davey Head. Lithological map base is from Mineral Resources Tasmania 1:250000 digital atlas series. Geographic locations are shown. The rectangle outlined by the fine dashed line is the area extending from the Lawson Range to Nye Bay discussed in Section 3.1.

*2.1.2 Tight to isoclinal F1 and F2 folds (early folds)*

The earliest folds have a spaced slaty cleavage that is sub-parallel to compositional layering except in fold hinges (Figures 11, 12 and 13) (McNeill, 1985). These were identified as F1 by McNeill (1985).

There is a change to folds with a spaced crenulation fabric in their hinge zones (Figure 14, 15 and 16). These are common north of Ummarah Creek and were designated as F2 folds by McNeill (1985) and in the graphitic phyllite approaching the high-grade schists.

*2.1.3 Relict Bedding/Sedimentation Features*

Despite the transposition nature of the layering through the phyllite sequence the bedded quartzite sequence contains some elements or relicts of sedimentation features. These include ripple marks (Figure 17), scour or erosional surfaces (Figure 18), large-scale cross bedding (Figure 19) and plane laminated bedding (Figure 20).

Figure 7. Intensely developed bedding-parallel foliation in graphitic phyllite containing thin boudinaged quartzite layers (Photo credit: A. W. McNeill).

Figure 8. Bedding-parallel foliation So/Sm in a "thin-banded" quartzite-phyllite sequence. Small isoclinal folds within the layering as well as a strong bedding-parallel foliation in the phyllite bands indicate that the layering has been transposed. This S0/Sm layering has been re-folded by an upright Devonian fold that has a spaced crenulation cleavage axial surface to the fold (Photo credit: A.W. McNeill).


Figure 9. Low-grade quartz-rich phyllite with a strong foliation parallel to apparent bedding "lamination". Quartz pressure shadows (fringes) on pyrite/magnetite (circled) indicate extension (X) within this So/Sm metamorphic foliation. There is a suggestion of an internal boudin termination below the coin that has been offset by a late stage brittle normal fault (Photo credit: A. W. McNeill).


Figure 10. Tectonic banding as transposed layering in low-grade phyllite and quartz-phyllite . The intense transposition foliation (Sm) results from marked isoclinal folding with development of a coarse, "ropy" style crenulation cleavage sub-parallel to So/Sm and axial surface to the folds. Remnant, small-scale isoclinal fold hinges are highlighted by the white circles. (Photo credit: A. W. McNeill).

Figure 11. Thinly layered phyllite, quartz-rich phyllite and thin quartzite band with a tight to isoclinal, early-stage asymmetric fold and a spaced axial surface cleavage (McNeill, 1985, fig. 2.1).


Figure 12. "Similar" style chevron folds in phyllite and graphitic phyllite (darker layers) (Photo Credit: A McNeill).

Figure 13. Spaced disjunctive cleavage in low-grade psammite (Photo Credit: A McNeill).

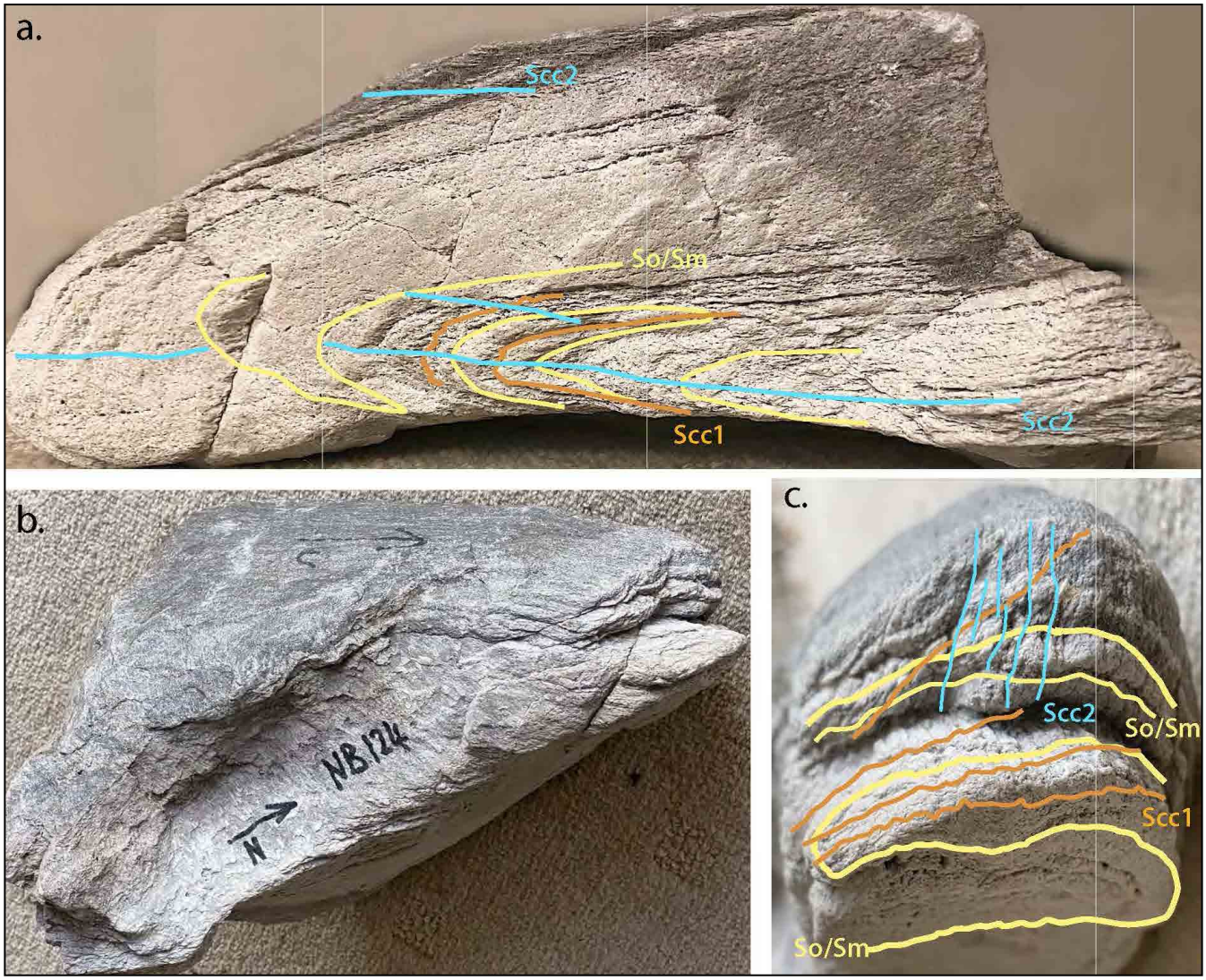


Figure 14. F2 isoclinal fold in quartzite sequence from coastline west of Ummarah Creek. a) Oblique view of fold hinge in S0/Sm (yellow line traces) showing an axial surface crenulation cleavage (Scc2: blue line traces), and an early F1 isoclinal fold pair also in So/Sm with an axial surfrace cleavage (S1/Scc1: orange line traces). b) View of fold approximately normal to the fold axis showing a curved, porpoise-like hingeline. c) Profile view of fold nose showing an early F1 isoclinal fold pair with an axial surface slaty-like cleavage (orange line traces). Blue line traces are the crenulation cleavage (Scc2) axial surface to the main F2 fold.

Figure 15 (left). Upright F2 fold with sub-vertical crenulation cleavage (Photo Credit: A McNeill).


Figure 16 (above). Typical crenulation cleavage in the hinge of an upright F2 fold (Photo Credit: A McNeill).

Figure 17. Ripple marks on the top of a quartzite bed indicating this bed is right way up (Photo Credit: A McNeill). See Section 3.1.1 *Way-up Determination in Quartzite* for discussion.


Figure 18. Thicker sandstone beds within a pelite-dominated part of the low-grade sequence showing scalloped erosion on the upper contact (Photo credit: A. McNeill). These scalloped erosion surfaces occur on the tops of the sand layers and are preserved by the next mud depositional phase suggesting that this part of the sequence is right-way-up.

Figure 19. Inclined bedding typical of larger scale cross-bedding reactivated as bedding parallel faulting, to form a small-scale duplex fault system (Photo credit: A. McNeill).

Figure 20. Thick plane-laminated quartzite beds separated by a black graphitic phyllite with So/Sm parallel quartz veins and a brittle fault plane (Photo credit: A. McNeill).

*2.1.4 Microstructure of the Low-Grade Sequence*

Spaced dissolution cleavage in the low-grade pelitic rocks show typical effects of pressure solution with dark, residue rich cleavage lamellae (Figures 21 and 22). The inter-cleavage lithons show mica beard growth on relict detrital quartz grains indicating phyllosilicate growth in the matrix during the early fabric development (Figure 21).

The presence of the primary spaced S1 fabric with mica beard growth shows that transposition of the layering has not totally obliterated or completely overprinted the early, primary tectonic fabrics in parts of the low-grade sequence. This shows that the early stages of transposition occur in certain zones that eventually grow laterally with increasing shear strain.

**2.2 Structure of the High-grade Sequence**

The high-grade sequence consists of compositional banding defined by alternating mica-rich (muscovite and biotite), quartz-rich ± plagioclase-rich layers with varying amounts of garnet and mica (McNeill, 1985; Meffre et al., 2001). Biotite-garnet-kyanite boudins and isolated lenticular blocks of amphibolite also occur within the sequence. Much of the following description and photographs following are from McNeill (1985) with additions from Mulcahy Bay and Bond Bay in Port Davey.

*2.2.1 Nature of the Sm Foliation*

The dominant foliation Sm in the West Coast high-grade schists is a schistosity/transposition layering sub-parallel with compositional banding (Figures 23 and 24). The dominant schistosity Sm has developed from micro-folding of an older, earlier-formed schistosity into crenulation cleavage with transition into schistosity by transposition (Figures 24, 25, 26, 27 and 28). This can be seen at the outcrop-scale as heterogeneous zones of the dominant foliation up to 1-2 metres enveloping pods folds that contain isoclinal fold relicts folded by the schistosity forming deformation (Figures 24 and 25). At the micro-scale relicts of the early crenulation cleavage fabric are commonly preserved between the foliation lamellae (Figures 26, 27 and 28).

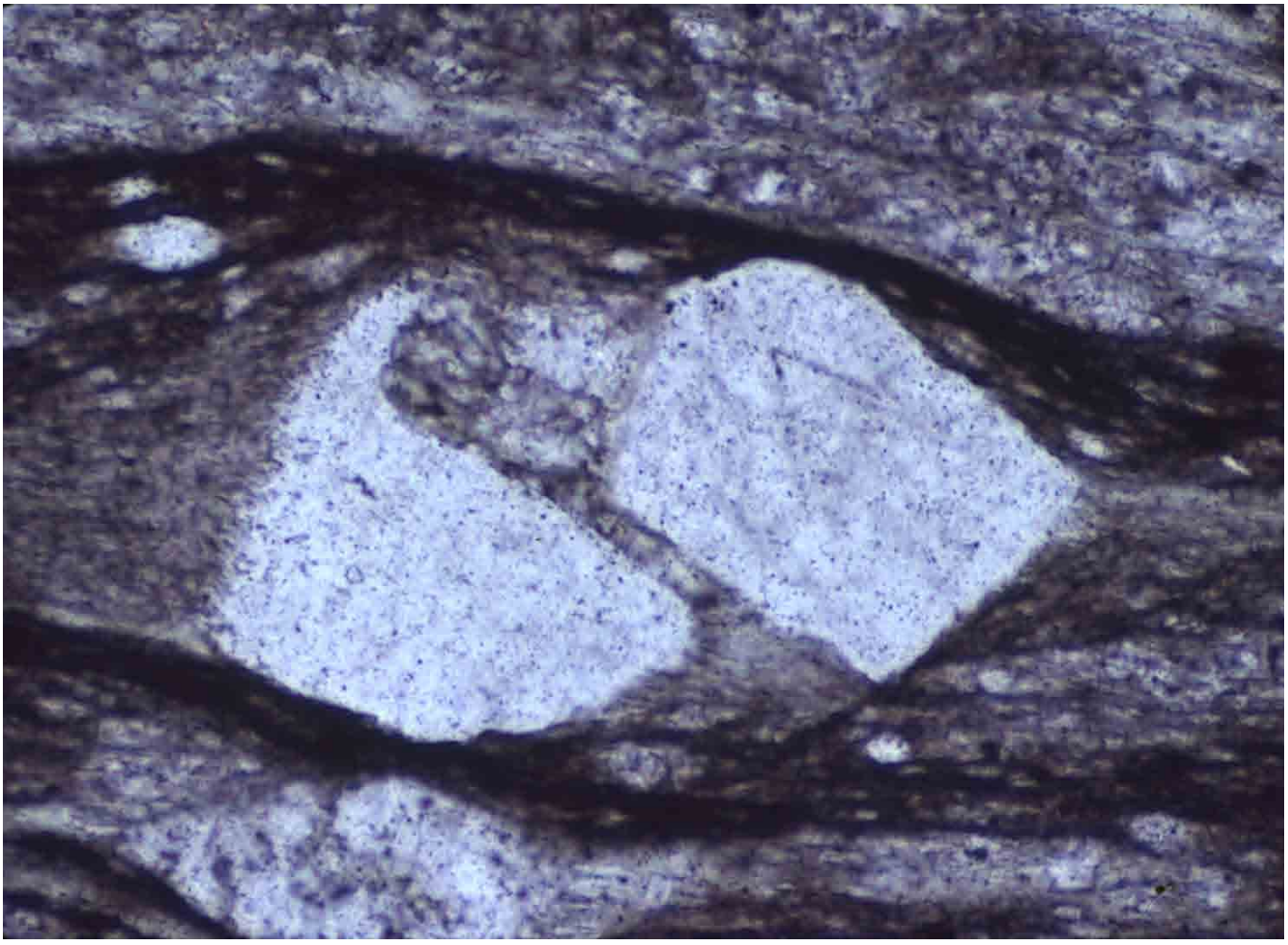

Figure 21. Microstructure of an S1 spaced cleavage showing dark quartz-depleted dissolution zones bounding quartz clasts with mica beard growth. (Photo credit: A.W. McNeill)

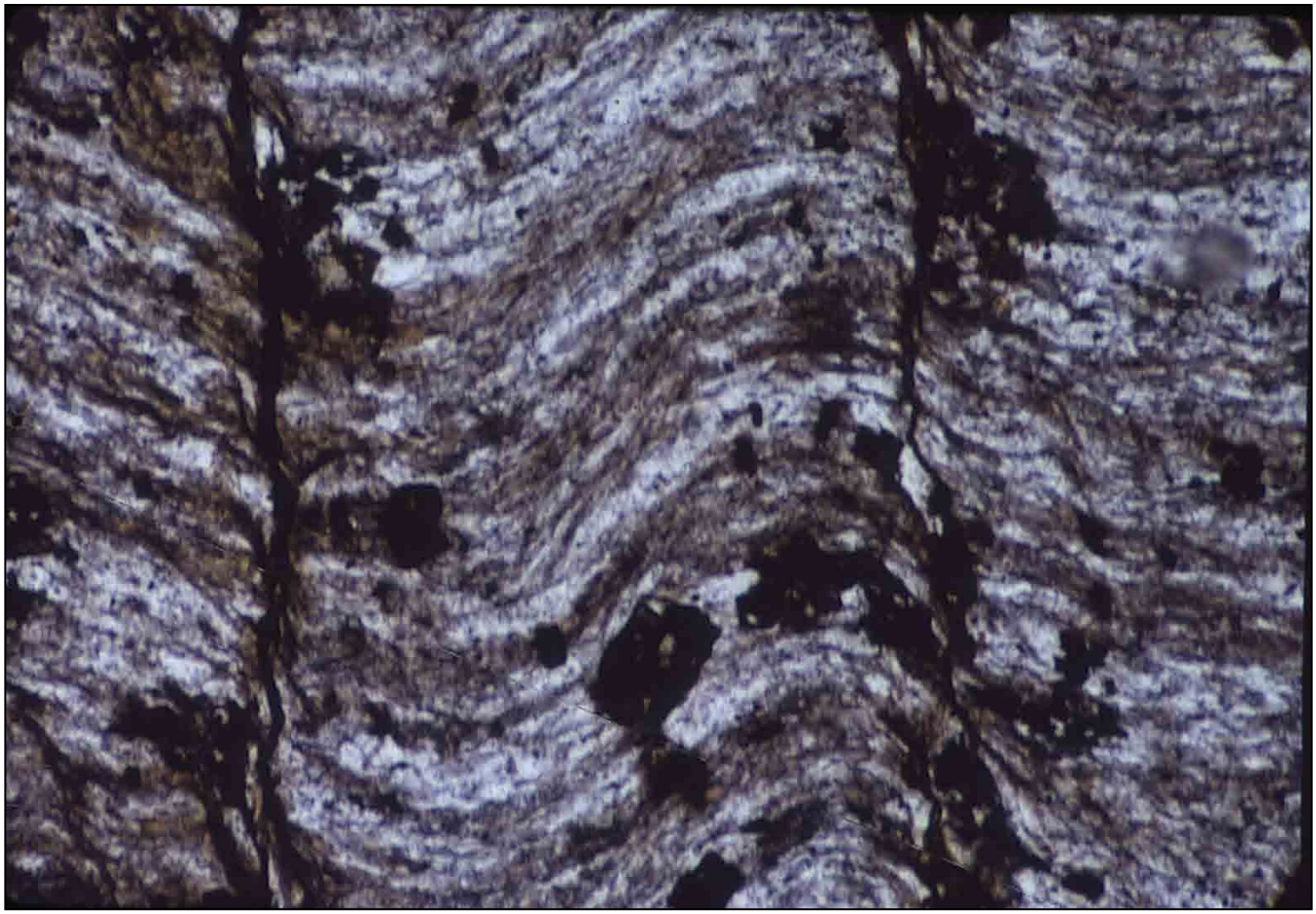

Figure 22. Discrete crenulation cleavages typical of pressure solution as sub-vertical, thin dark, residue rich, "crack-like" surfaces. The intervening microlithons show open crenulations of the primary first phase slaty cleavage. The discrete crenulation cleavage is axial surfaces to the upright F2 folds (Figures 15 and 16). (Photo credit: A.W. McNeill)

Figure 23. Compositional banding in coarse, gneissic schist showing a flattened extremely attenuated isoclinal fold hinge (Station AM70) (Photo credit: A.W. McNeill).

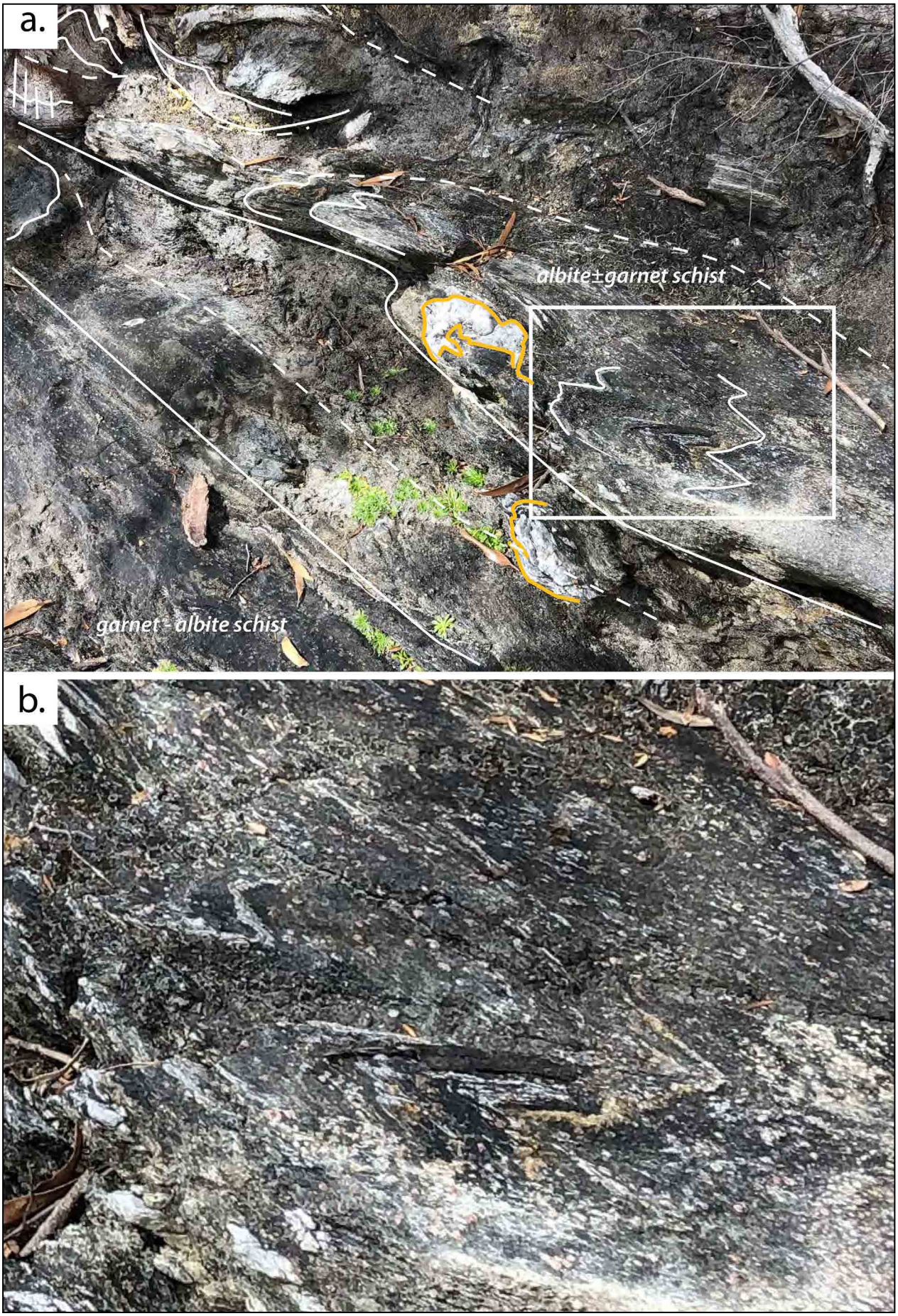


Figure 24. High-grade garnet-albite schist at Bond Bay, Port Davey. a) Foliation-parallel compositional banding with layers of garnet-albite schist and albite ±garnet schist showing extremely heterogeneous deformation. Zones of dominant schistosity envelope folded domains as metre-scale, augen-like pods preserving folds in an older schistosity. b) Close up of the folded layering in albite schist with an axial surface crenulation cleavage. This cleavage transitions into the dominant schistosity at the edges and tips of the pods. Relict isoclinal folds cored by dark graphitic schist occur within an even earlier-formed layering (Photo credit: E. P. Ambler).


Figure 25. Dark graphitic garnet schist from Bond Bay, Port Davey. a) b) Annotated photo showing the heterogeneous nature of the dominant schistosity. This schistosity encloses garnet porphyroblasts and phacoid-lenses that show the schistosity transitioning from a sub-parallel crenulation cleavage in an older schistosity. Some of the garnets have tails as overgrowths (pale yellow beards) (Photo credit: E. P. Ambler).

Figure 26. Photomicrograph of schistosity in high-grade garnet schist showing mica-rich domains with intensely flattened and aligned mica alternating with quartz-mica lamellae and occasional stringers of quartz vein relicts (photo bottom right) (Photo credit: R. F. Berry).

Figure 27. Photomicrograph of the schistosity/compositional banding with alternating mica-rich bands and quartz-rich bands that preserve evidence of microfolding of an earlier fabric preserved as mica trains in the quartz-rich microlithons. The foliation augen (photo centre) shows a micro-fold hinge defined by mica trains within an original quartz rich layer that was isoclinally folded, flattened with complete limb attenuation. (Photo credit: R. F. Berry).

Figure 28. Photo-micrograph of coarse, gneissic-like, compositional banding showing relict isoclinal hinges in now attenuated and transposed quartz-rich layers. Location is Bottom Rocks RB97-626B. (Photo credit: R.F. Berry)

*2.2.2 Nature of the Early F1/F2 Folds*

Early isoclinal F1 folds occur as isolated rootless intrafolial fold closures within transposed compositional banding (So/Sm) in gneissic schists and quartzites (Figures 23 and 29).

The F1 fold hinges are thickened with highly attenuated limbs (Figures 23, 29 and 30). Fold axial surfaces are either north-south striking and west dipping or east-west striking and south dipping (McNeill, 1985). Fold geometry is gently plunging and moderately inclined.

Most of the preserved isoclinal folds within the high-grade sequence are small-scale and intra-folial to the So/Sm transposed layering (Figures 29 and 30). Some larger scale examples of isoclinal fold pairs up to 1 metre have developed augen or pod-shaped form within strongly flattened transposed zones within the quartzite (Figure 31).

Within the general homoclinal, steeply west-dipping, high-grade sequence a zone of steeply dipping So/Sm with a flat-lying, strong to intense Sm axial surface fabric is suggestive of a relict, early-formed, larger scale, second or first order hinge (Figure 32).

Mesoscopic, plunging upright folds with axial surface crenulation cleavage, designated F2 folds by McNeill (1985), are most common and occur on all scales (Figure 33). They include some major, second-order closures with a wavelength of approximately 200 metres (CN921373 and CN914327). Vergence folds are common on the eastern limb of the former of these, and are open, moderately angular, upright and gently plunging structures with a wavelength of 2 to 3 metres. Parasitic to these are chevron folds with variable wavelength, dependent on lithology, although it is generally less than 2-3cm. They are symmetrical and open, having the same axial plane and hinge orientation as the vergence folds. A north-south strike with a steeply west-dipping axial plane and a hinge line plunging at an average of $20^{o}$ to $220^{o}$ are characteristic (McNeill, 1985). Some refraction of strain may occur in quartzites that generally have steeply east-dipping axial planes.

*2.2.3 Amphibolite Boudins*

Amphibolites occur as rounded to lenticular boudin-like bodies enveloped by Sm and So/Sm in the high-grade schists (Figure 34). They are a minor component of the Nye Bay high-grade rocks, have three mineralogical associations and occur principally at two locations (McNeill, 1985).

Figure 29. Flattened isoclinal fold in quartzite within the high-grade garnet schist sequence at CN921324 (Station AM73). The enclosing So/Sm layering has attitude 150/44W. Photo from McNeill (1985, Figure 3.1).


Figure 30. Isoclinal fold pair in quartzite showing limited axial surface foliation (Photo credit: A.W. McNeill).

Figure 31. Flattened isoclinal fold pair forming a "pod" with attenuated limb segments within quartzite of the high-grade sheet (Photo credit: A. McNeill).

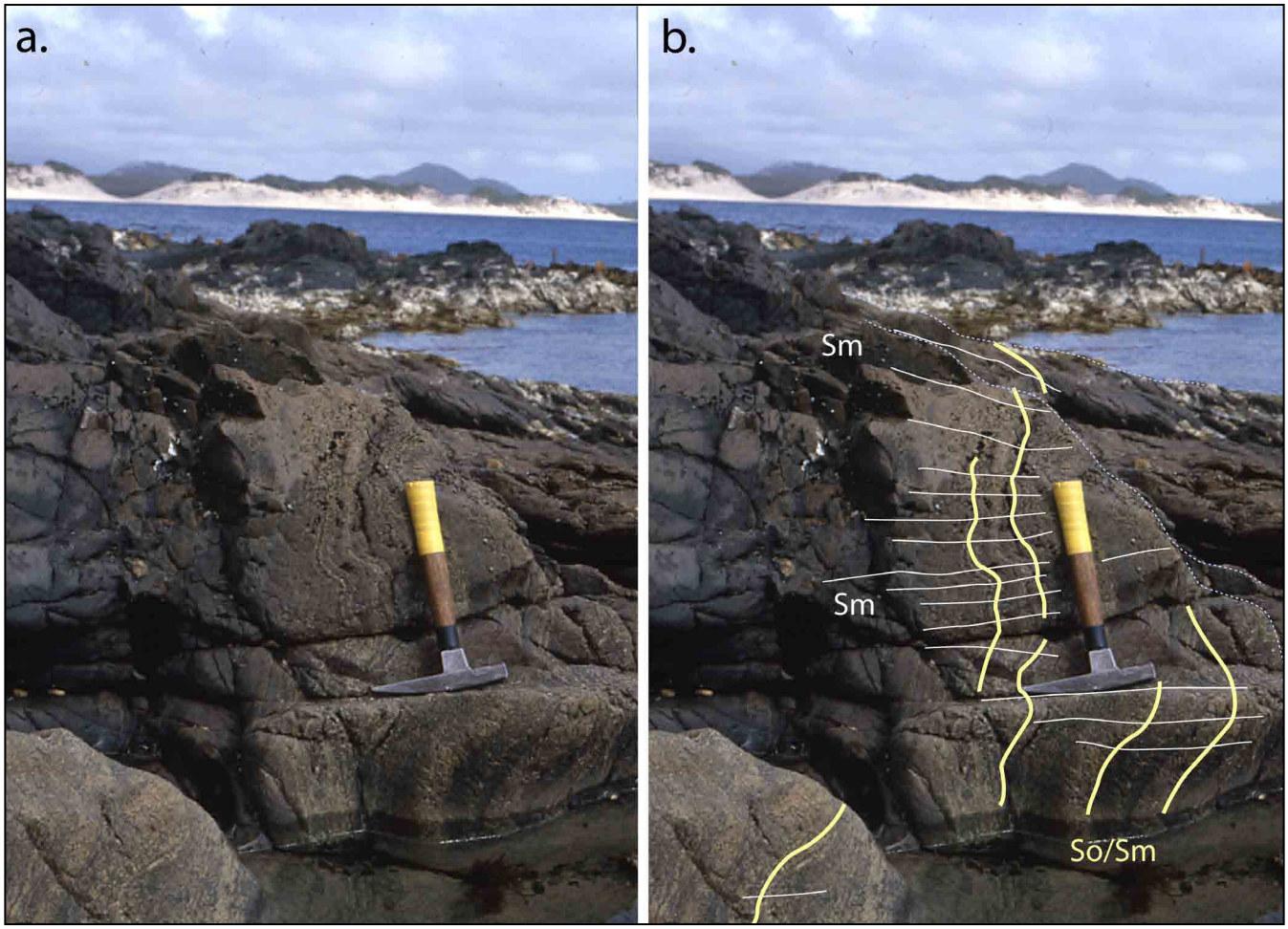


Figure 32. Large-scale recumbent fold closure in H-G psammitic schists with Nye Bay in the background. (Photo credit: A. McNeill)

Figure 33. Plunging F2 fold with sub-vertical axial surface crenulation cleavage typical of the Nye Bay high-grade sequence. The convergence of the differentiated metamorphic layering in places is suggestive of remnant intrafolial F1 isoclines (see circled areas). (Photo credit: A.W. McNeill)

Figure 34. Small amphibolite boudins within and enveloped by high-grade schist. (Photo credit: A.W. McNeill)

1. Hornblende-plagioclase-quartz amphibolite occurs as three large boudins, up to 10 metres in length and 3 metres wide at CN921324 (Figure 35). Boudin sectional views in outcrop plan give aspect ratios of 2.5: 1 to ~4:1. These approximate X/Z strain ratios where X is the long dimension shape-axis sub-parallel to the regional stretch direction (mineral lineation Lm) and Z is the maximum-width shape axis normal to the enveloping foliation.
2. Garnet-hornblende amphibolite occurs as an isolated boudin adjacent to the three large three large hornblende-plagioclase-quartz amphibolite boudins at CN921324 (McNeill, 1985).
3. Garnet amphibolite occurs as numerous 1-3 metre long boudins at CN918325 (Figure 36) and as scattered bodies further west at CN914327. These occur as isolated boudin trains within the dominant So/Sm foliation and show marked variations in aspect ratios indicative of heterogeneous strain (Figures 36a and b). In the highest strain zones the shape ratios are up to 9:1 with a range of 5:1 to 9:1. Another zone show aspect ratios less than 3:1. These approximate X/Z strain ratios where X is the long dimension shape-axis sub-parallel to the regional stretch direction (mineral lineation Lm) and Z is the maximum-width shape axis normal to the enveloping foliation.

Outcrop sectional views at high angles to the regional stretch direction (Figure 36c) give shape aspect ratios of 4:1 with the occasional approaching 1. These equate to Y/Z strain ratios where Y: is the intermediate strain axis and Z is the minimum strain axis.

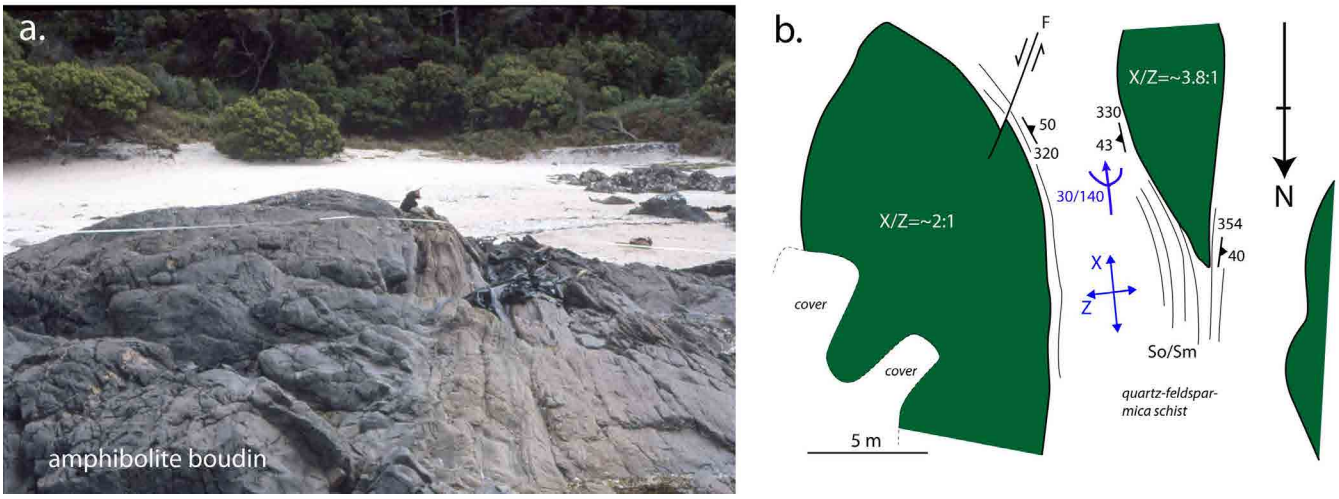


Figure 35. Large hornblende-plagioclase-quartz amphibolite boudins within quartz-felspar-quartz mica schist at outcrop at CN921324. a) Photo of contact between large amphibolite boudin and high-grade schist. b) Map of boudins showing shapes and relationships with the enveloping foliation Sm and So/Sm. Boudin shape aspect-ratios from the mapped outcrop sectional views are shown as X/Z ratios in white text for individual boudins, where X is the maximum principal elongation (stretch) and Z is the minimum principal elongation (shortening direction). (McNeill, 1985)

### 2.3 Contacts Between the Low-grade and High-grade Sequences

Contacts between the high-grade and low-grade rocks are ductile high strain zones but many have been overprinted by later brittle deformation (Meffre et al., 2001) (Figure 37). The nature of the contacts in the Nye and Mulcahy Bay areas have been described and discussed in detail by Meffre et al. (2001). These contacts will be described here in their geological and geographic context with respect to the different coastal segments (see Section 3).

## 3.0 STRUCTURE OF THE HIGH-GRADE COASTAL BELT

### 3.1 Top Rocks - Nye Bay - Mulcahy Bay

The Top Rocks-Nye Bay-Mulcahy Bay region is cored by high-grade garnet-mica schist from the Lawson Range to Nye Bay through to Elliott Point (Figure 38). These high-grade schists are bounded by low-grade pelite and quartzite from Nye Bay to Top Rocks on the west and from Elliot Point to Mulcahy Bay on the east (Figure 38). The repeated, homoclinally-dipping litho-tectonics units are reminiscent of folded flanking-layers about a recumbent fold core of high-grade schist (Figure 40c). The inferred recumbent fold (see Section 3.1.4) has a inferred plunge of 48°/259° based on mesoscopic isoclinal fold attitude at Elliott Point (Figure 38). This is folded by open, north-south trending, south-plunging, younger Devonian folds including the Giblin Syncline (calculated plunge 19°/178°) and the Lawson Range Anticline (calculated plunge 30°/185°) (Figures 39 and 40).

Early F1/F2 isocline axial surface attitudes and fold axis plunges (Figure 39) show a marked variability related primarily to folding of the early mesoscopic isoclines by the large, regional scale fold-nappe, and secondly by the younger Devonian folds.

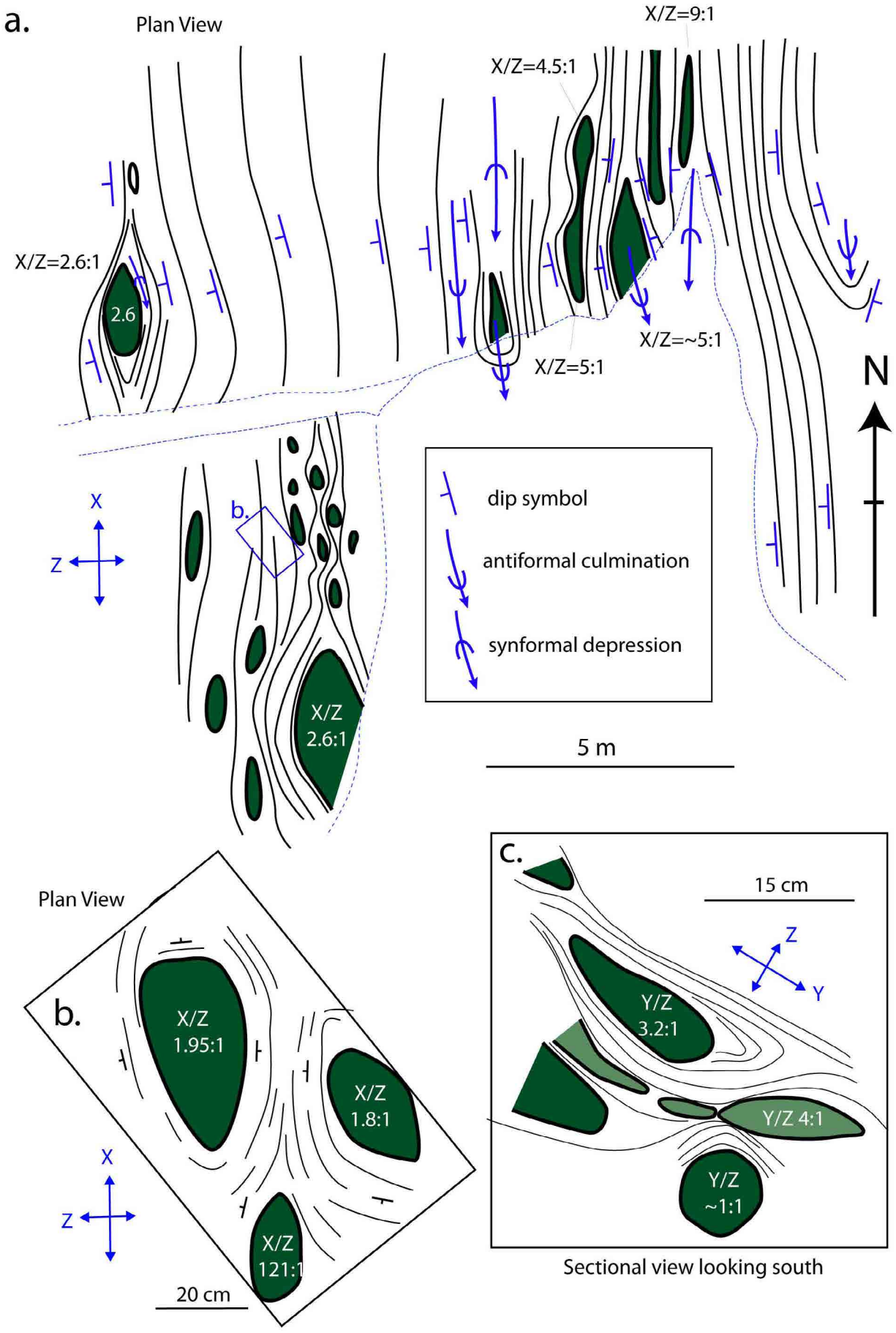


Figure 36. Structural relationships of the small (< 3 metres) garnet-quartzite amphibolite boudins at CN918325. a) Outcrop map with enlargement of area shown in (b) providing XZ sections through the boudins , where X is the maximum principal elongation (stretch) and Z is the minimum principal elongation (shortening direction). Boudin shape aspect-ratios from the mapped outcrop views are shown as X/Z ratios in white text for individual boudins. c) Sub-vertical sectional profile view of part of the exposure. Boudin shape aspect-ratios are shown as Y/Z ratios in white text for individual boudins, where Y is the intermediate principal elongation. (McNeill, 1985)

The litho-structural map (Figure 38) shows key elements including

1. A southwards tapering or thinning of the high-grade schist (Ptpg) towards Elliott Point.

2. A loss of high-grade schist (Ptpg) north of the Lawson Range, across a northwest-trending cross-fault.

3. Thinning northwards of the low-grade pelite (Ptp) units that enclose the high-grade schists away from the inferred macro-fold hinge at Elliott Point (i.e. layer thickening within the inferred hinge and layer thinning and attenuation along the fold limbs).

4. A pinch out of low-grade pelite (Ptp) north of the Giblin River along the eastern flank of the high-grade schist, such that north of Nye Bay the high-grade schists sit directly on quartzite.

5. A re-appearance of low-grade pelite north of the Giblin Syncline closure.

6. High-strain, mylonitic, platy schistose quartzite is more common along the eastern contacts of the quartzite unit.

7. Fault-offsets of contacts by a northwest-trending dextral-oblique slip fault set and a northeast-trending sinistral-oblique fault set.

**These relationships suggest a lack of continuity of the major layering due to high strain transposition of units at a regional scale with extreme flattening and elongation of litho-structural units with high strain zones developed along their bounding contacts (see Section 2.3).**

*3.1.1 Top Rocks to Nye Bay*

The coastal sequence from Top Rocks to Nye Bay (area 1, Figure 6) consists of a homoclinal-dipping, foliated sequence of low-grade quartzite (Pts), overlying low-grade quartz phyllite (Ptpq), overlying graphitic phyllite (Ptp) overlying high-grade garnet schist (Ptug) (Figures 41a and 42a, b). Structural mapping by McNeill (1985) provides the map base and structural data presented in Figure 41.

Figure 37. Steeply-dipping L-S fabric in the low-grade phyllite at the boundary with the high-grade schist west of Nye Bay (Photo from McNeill, 1985, fig. 3.1). (AMG grid location 391204E 5233266N)

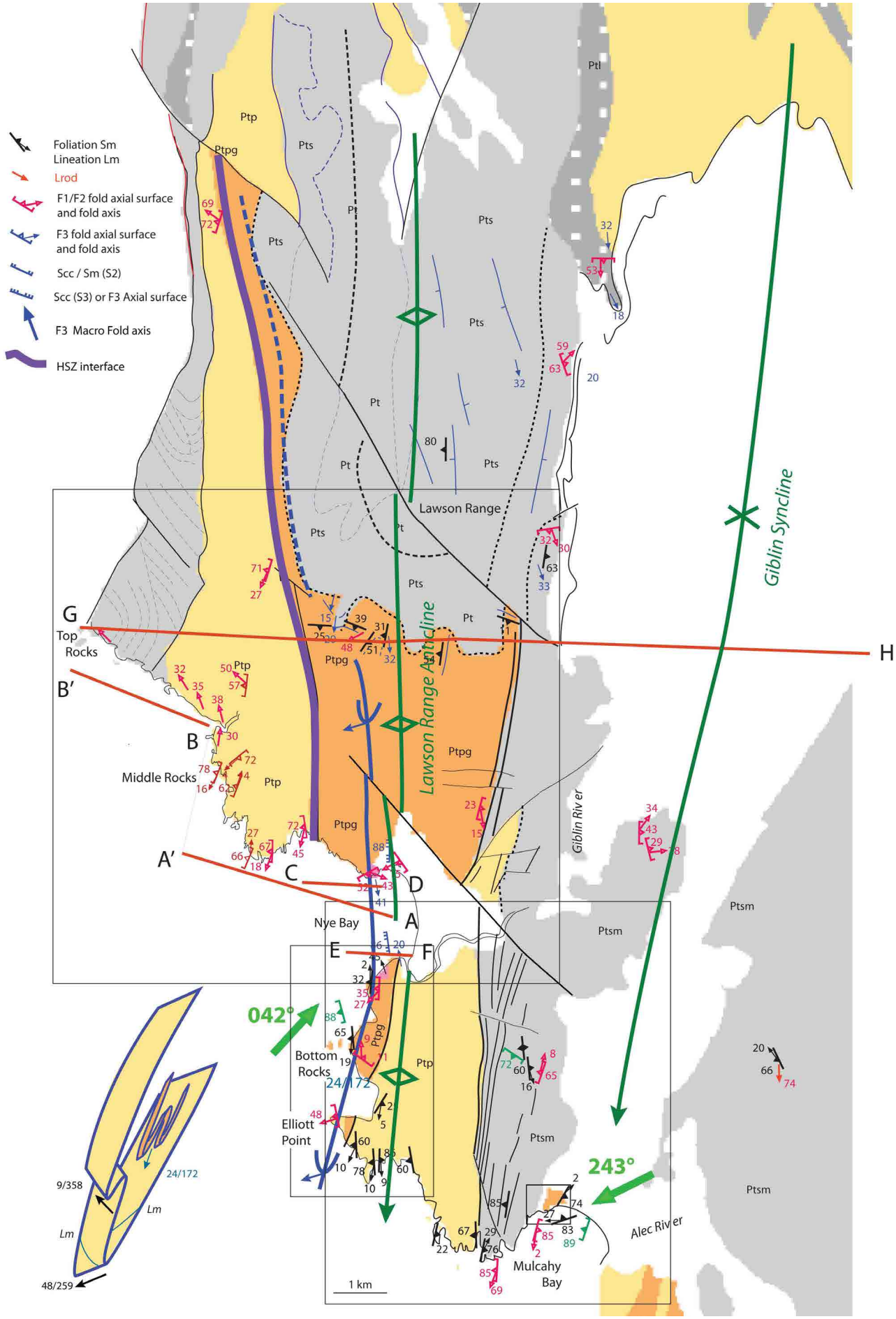


Figure 38. Lithological and structural relationships in the Nye-Mulcahy Bay area. Base map is the Mineral Resources Tasmania digital geological atlas Lewis, Elliott, and Mulcahy 1:25000 map sheets. Positions of section lines A-A', B-B', C-D, E-F and G-H are shown by the thick red lines. Heavy green arrows are calculated transport directions TD (see Section 5.0).

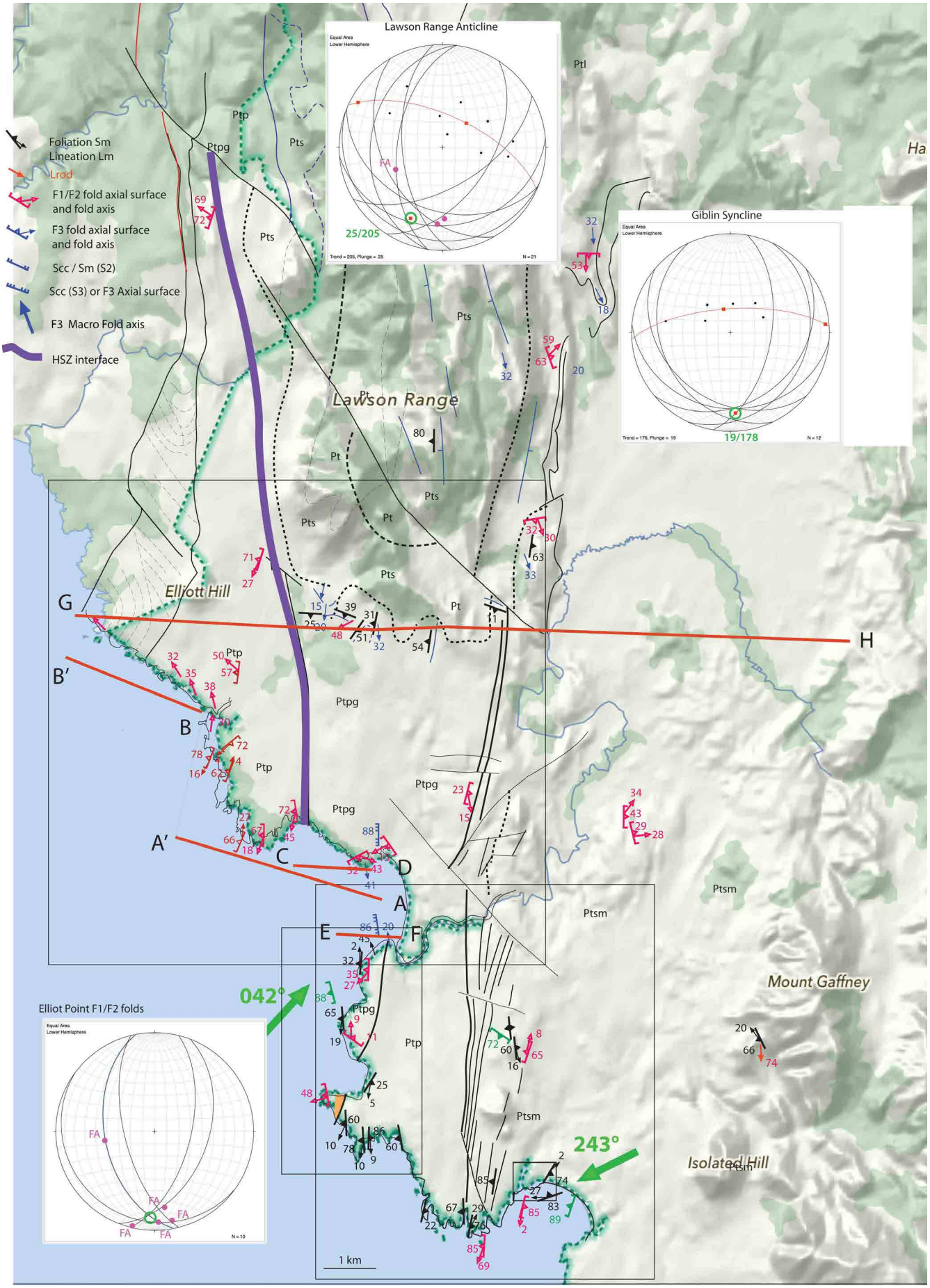


Figure 39. Early F1/F2 fold axis and axial surface data plotted on a MapOutTM DEM base with some formline traces (black full and dashed lines). Positions of section lines A-A', B-B', C-D, E-F and G-H are shown by the thick red lines. The heavy purple line represents the high strain zone contact between the low-grade phyllites and the high-grade schists west of Nye Bay. Stereonet insets show the plunges and plunge directions of the inferred Nye Bay fold-nappe (25°/205°) and the younger Devonian Lawson Range Anticline (30°/185°) and Giblin Syncline (19°/178°).

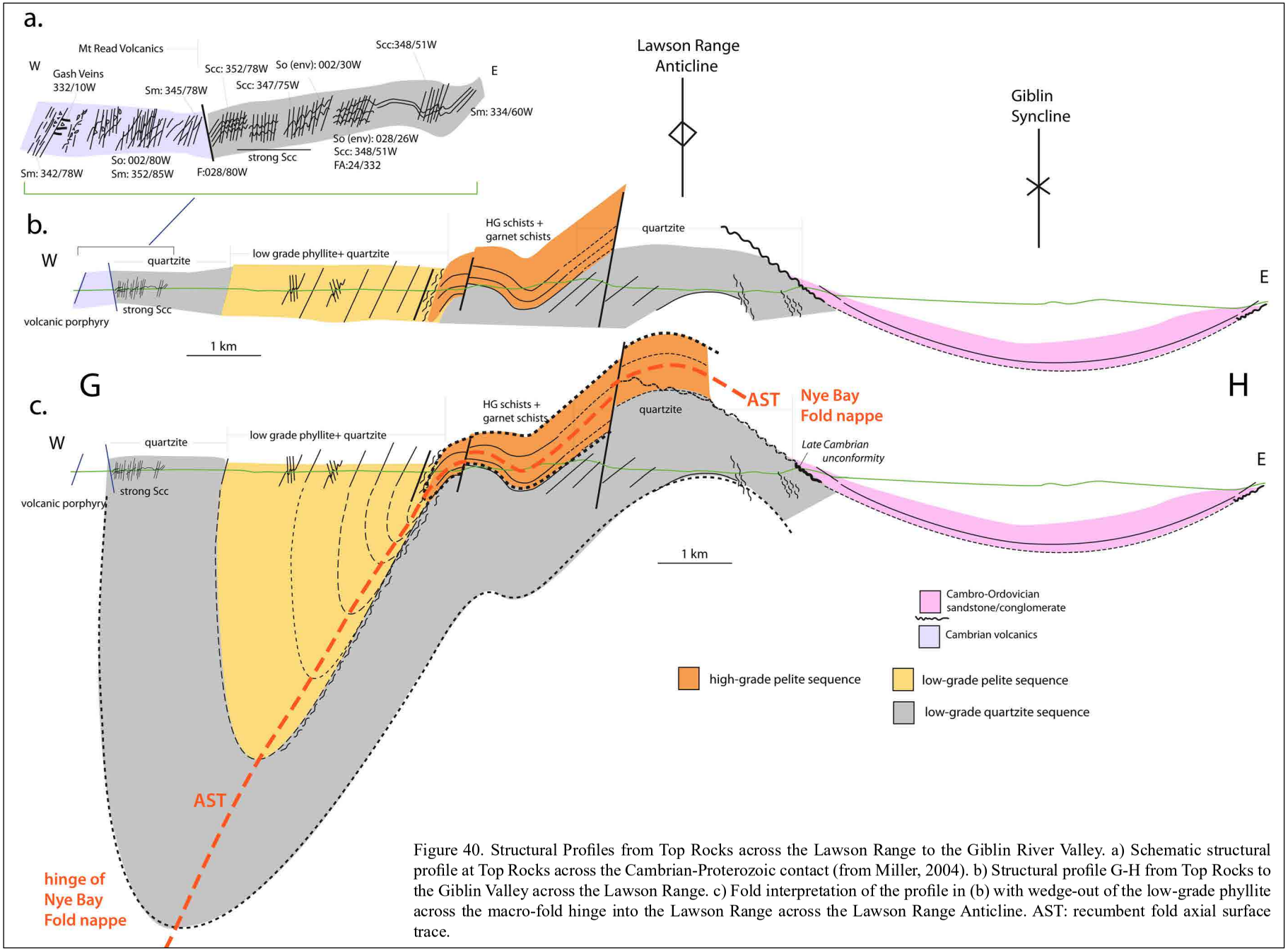


Figure 40. Structural Profiles from Top Rocks across the Lawson Range to the Giblin River Valley. a) Schematic structural profile at Top Rocks across the Cambrian-Proterozoic contact (from Miller, 2004). b) Structural profile G-H from Top Rocks to the Giblin Valley across the Lawson Range. c) Fold interpretation of the profile in (b) with wedge-out of the low-grade phyllite across the macro-fold hinge into the Lawson Range across the Lawson Range Anticline. AST: recumbent fold axial surface trace.

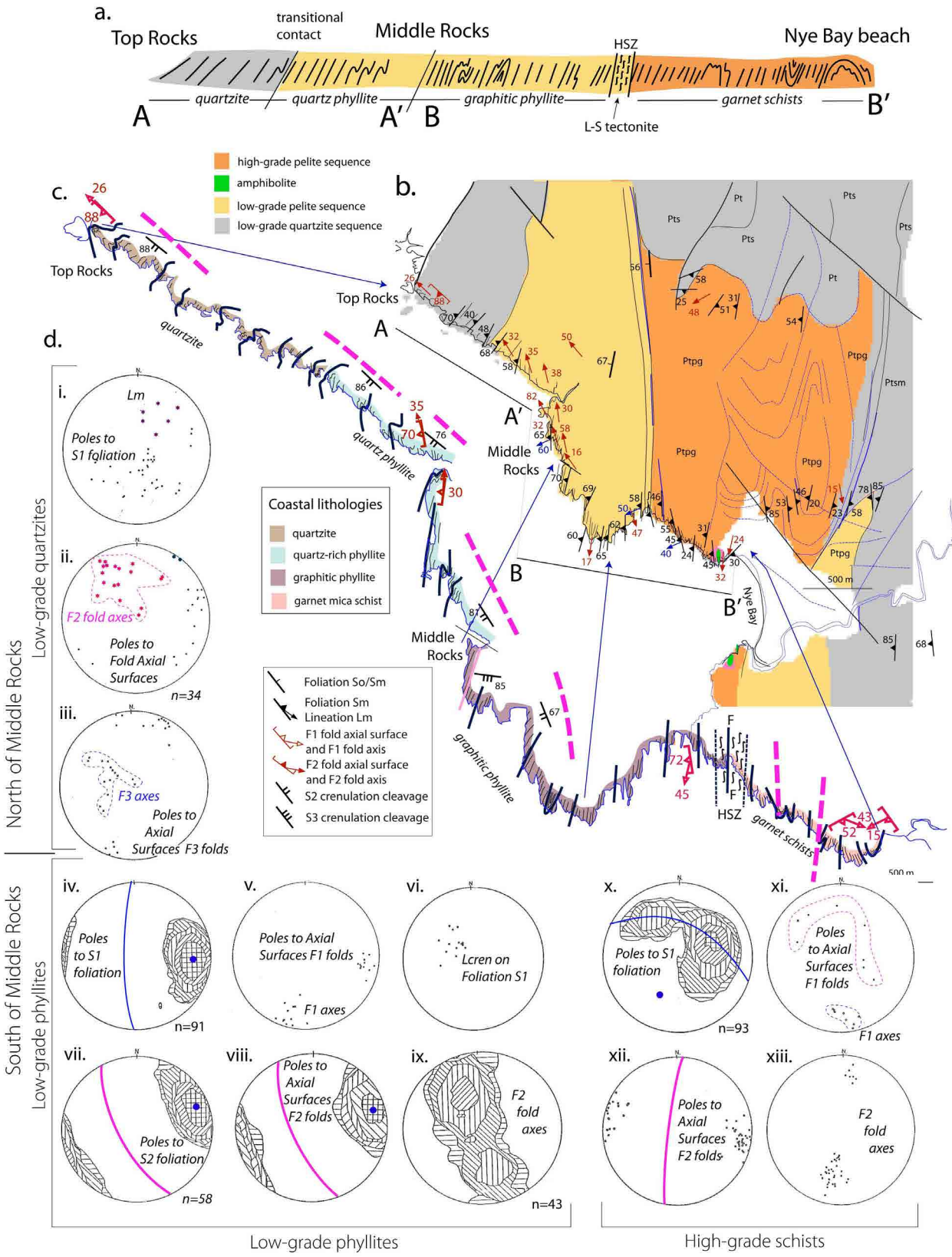


Figure 41. Structure of the Top Rocks to Nye Bay region. a) Stepped structural profile A-A' and B-B' from Top Rocks to Nye Bay beach adopted from McNeill (1985). b) Geological map of the Top Rocks-Nye Bay area adapted from McNeill (1985) and Hall and Vicary (2010b). c) Coastal formline map adapted from McNeill (1985). Pink dashed lines highlight the swing in S2/F2 orientation. d) Structural data summary in stereonet form for the three litho-tectonic packages low-grade quartzite and quartz phyllite (stereonets i, ii and iii), low grade phyllites (stereonets iv, v, vi, vii, viii and ix) and high-grade schists (stereonets x, xi, xii and xiii).

Despite the apparent homoclinal, west-dipping sequence (Figure 41a) there are significant changes in the geometry and attitude of the early F1/F2 isoclinal folds (Figures 39, 41b and 41d). These include:

1. A change in the S1 pole patterns from a complex girdle pattern with a north-plunging p axis north of Middle Rocks (stereonet i, Figure 41d), to a unimodal pattern indicating north-south trend and steep west dip in the graphitic phyllite south of Middle Rocks (stereonet iv, Figure 41d), to an approximate girdle pattern with a southwest plunging p axis in the Nye Bay high-grade schists (stereonet x, Figure 41d).
2. F1 fold axis changes from a northwest plunge north of Middle Rocks (stereonet ii, Figure 41d), to a south-southwest plunge south of Middle Rocks (stereonet v, Figure 41d), to a south or south-southeast plunge in the Nye Bay high-grade schists (stereonet xi, Figure 41d).
3. F2 fold-axis plunge direction changes and variability.

Top Rocks to Middle Rocks: isocline fold plunges are to the northwest (stereonet ii, Figure 41d).

Middle Rocks to Nye Bay are south-plunging and associated with more upright folds.

Further to this, the lineation pattern changes from a north-northeast plunge in the quartz-phyllites near Ummarah Creek (stereonet i, Figure 41d) to gently southwest plunging in the high-grade rocks west of Nye Bay (Figure 41b).

Formline mapping of the bedding foliation So/Sm by McNeill (1985) shows the hinge of a broad northwest-plunging antiformal fold in the quartzite at Top Rocks and in the quartz-phyllite north of Ummarrah Creek (Figure 41c). Plunges of the accompanying mesoscopic folds, designated F2 by McNeill, are northwest-plunging but show variable plunge to the northwest (stereonet ii, Figure 41d). South of Ummarrah Creek the coastline mapping shows a swing to a more north-south strike of So/Sm with a convergence to a more north-south trend through to the high-grade schists at the north end of Nye Bay (Figure 41c).

The S2 foliation and axial surfaces of the F2 folds in the graphitic phyllite south of Middle Rocks are northwest-trending with a steep west-southwest dip (stereonets vii, viii and ix, Figure 41d), but change to a north-northeast trend with a steep west dip in the high grade schists at the north end of Nye Bay (stereonet xii, Figure 41d). The F2 fold plunge is markedly variable in the graphitic phyllites with fold plunges defining a girdle pattern with both northwest and southeast plunges, indicative of fold hinge migration at shear increasing strain (stereonet ix, Figure 41d). Within the Nye Bay high-grade schists the fold plunges are consistent moderately to gently south-southwest plunging (stereonet xiii, Figure 41d).

In summary, there is a marked swing in S2 strike and F2 fold plunge direction from Top Rocks to the north end of Nye Bay beach (pink dashed lines in Figure 41c). The F2 fold axis pattern changes dramatically (compare stereonets ii, ix and xiii, Figure 41d).

Profiles A-B' (Figure 41a), C-D and E-F (Figure 42a and b) show a homoclinal west-dipping sequence of high-grade schists across the inferred hinge zone of the fold-nappe, not unlike those seen along the Mt McCall road traverse (see Gray and Vicary, 2021b). The high-grade schists are bounded by the low-grade phyllite sequence (Figures 42a and b), although the western low-grade phyllite is offshore and not exposed along the coastline at Elliott Point (Figure 42).

The contact between the high-grade schists and the low-grade phyllite north of Nye Bay (Figures 41a and 42a) is a 60m wide zone of highly sheared rocks, some of which have an L-S fabric (McNeill, 1985; Meffre et al., 2001. The foliation in this zone is sub-parallel to Sm of both the phyllites and adjacent schists, with an orientation of 360/57W. The dominant phyllite lithology in this zone has a black matrix with quartz and calcite-rich porphyroclasts (Figure 37). These are elongate parallel to the foliation and form a strong lineation trending 270° and plunging at 60°. Microscopically, sub-rounded quartz grains are set in a matrix of fine-grained quartz and mica, showing strong crystallographic preferred orientation (McNeill, 1985). The matrix has undergone strong grainsize reduction, whilst porphyroclasts have been brittlely deformed. Fractured grains, with calcite infilling between fragments, asymmetric augen and pressure shadows indicate a west-side down or normal sense of movement (Meffre et al., 2001).

*Way-up Determination in Quartzite*

Analysis of the structure in quartzite and quartz phyllites northwest of Ummarah Creek (Figure 43a), utilising way-up determined from ripple marks preserved in quartzite (Figure 43b), indicate that this coastal litho-section is upside down. Despite a lack of So/Sm attitude data at AM57 formline mapping by McNeill (1985) shows that the So/Sm containing the ripple marks is northwest striking (Figure 43a). Other mapped So/Sm northwest-striking segments (AM116 and AM62) have northeast-dip that swing into a northeast-strike with northwest dip that must be overturned with overall younging to the southeast (see Figure 43d and compare with mapped coastal formline patterns in Figure 43a). The mapping (Figure 43a) and the stereonet plot (Figure 43c) show the two sets of folds interfere in the succession; the dominant northwest striking and plunging set (F2 by McNeill, 1985) is refolded and/or overprinted by a northeast trending set (see Figure 43a and c).

The significance of the overturned succession from Top Rocks to Middle Rocks will be discussed in Section 3.1.4 and Section 4.

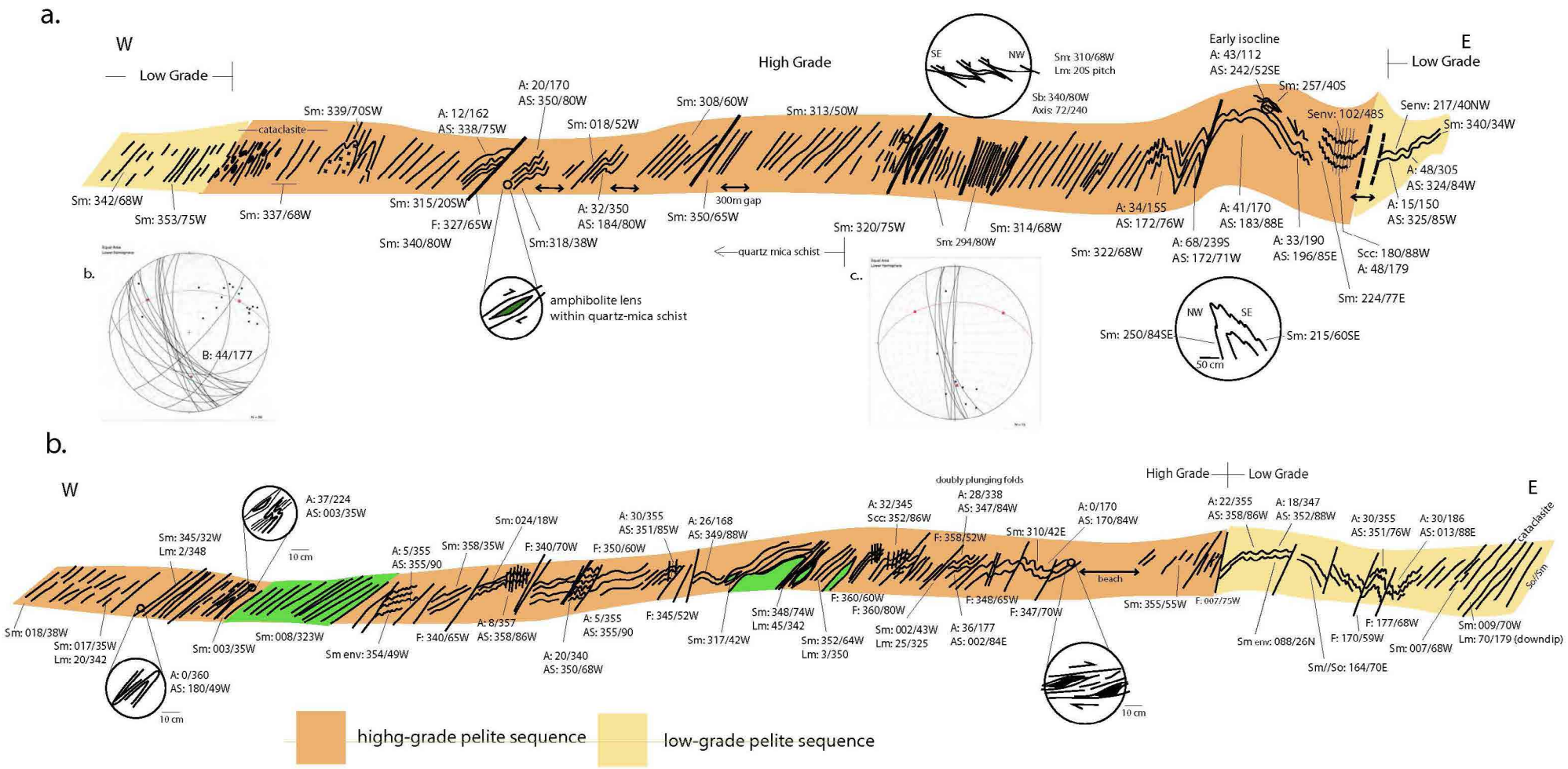


Figure 42. Schematic structural profiles constructed by John Miller during coastal field mapping in 2004 (Miller, 2004). a) Profile C-D is at the north end of Nye Bay. b) Profile E-F is from the south end of Nye Bay. Profile locations are shown on Figure 38.

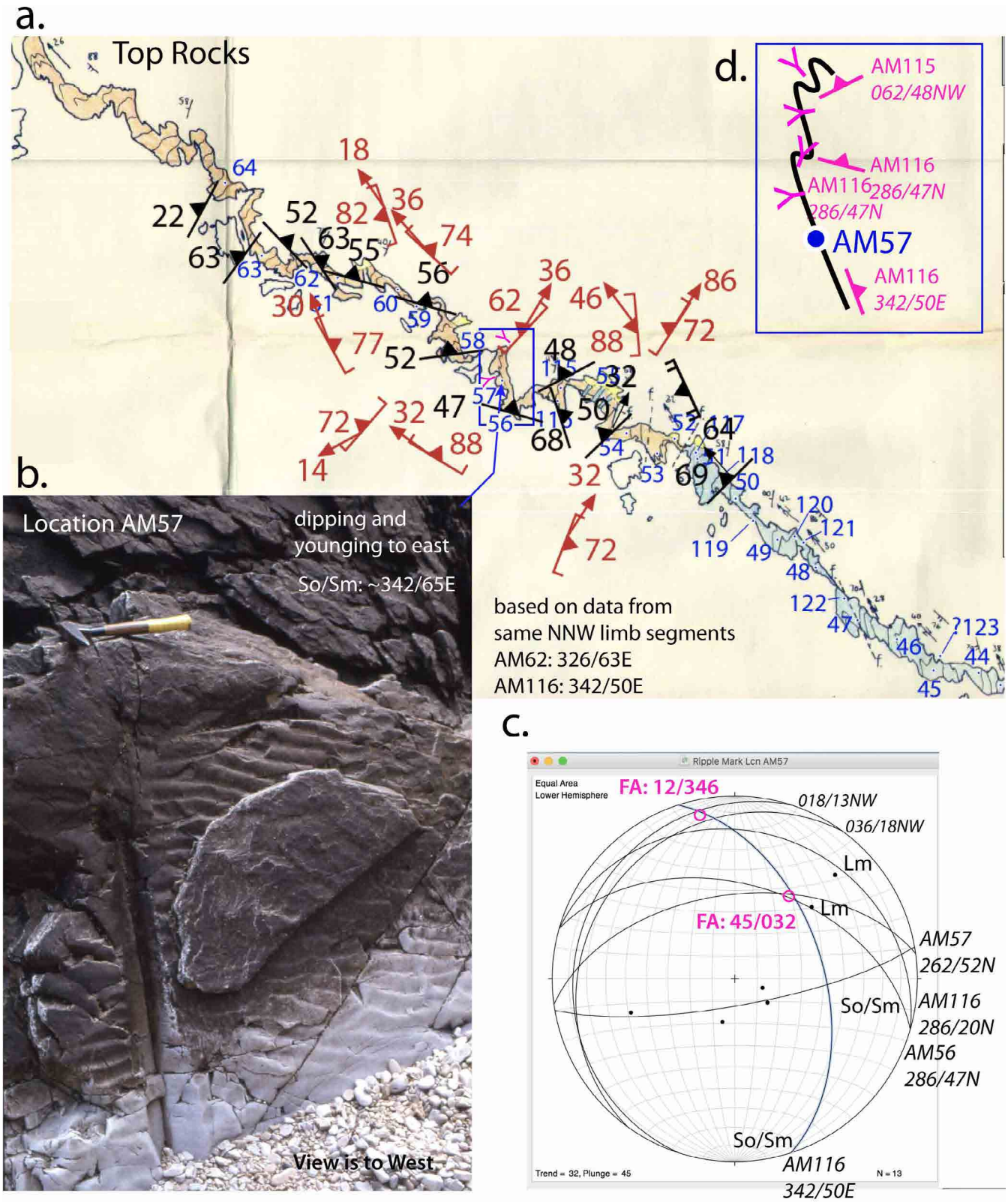


Figure 43. Structure of quartzite and quartz phyllites northwest of Umarrah Creek to Top Rocks. a) McNeill (1985) map with formlines in So/Sm, AM station location numbering (blue) and structural data (Black: So/Sm foliation and lineation attitudes; Red: Fold axial surface and fold axis attitudes). b) Photo of ripple marks on inferred northeast-dipping bedding So/Sm in quartzite at AM57 indicating younging is to the northeast. c) Stereonet plot of So/Sm great circles and poles, and mineral lineation Lm.

*3.1.2 Nye Bay to Mulcahy Bay*

This map area extends from the Giblin River mouth at the south end of Nye Bay to the south end of Mulcahy Bay (area 2, Figure 6). Belts of west-dipping high-grade garnet ± kyanite schist flanked by low-grade phyllite/schistose quartz and quartzite occur along the coast from the Giblin River Mouth through Bottom Rocks to Elliott Point, and on the northern and southern margins of Mulcahy Bay (Figure 44). Detailed maps are presented for the coastal strip from Giblin River through Elliott Point (Figure 44 and Appendix 2), the high-grade rocks north end of Mulcahy Bay (Figure 47) and the contact at the south end of Mulcahy Bay (Figures 49 and 50).

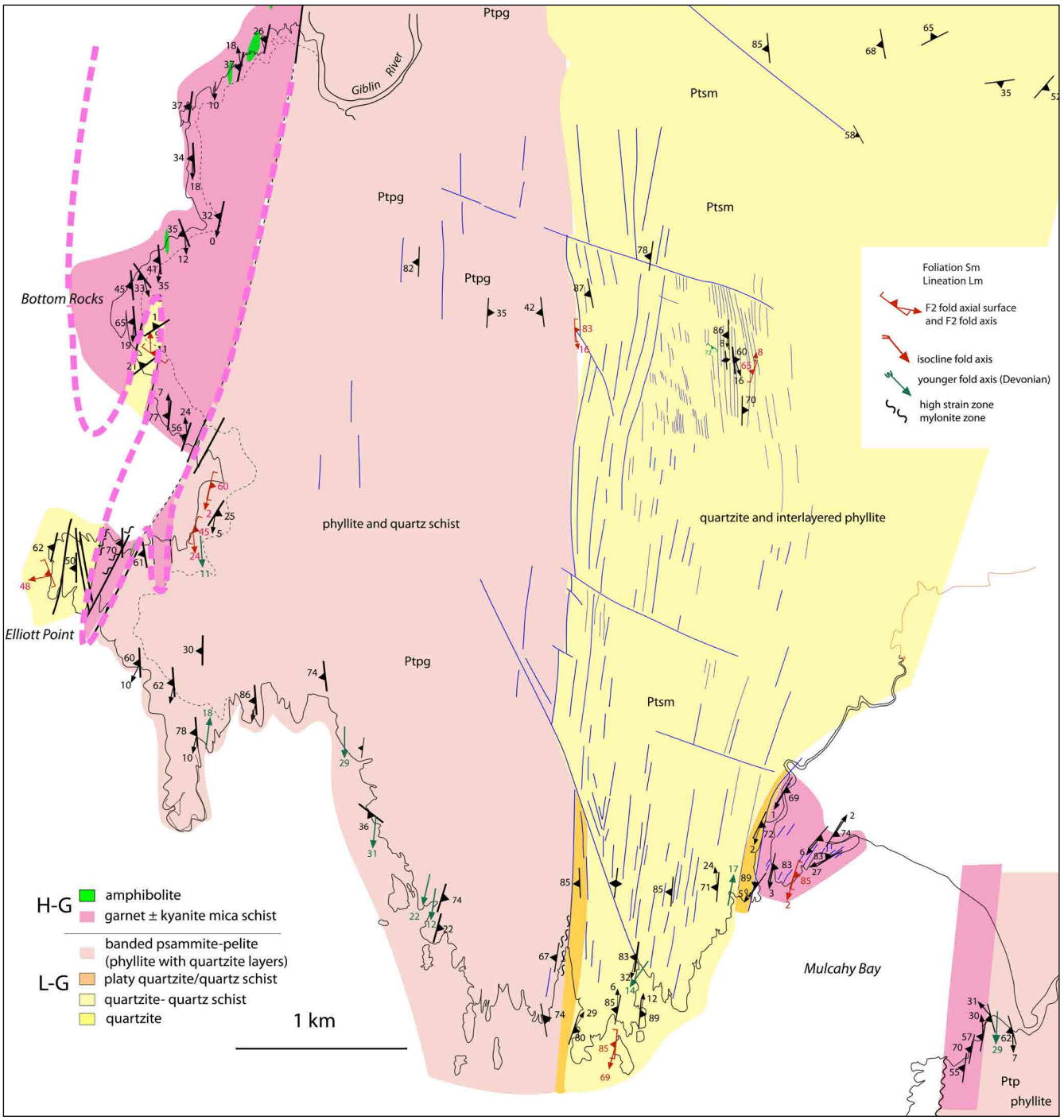


Figure 44. Mulcahy Bay-Elliott Point structure map based on mapping by Ron Berry and Sebastien Meffre in 1997 and Mike Hall and John Miller in 2004. Mapping and structural data also from the 1:25000 digital map series map sheets of Elliott (Hall & Vicary 2010a) and Mulcahy (Hall & Vicary, 2010b).

The high-grade schists south from Giblin River are in-folded with quartzite at Bottom Rocks through to Elliott Point and show a pronounced tapering or wedging out of the high-grade schists south of Bottom Rocks and at Elliott Point (Figures 44 and 45). At Elliott Point garnet schist in the pinch-out wedge is shear zone bounded (Figure 45), but there is a pronounced albitisation with almost massive quartz-feldspar present. The eastern contact of the high-grade schist with pelite in the bay south of Bottom Rocks is a 5m wide mylonite zone (Meffre et al., 2001) that shows a strong S-C' fabric (Figure 46).

Contacts defining the high-grade termination south of Elliott Point are marked by 20 m wide zones of phyllite, with strong to intense L-S tectonite fabrics (Meffre et al., 2001). Both contacts have been reactivated as brittle faults marked by cataclasite and dip-slip quartz-fibre lineations (Meffre et al., 2001). The phyllites have an intense cleavage but are not mylonitic. Within the feldspathic rocks of Elliott Point (RB97/611) the contact between garnet schist and the more massive garnet absent rocks on the Point is a 20 m zone of strong L-S schists with a shallow plunging lineation (Meffre et al., 2001).

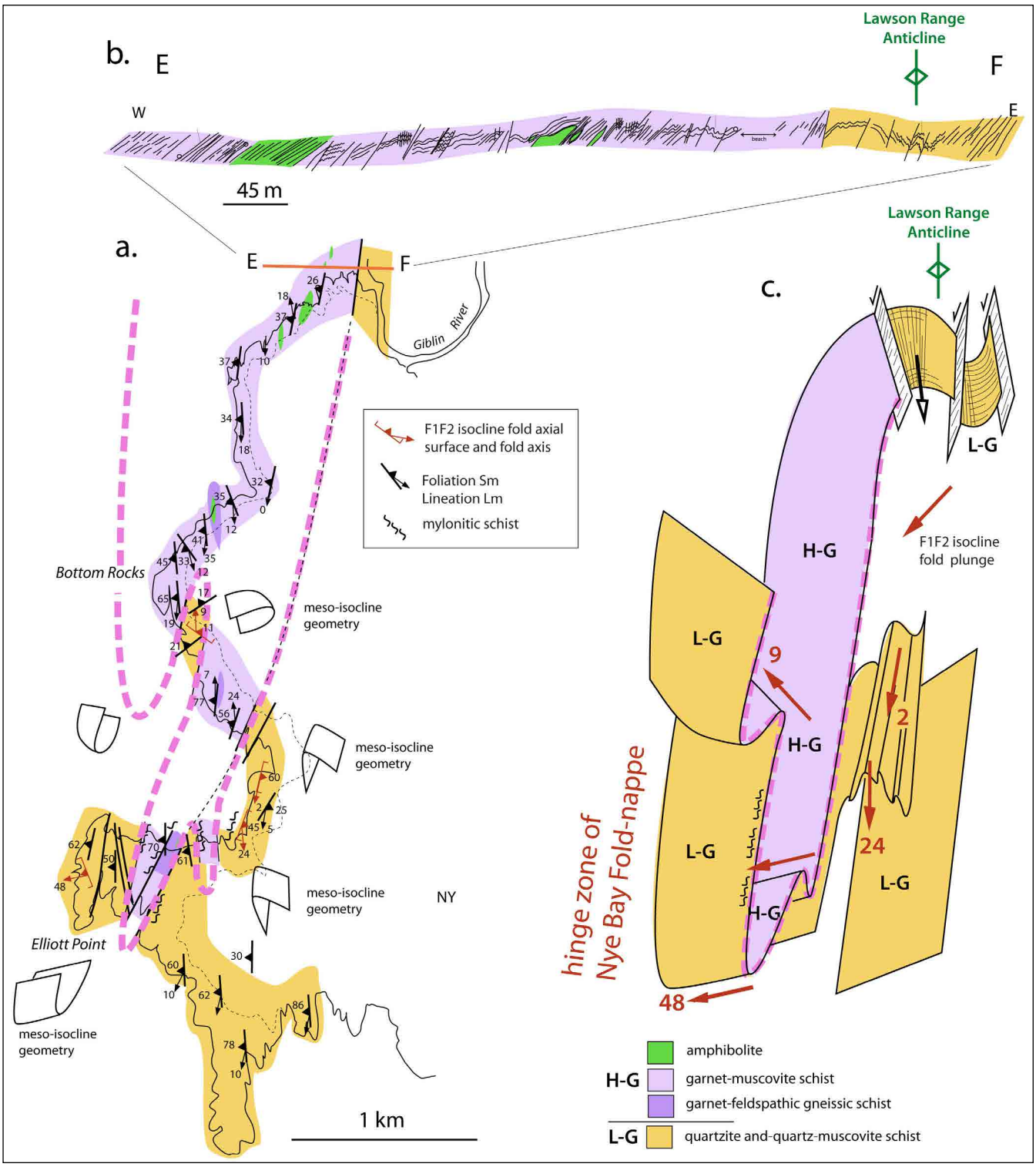


Figure 45. Structural-geological coastal strip map from the Giblin River mouth at the south end of Nye Bay to south of Elliott Point showing the distribution of high-grade garnet schists and low-grade phyllite sequences. Map base and structural data is combined from mapping by 1) Ron Berry, Sebastian Meffre and Mike Hall in 1997, and 2) Mike Hall and John Miller in 2004. a) Map base with outcrop contact interpretation shown b y pink dashed line. b) Schematic sketch profile across the high-grade low-grade contact west of the Giblin River mouth (from Miller, 2004). c) Reclined macro-fold hinge interpretation of the high-grade schist pinch-out at Elliott Point with macro-geometry based on mesoscopic isocline attitudes.

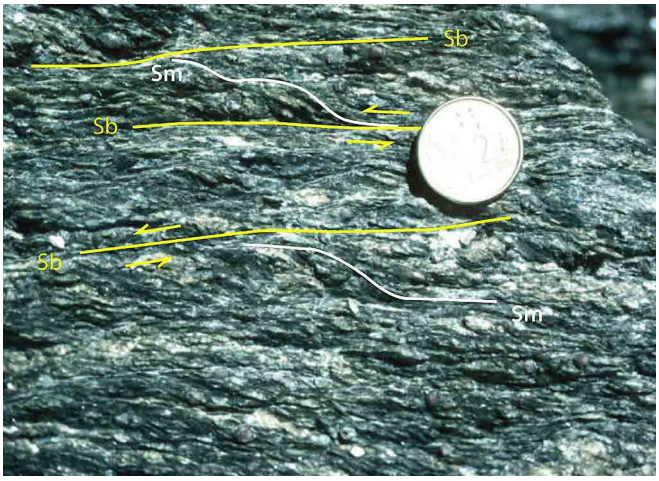


Figure 46: Intense shear band (S-C') schistosity (horizontal) where the C' (cisaillement) or shear planes are the dominant foliation. Relicts of the original schistosity trend top left to bottom right with extensional crenulation form showing sinistral shear sense. Garnet-albite schist from Bottom Rocks. (Photo credit: Ron Berry).

To the east of Elliott Point towards Mulcahy Bay the contact between pelite (Ptp) and quartzite (Ptsm) is a steeply dipping high strain zone (HSZ) in platy quartzite/quartz schist. The HSZ widens northwards from ~100m at the coast to ~300m inland (Figure 45). The contact is offset by late WNW-trending brittle faults (right lateral sense) and is also folded across the Lawson Range Anticline (Figure 38).

The nose of the south-closing fold nappe, that correlates with the Franklin fold-nappe to the north, is inferred in the outcrops at Elliott Point where the high-grade garnet schist taper or close out (Figure 45).

*3.1.3 Structure of the high-grade sequence at Mulcahy Bay*

High-grade schist outcrops occur at the north and south ends of Mulcahy Beach (Figure 44). The schist/mylonite at the northern end has a general northeast-strike with both southeast and northwest dips (Figure 47), whereas at the southern exposure just south of the Alec River mouth the schist/mylonites have a north-south strike with a west-dip (Figures 49 and 50). This outcrop sits beneath the Late Cambrian-Ordovician Owen conglomerate (Figure 50).

At the northern end of the beach, a shear zone-bounded wedge of high-grade garnet schist crops out east of the Mulcahy River mouth. The western contact with the low-grade quartzite sits along the Mulcahy River but does not crop out. The linear stretch of the river sub-parallel to Sm in both the low-grade quartzite and the high-grade schist there suggest a high-strain platy quartzite -mylonitic zone that has been eroded.

In the easternmost part of the exposure of the high-grade rocks (RB97/514) a northeast-trending mylonite zone shows sinistral sense of shear (Figure 48). Narrow dextral mylonites are exposed at RB97/515 represent the conjugate direction (strike 035°) but with angle at 20° to the main sinistral zones.

The contact between chloritised meta-sedimentary rocks and amphibolite facies schists south of Mulcahy Bay (grid location 396521E 5224834N) is occupied by a 10m wide zone of muscovite-albite-quartz mylonite (Figure 50). The mylonite has a strong L-S fabric and contains dismembered vein quartz fish that have asymmetric boudin shapes and a strong shallowly south plunging grooves along the edges (Figure 51). The schistose rocks have very common shear band geometry visible in outcrop. Oriented thin sections support a sinistral sense of shear with shear band geometry, sigma-shapes on albite porphyroblasts and subgrain textures in quartz grains (Meffre et al., 2001).

Restoration of the Ordovician unconformity surface to Ordovician orientation shows the contact zone mylonites (from 561 using 554 for unconformity surface) dip 40°/214° with a mineral lineation plunging 36°/180° and give a top-to-the-south (normal) sense of movement (Meffre et al., 2001).

*3.1.4 Top Rocks-Nye Bay-Mulcahy Bay Structural Interpretation*

The following observations based on the structural mapping and structural data presented in Sections 3.1.1 and Section 3.1.2 have been used to construct a three dimensional interpretation of the Top-Rocks-Nye Bay-Mulcahy Bay domain (Figure 52). These are:

1. S2-F2 changes from Top Rocks to Nye Bay.
2. The tapering or wedge-out of the high-grade schists across Nye Bay through to Elliott Point.
3. The apparent repetition of litho-tectonic "stratigraphy" and the upside down sequence from Top Rocks through to Middle Rocks.

The 3D model depicts the inferred, south-closing, west-plunging Nye Bay Fold-nappe with overall reclined geometry (Figure 52). The macro-fold is re-folded by the younger, Devonian, north-south trending, south-plunging open Lawson Range Anticline and the Giblin Syncline.

*3.1.5 Implications of MRT Geophysical data for the Nye Bay-Mulcahy Bay Structure Interpretation*

The Mineral Resources Tasmania statewide stitch of the old, wide spaced aeromagnetic data provides another constraint on the macro-structure of both the high-grade and low-grade sequences of the Southwest high-grade coastal belt. The Total Magnetic Intensity (TMI) images and the RTP1st-Vertical Derivative of the data (Figure 53) were used to better define and refine the macro-structure of the Top Rocks-Nye Bay-Mulcahy Bay area shown in Figure 38.

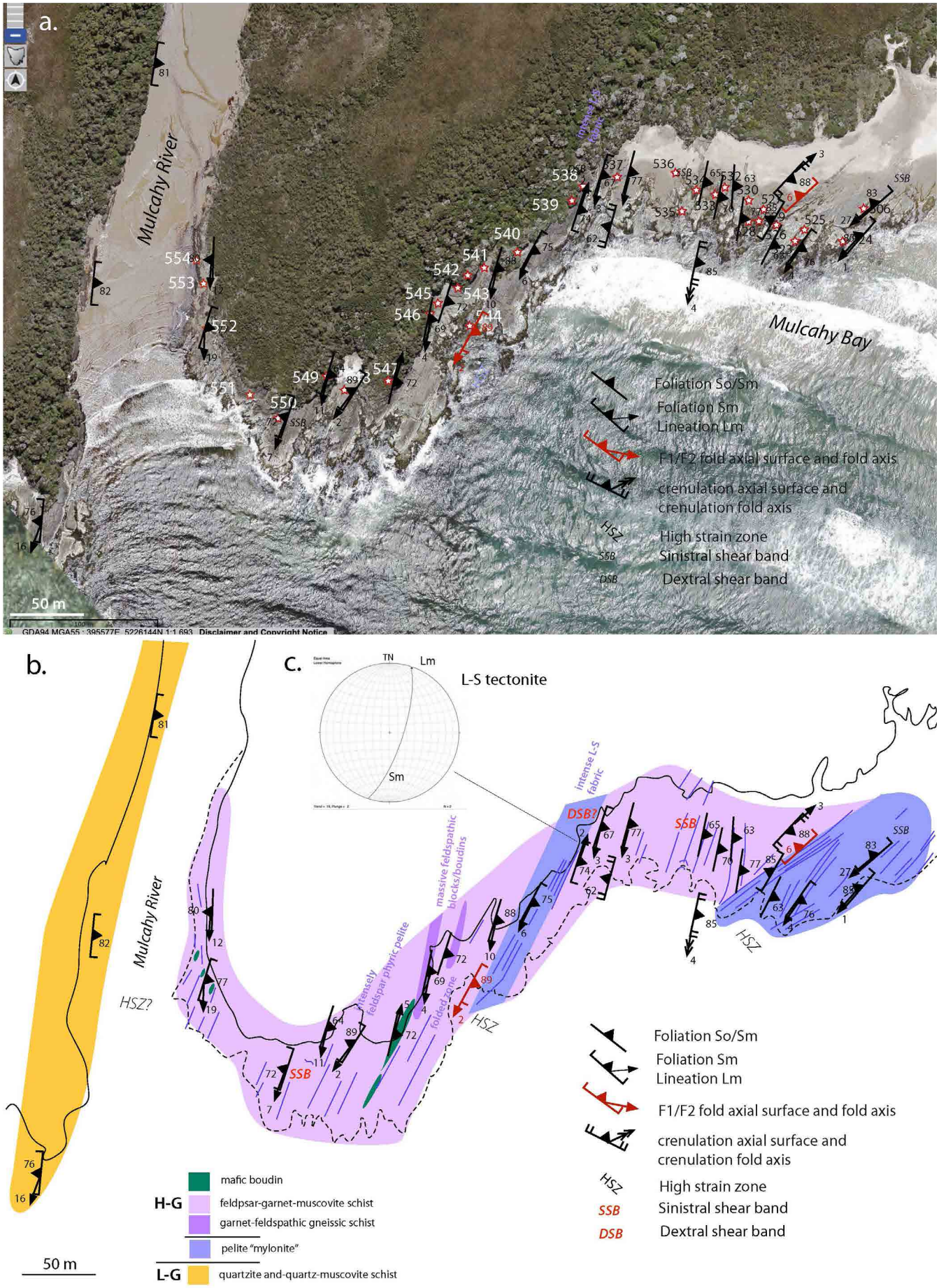


Figure 47. Structural relationships within high-grade garnet schists at the Mulcahy River mouth, north end of Mulcahy Bay. a) ListMap aerial photo as map base with structural data from Berry (1997) with RB 97 field stations in white. Data in the quartzite on the west side of the Giblin River are from (Hall, 2005). b) Structure map on lithology map base with lithology from Hall (2005) and Berry (1997). The stereonet inset shows Sm and Lm relationships in L-S tectonite.

Figure 48 (left). Fragmented and dismembered quartz veins in mylonite north end of Mulcahy Bay showing sinistral shear bands (photo credit Ron Berry)

Figure 49 (below). Outcrop map south end of Mulcahy Bay, just south of the Alec River mouth. a) Air photo RB97 locations (courtesy Ron Berry). b) Google image of the mapped section shown in (c). c) Outcrop map from Meffre et al. (2001) showing the mylonite contact between the low-grade quartzite and phyllite at the Alec River mouth with the high-grade sequence of meta-quartzite, albite schist and garnet-bearing schist to the west.

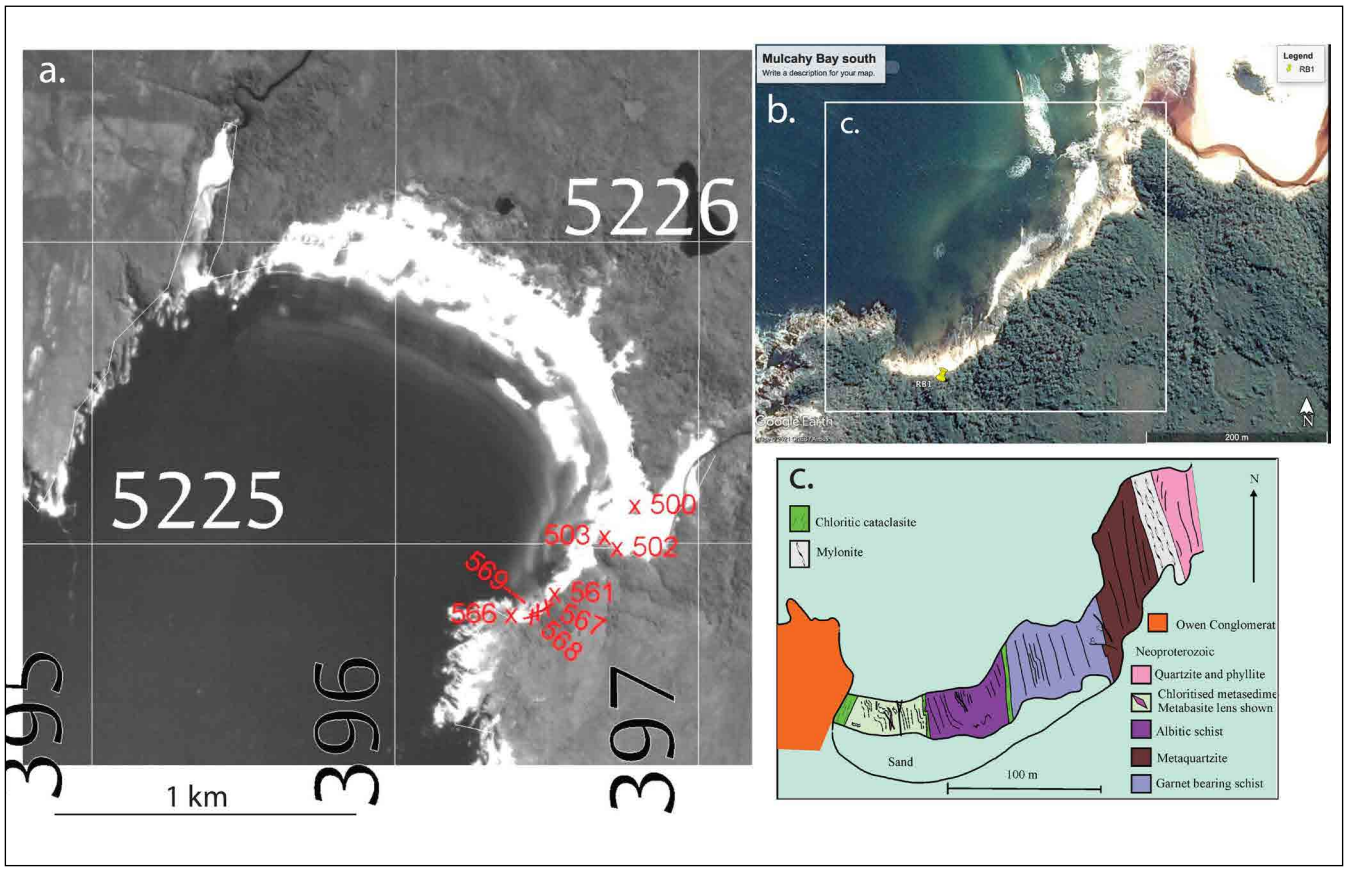


Figure 50 (right). Detailed geology at the south side of Mulcahy bay showing the mylonite contact between the low-grade and high-grade rocks and normal fault against siliceous conglomerate (Owen Conglomerate or Pioneer Sandstone). 1997 Mapping by Ron Berry and Sebastian Meffre (Meffre et al., 2001, fig.2).

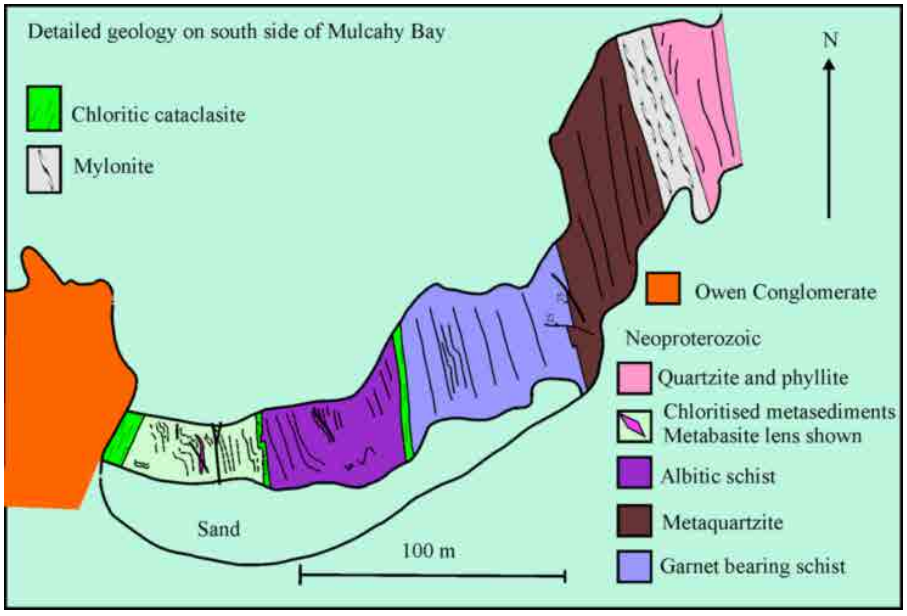

Figure 51 (right). Close-up view of fragmented and dismembered quartz veins in mylonite at the south end of Mulcahy Bay. (photo credit Ron Berry)

Figure 52 (below). 3D oblique model of the inferred Nye Bay fold-nappe geometry. The diagram shows the distribution of the litho-tectonic layering, the changes in minor fold geometry and attitude across the macro-fold, from the structurally higher, over-turned western limb at Top Rocks-Ummarah Creek through to the fold-nappe hinge at Nye Bay. The minor fold geometries as well as their respective fold plunges are shown in aquamarine. Positions of geographic locations in the 3D model are shown in blue text.

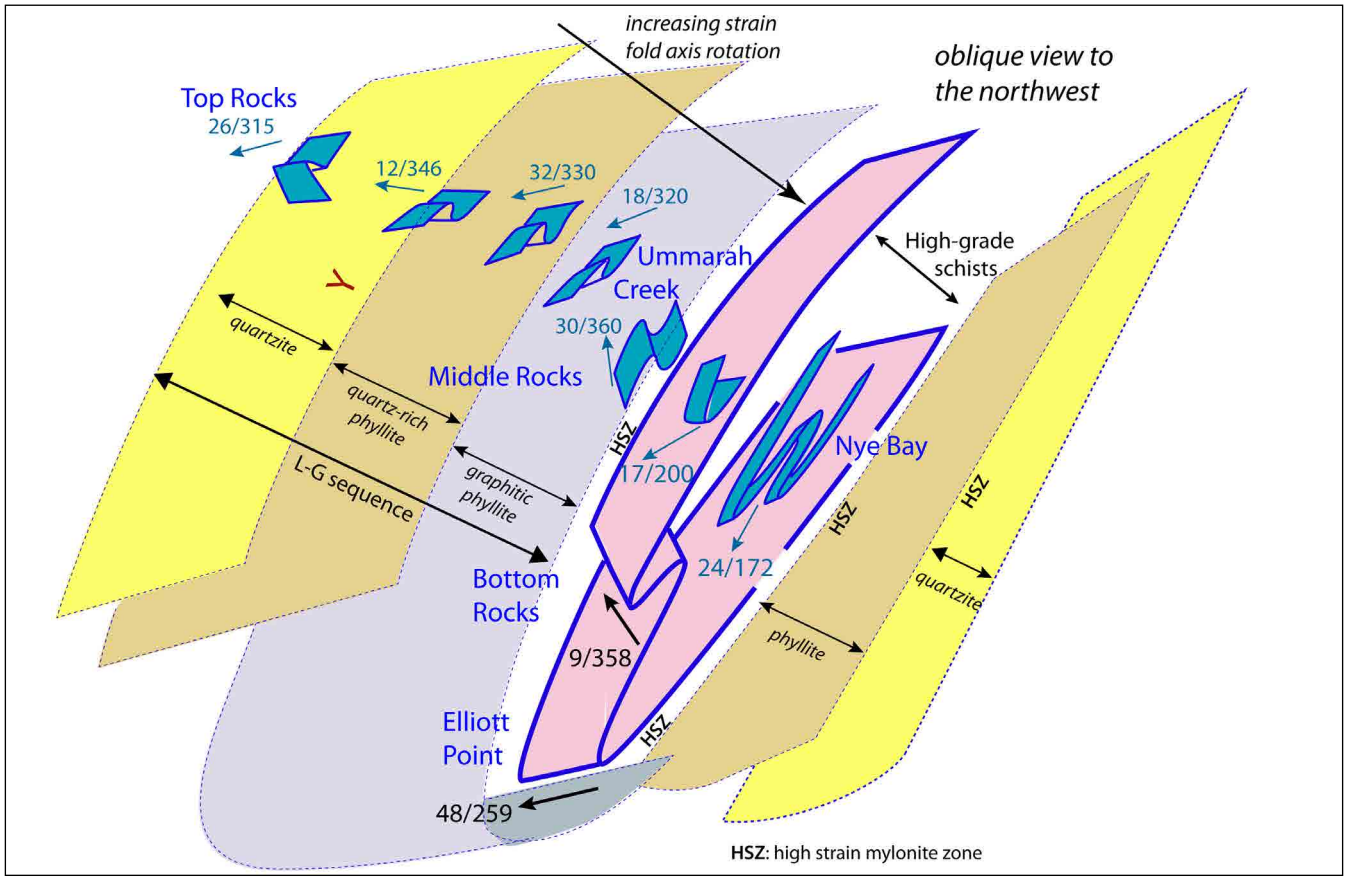


Features include:

1. The under-cover elongated nose of the south-plunging fold-nappe through the Lawson Range.
2. The higher magnetic intensity of the nose region suggesting graphitic phyllite above the quartzite exposed in the Lawson Range. This supports a stacking of high-grade schist, above a more magnetic graphitic phyllite, above a low magnetic quartzite on the proposed fold-nappe lower limb, matching the quartzite overlying quratz-phyllite and graphitic phyllite overlying high-grade schist on the inverted upper limb.
3. A possible ~15km long macro-fold pod within the quartz-phyllite and graphitic phyllite unit on the inverted western limb of the fold-nappe.
4. A possible second-order north-closing hinge along the eastern edge of the Lawson Range

These defined features are highlighted in Figure 55 and should be compared with the raw or non-interpreted image in Figure 54. The geophysical formline interpretation superimposed onto the geological map (Figure 56) suggests the presence of second-order isoclinal fold pairs as part of the major south-closing Nye Bay fold-nappe.

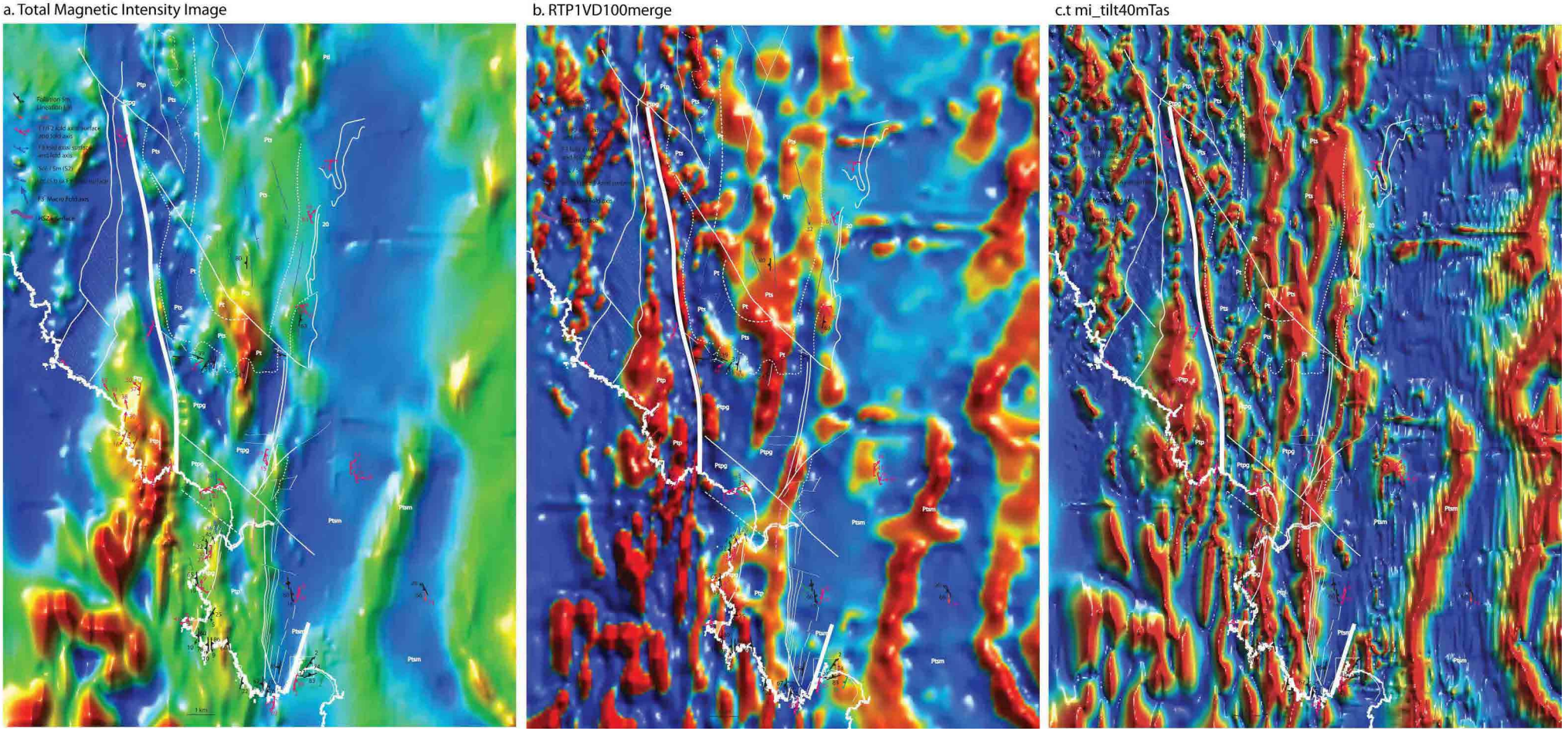


Figure 53. West Coast High-Grade belt aeromagnetic data. a) Total Magnetic Intensity image 40m spacing. b) Reduced to Pole First Vertical Derivative aeromagnetic image. c) Total Magnetic Intensity Tilt Image.

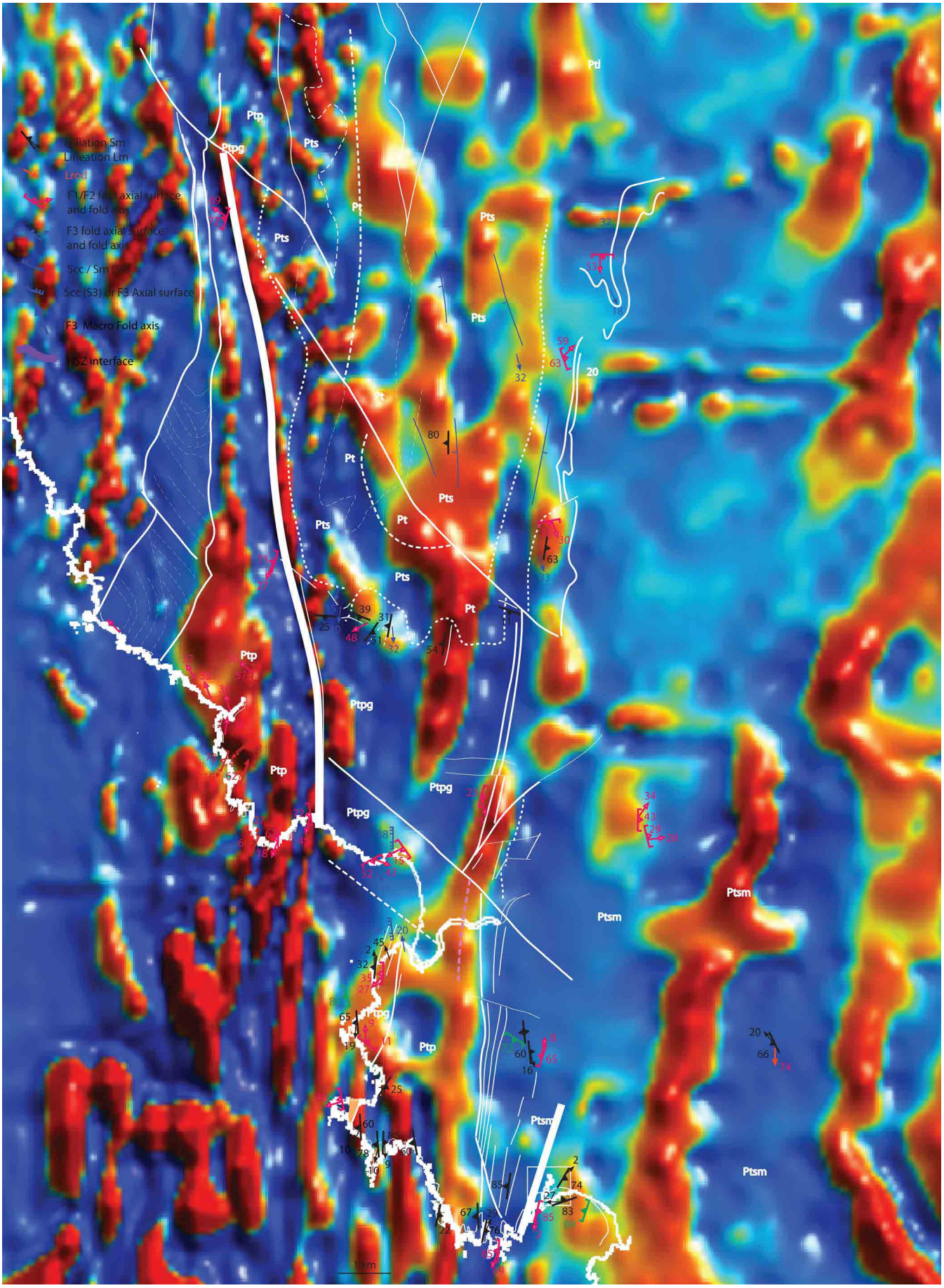


Figure 54. RTP 1st Vertical Derivative of the aeromagnetic dataset with geological contacts, structural data and formlines adapted from Figure 38.

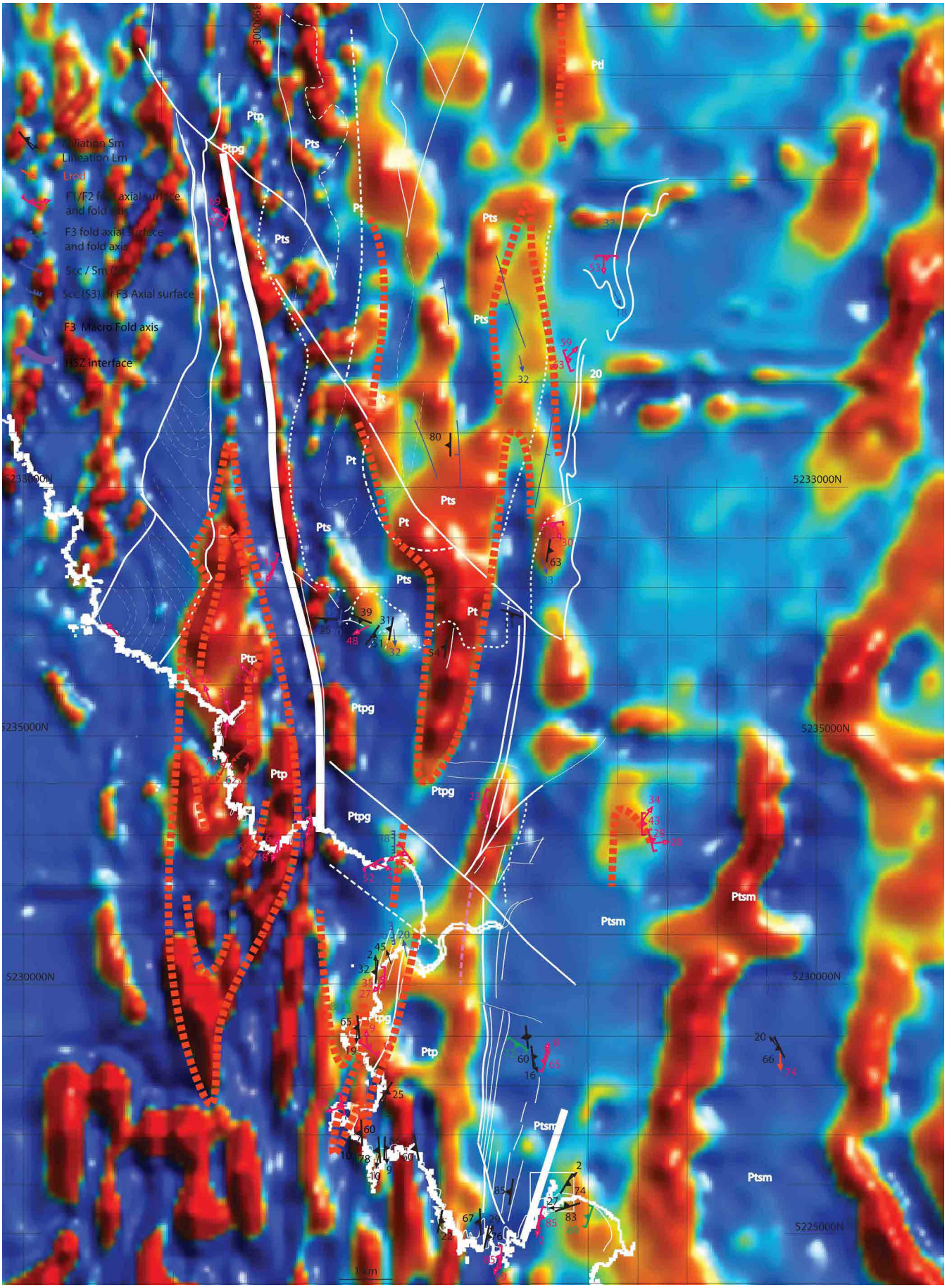


Figure 55. Structural interpretation of the RTP1stVertical Derivative of the aeromagnetic dataset. Mapped and interpreted formlines are shown as white line traces. Structural field measurements are also shown.

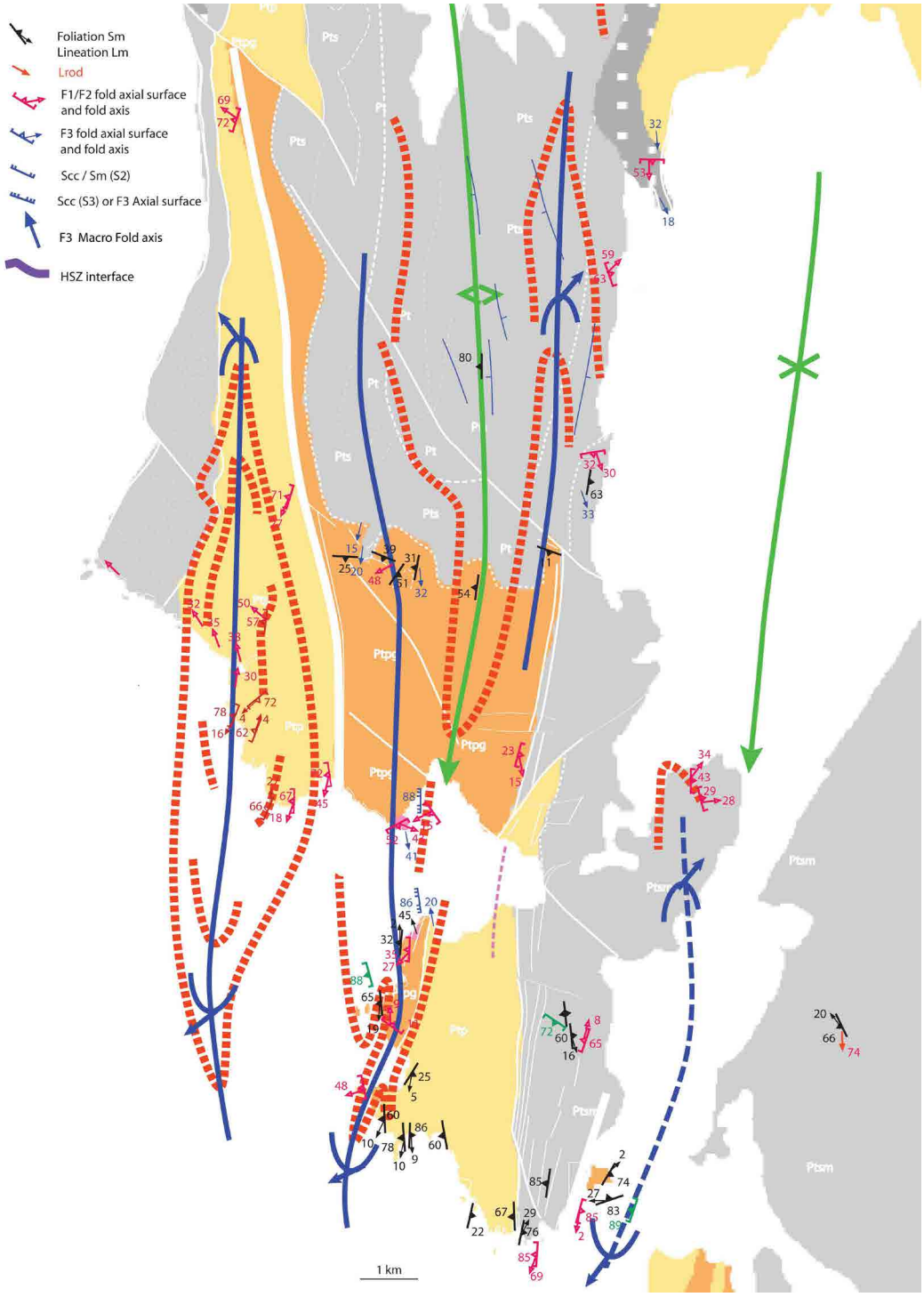


Figure 56. Revised structural interpretation incorporating the interpretation of the aeromagnetic dataset with second-order isoclinal fold pairs along the limbs of the regional scale Nye Bay fold-nappe. Axial surface traces of large-scale folds are shown with the early F1/F2 macro-fold axial traces in blue and the younger Devonian fold axial surface traces in green.

### 3.2 Mulcahy Bay to Wreck Bay

This region extends from the south end of Mulcahy Bay at the Alec River Mouth through Brier Holme Head to Svenor Point and to the north end of Wreck Bay (Figure 57). Two zones of quartzite occur intercalated with garnet-schist in an essentially west dipping sequence. These zones comprise quartzite as three bands just east of Brier Holme Head, and a zone approximately midway along the coast between Brier Holme Head and Svenor Point.

Repetition of quartzite in smaller zones east of Brier Holme Head (Figure 57) suggests a more complex high-grade to low-grade contact zone there with series of faulted out second- or third-order isoclinal folds. Amphibolite pods also occur at this structural level (Figure 57). In the coastal strip between Brier Holme Head and Svenor Point a "zone' of low-grade quartzite is intercalated within the overall west-dipping high-grade schist. With limited structural data/observations the structural interpretation is based on ListMap air photo interpretation (Figure 58). Both the schist and quartzite here are isoclinally folded by northwest-trending folds, many with faulted margins. The southern contact of quartzite and schist consists of a stack of isoclinal fold hinges separated by brittle faults with the quartzite on the west structurally overlying the high-grade schist on the east. The core of the quartzite zone consists of a zone of refolding by open folds with NE-trending axial surfaces. The northern contact with the schist appears as a sinistral shear zone, with the Sm foliation in the high-grade schist deflecting into the apparent high strain zone (Figure 58).

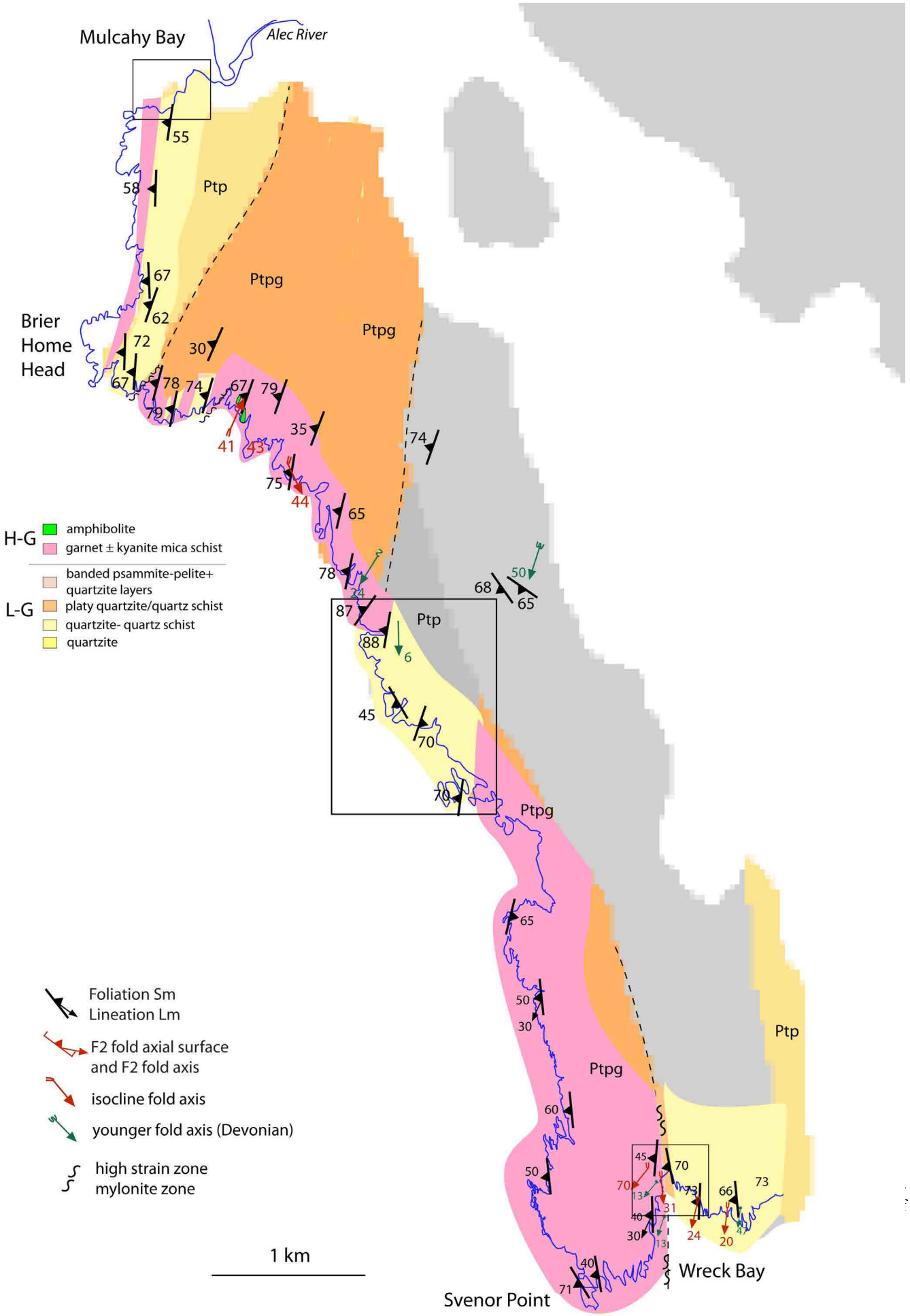


Figure 57a. Mulcahy Bay-Wreck Bay structure map based on the Mineral Resources Tasmania 1:25000 and 1:250000 digital geological atlas and coastal mapping by Hall (2005). Rectangles show the positions of detailed structural maps shown in Figures 50, 58 and 59.

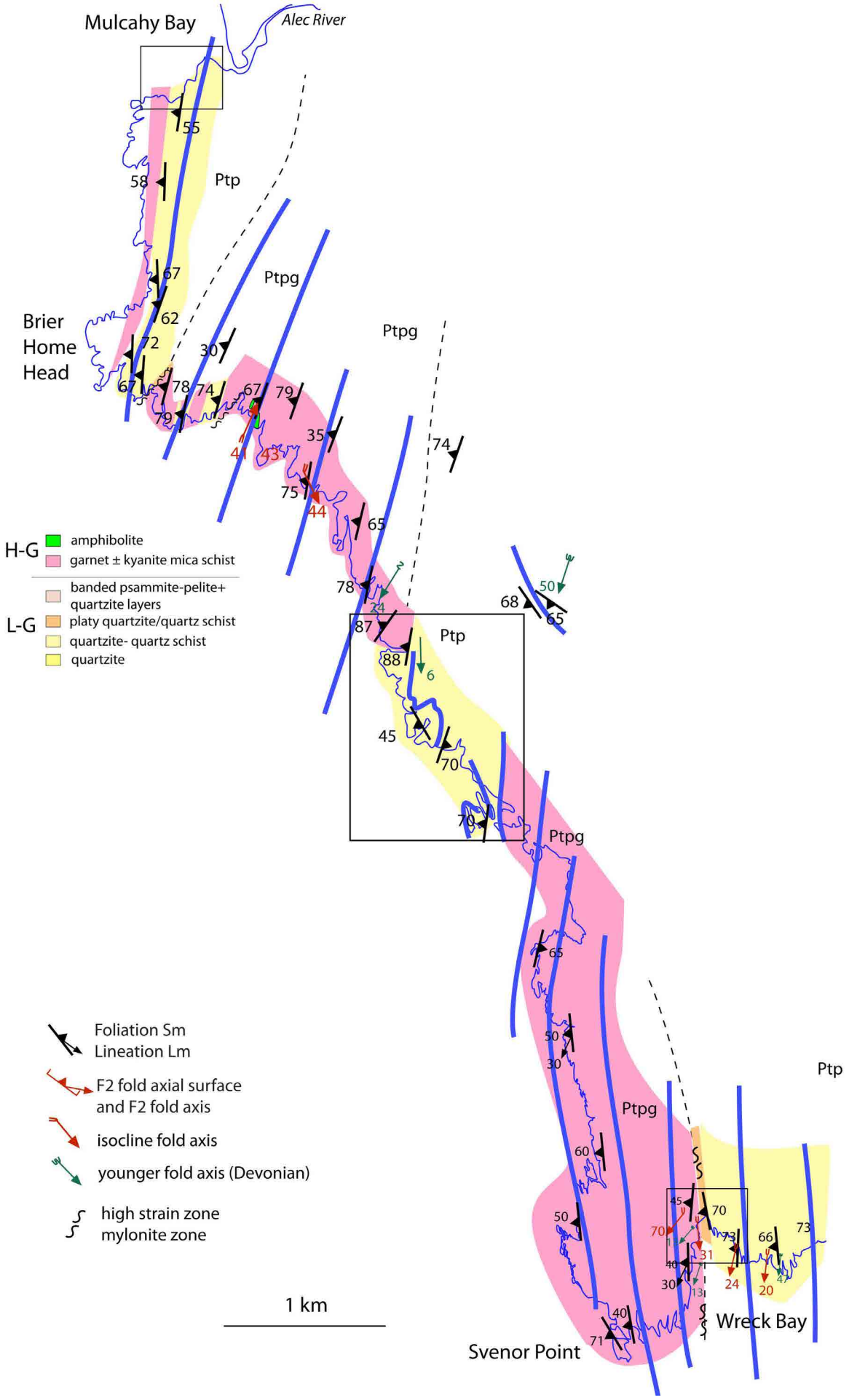


Figure 57b. Formline interpretation of the coastal segment Brier Holme Head to Wreck Bay showing an overall west-dipping, intercalated sequence of quartzite and high-grade schist. Rectangles show the positions of detailed structural maps shown in Figures 50, 58 and 59.

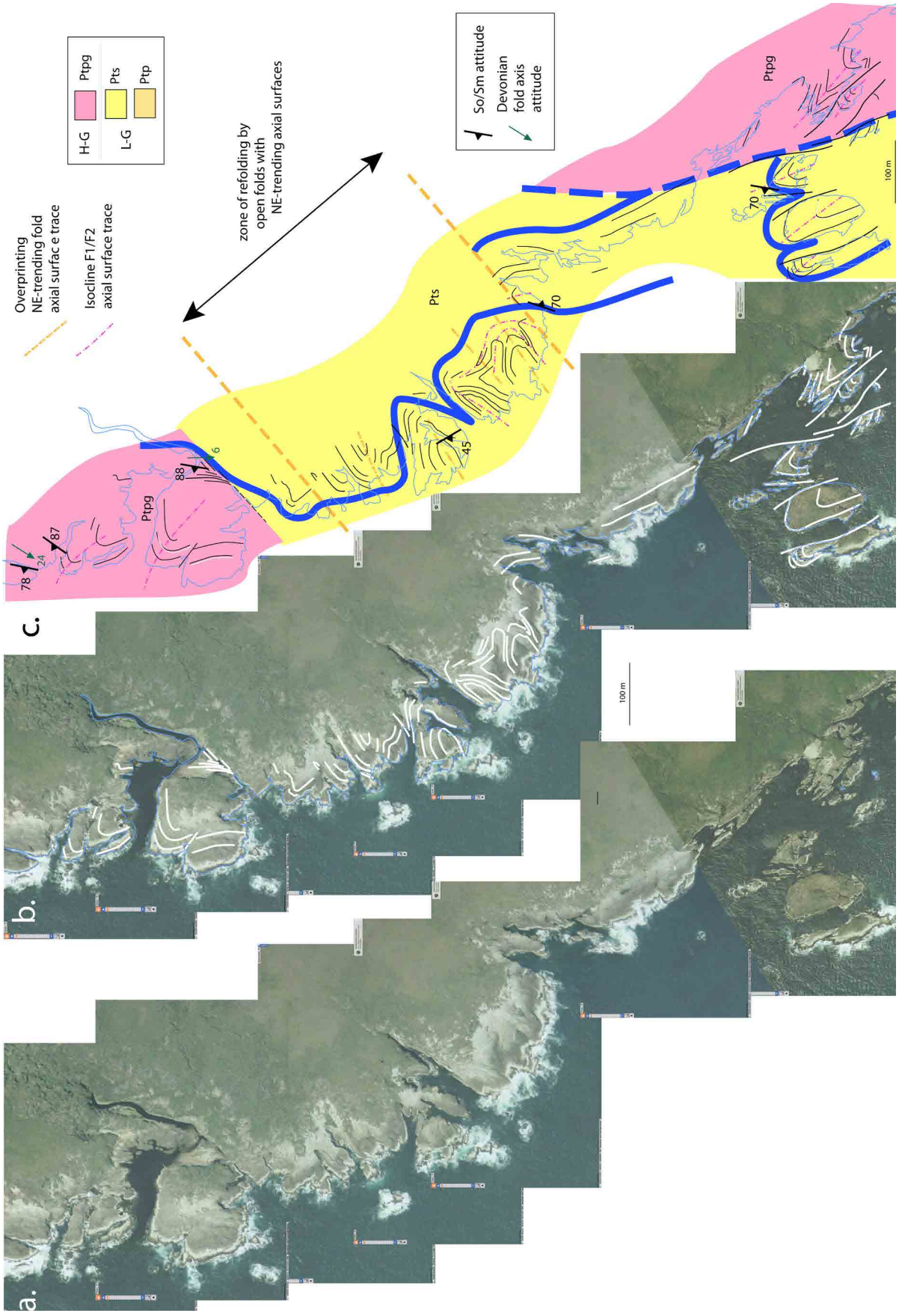


Figure 58. Quartzite outcrop belt between Brier Holme Head and Svenor Point. a) Stitched ListMap air photos of the coastal segment. b) Formline interpretation of So/Sm foliation on the stitched air photos. c) Structure - lithology map constructed by using formlines and coastal mapping data from Hall (2005).

At the southern end of the Brier Holme Head-Svenor Point coastal segment (Figure 57) the contact between the Svenor Point high-grade schists and the low-grade platy quartzite in the north end of Wreck Bay is a zone where an intense Scc in the high-grade rocks (Stations SW60 and SW61, Figure 59a) is sub-parallel to Sm in the platy mylonitic quartzite (Station SW63, Figure 59a) on the low-grade side (Figures 59b and c). So/Sm layering, visible in the high-grade schists (Figure 59a), is folded by a set of folds with an intense Scc fabric as axial surface. The highest strain occurs in the low-grade quartzite with strong to intense Sm development into the quartzite to the east (Figure 59b).

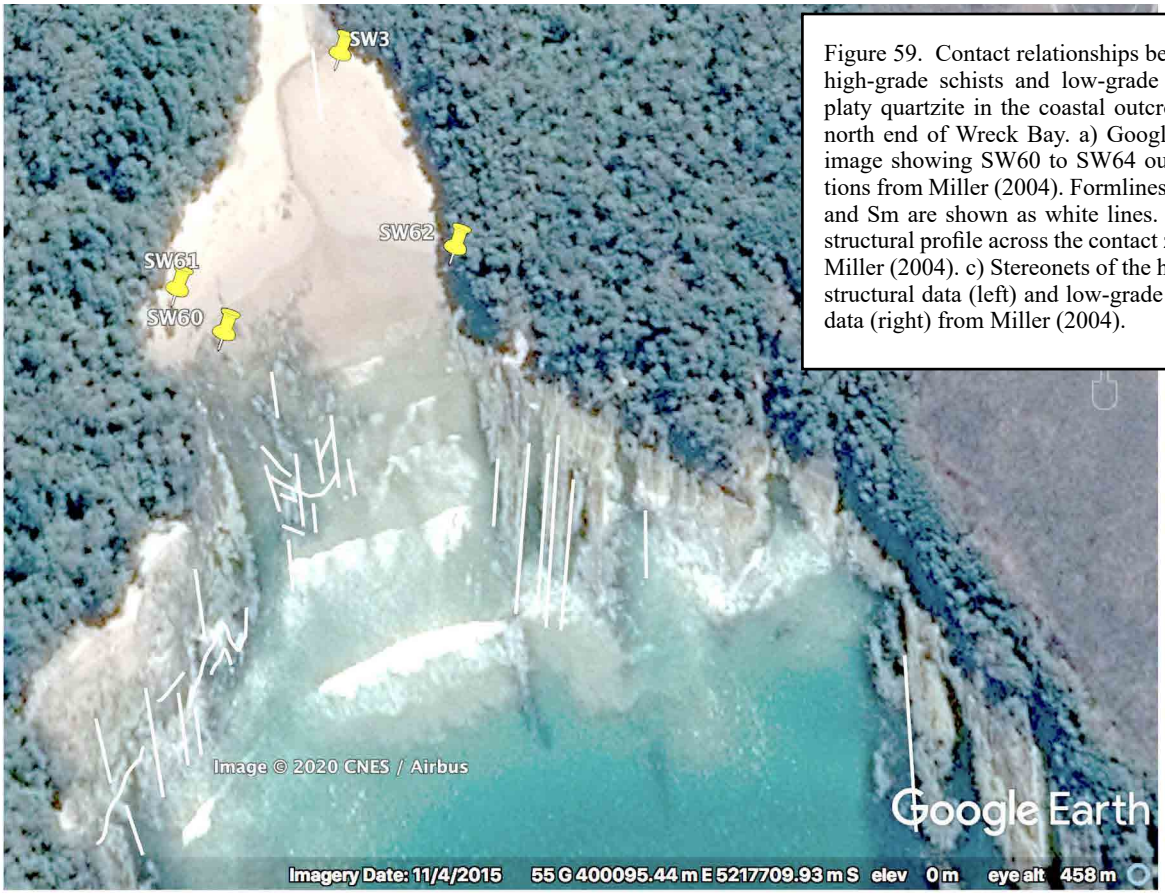


Figure 59. Contact relationships between the high-grade schists and low-grade quartzite/ platy quartzite in the coastal outcrops at the north end of Wreck Bay. a) Google satellite image showing SW60 to SW64 outcrop stations from Miller (2004). Formlines in So/Sm and Sm are shown as white lines. b) Sketch structural profile across the contact zone from Miller (2004). c) Stereonets of the high-grade structural data (left) and low-grade structural data (right) from Miller (2004).


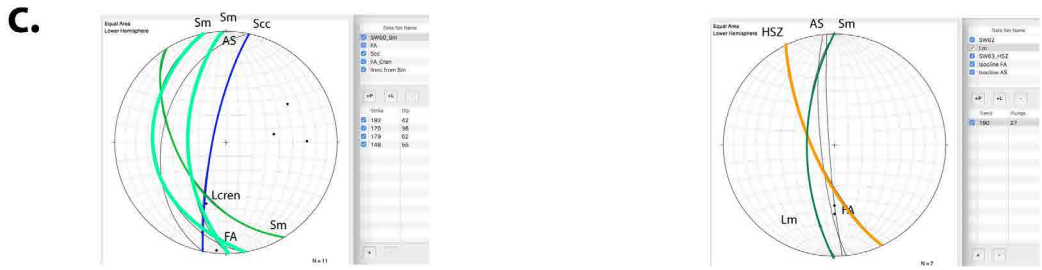


### 3.3 Wreck Bay to Sandblow Bay

This region extends from Wreck bay through Alfhild Bight to Sandblow Bay and contains several contacts between the high-grade schists and the low-grade phyllites and quartzites (Figures 60a and b). Detailed maps are provided for Alfhild Bight and Sandblow Bay (Figures 61 and 62).

The low-grade sequence at Wreck Bay consists of quartzite and banded psammite-pelite with a north-south strike in the north of Wreck Bay to an east-west strike southeast of Wreck Bay. Formline interpretation suggests the high-grade/low-grade contact is folded about a younger, southwest plunging Devonian anticline with an apparent second-order, northeast-trending isoclinal fold within the sequence east of the south end of the beach. Southwards to Sandblow Bay, formline interpretation suggests the sequence is folded into a series of open, northeast-trending, southwest plunging younger Devonian folds. These folds have been designated as the Wreck Bay Anticline, the Towterer Beach Syncline, the Sandblow Bight Anticline and the Southeast Bight Syncline (see Section 4.4).

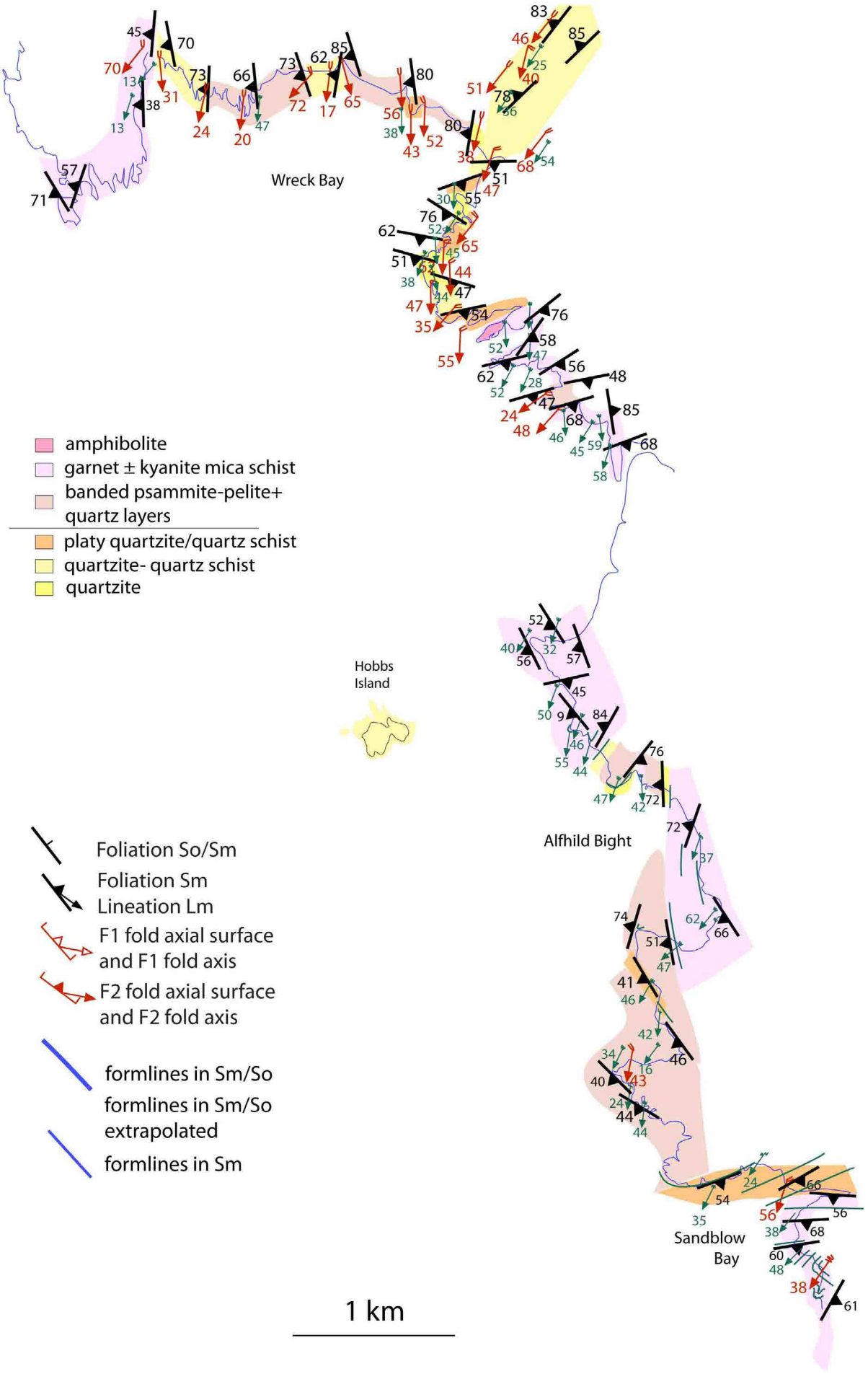


Figure 60a. Structural map of the coastal segment from Wreck Bay to Sandblow Bay based on coastal mapping by Hall (2008).

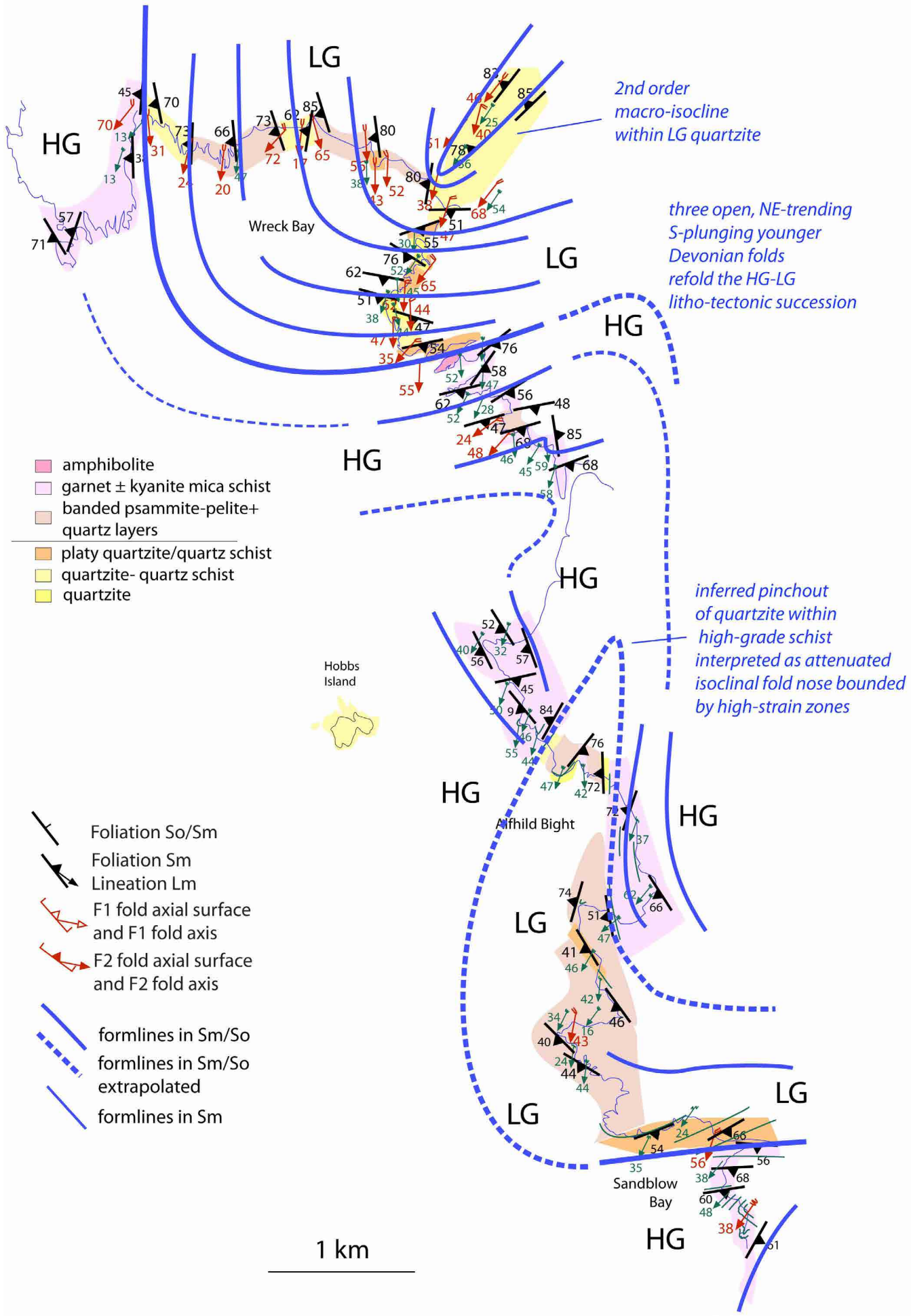


Figure 60b. Formline interpretation of So/Sm and Sm data in Figure 60a. HG: high-grade schist. LG: low-grade quartzite-pelite sequence.

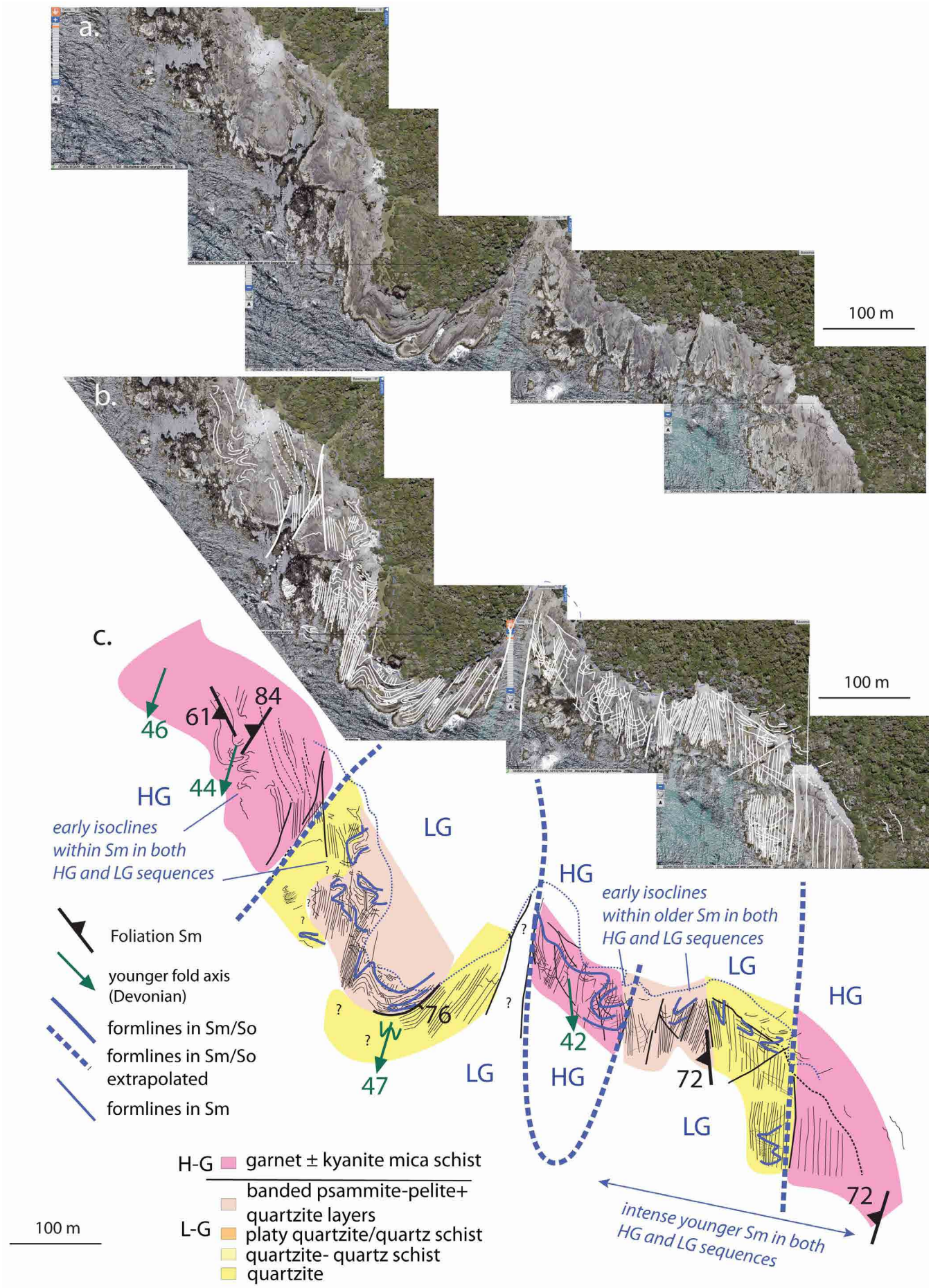


Figure 61. High-grade low-grade contact relationships in coastal outcrop in Alfhild Bight. a) TasMap airphoto stitch of the Alfhild Bight coastal outcrops. b) Formline interpretation (white lines) of Sm and So/Sm on the air photo stitch. c) Lithology-structure map of the Alfhild Bight coastal exposure based on coastal mapping by Hall (2008) and with the formlines from (b) superimposed.

The contact at Alfhild Bay is a complex zone of intensely foliated, intercalated high-grade schist, quartzite and banded psammite-pelite overprinted by late brittle faults. Within the low-grade banded psammite-pelite and quartzite sequence earlier folds within So/Sm are enveloped by zones of stronger Sm sub-parallel to the major interface zone (Figure 61). The larger scale geometry is difficult to establish from the limited structural data, the interpreted formlines and the map pattern of the litho-tectonic units.

Further south at Sandblow Bay the quartz-schist dominant zone at the contact with the high-grade schist also shows fold interference between early isoclinal folds within Sm and northeast-trending, south-southwest plunging younger folds (Figure 62). The dominant schistosity within the high-grade schist appears discordant to the structural interface shown by the blue dashed line. Air photo interpretation of the low-grade banded psammite-pelite and quartzite sequence (Figure 62a) suggests the presence of earlier folds within So/Sm enveloped by zones of stronger Sm that is sub-parallel to the major interface zone (Figure 62).

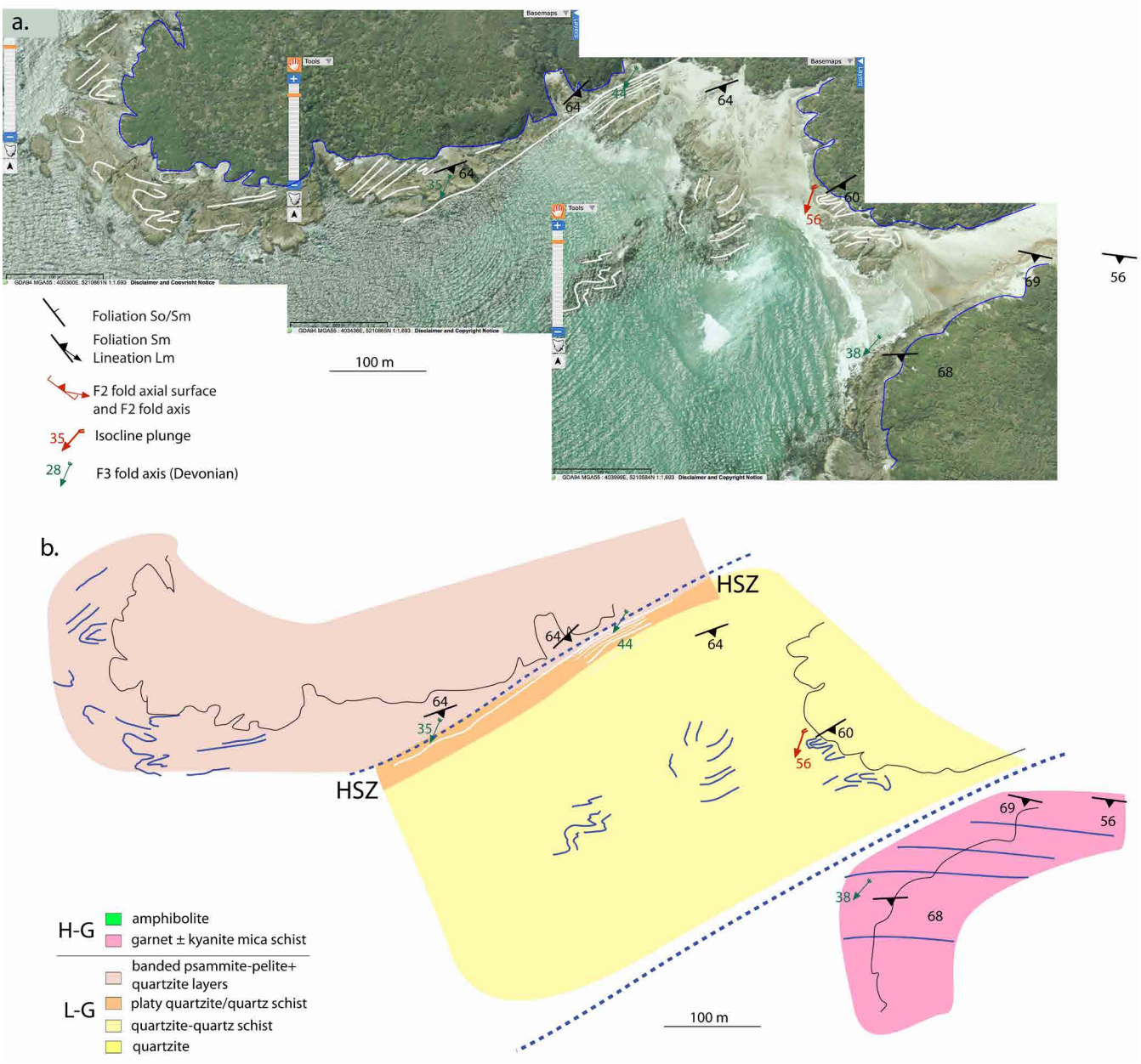


Figure 62. Structural relationships at the contact between low-grade quartzite and high-grade schist at Sandblow Bay. a) ListMap air photo stitch of the eroded contact zone between the high-grade schist and quartzite and quartz schist. b) Lithological map base with structural data and interpreted formlines based on Hall (2008) field mapping.

### 3.4 Sandblow Bay to Davey Head

The coastal segment from Sandlow Bay to Port Davey (Figure 63) is based on the mapping of Williams (1978) that identified large-scale, northwest-trending, reclined isoclinal folds at Whalers Point and Point Lucy (Figure 64). These early-formed isoclines are refolded by the open, northeast-trending and southwest-plunging Southeast Bight Syncline to give a mushroom-fold interference pattern (Figure 63).

The Port Davey map pattern (Figure 65) reflects interference between early northwest trending, approximately recumbent macro-isoclines (Figure 64) and northeast-trending, southwest plunging open folds west of South East Bight and more north-south trending, south-plunging folds east of South East Bight. The planar wings on the east side of the apparent mushroom-outcrop pattern (Figures 65 and 66) are due to the greater distance to the axial surface trace of the adjoining Port Davey Anticline. There is also an en echelon stepping eastwards of the younger axial surface trace (green dashed lines, Figure 66) across the earlier macro-isocline axial surface traces (pink dashed lines, Figure 66).

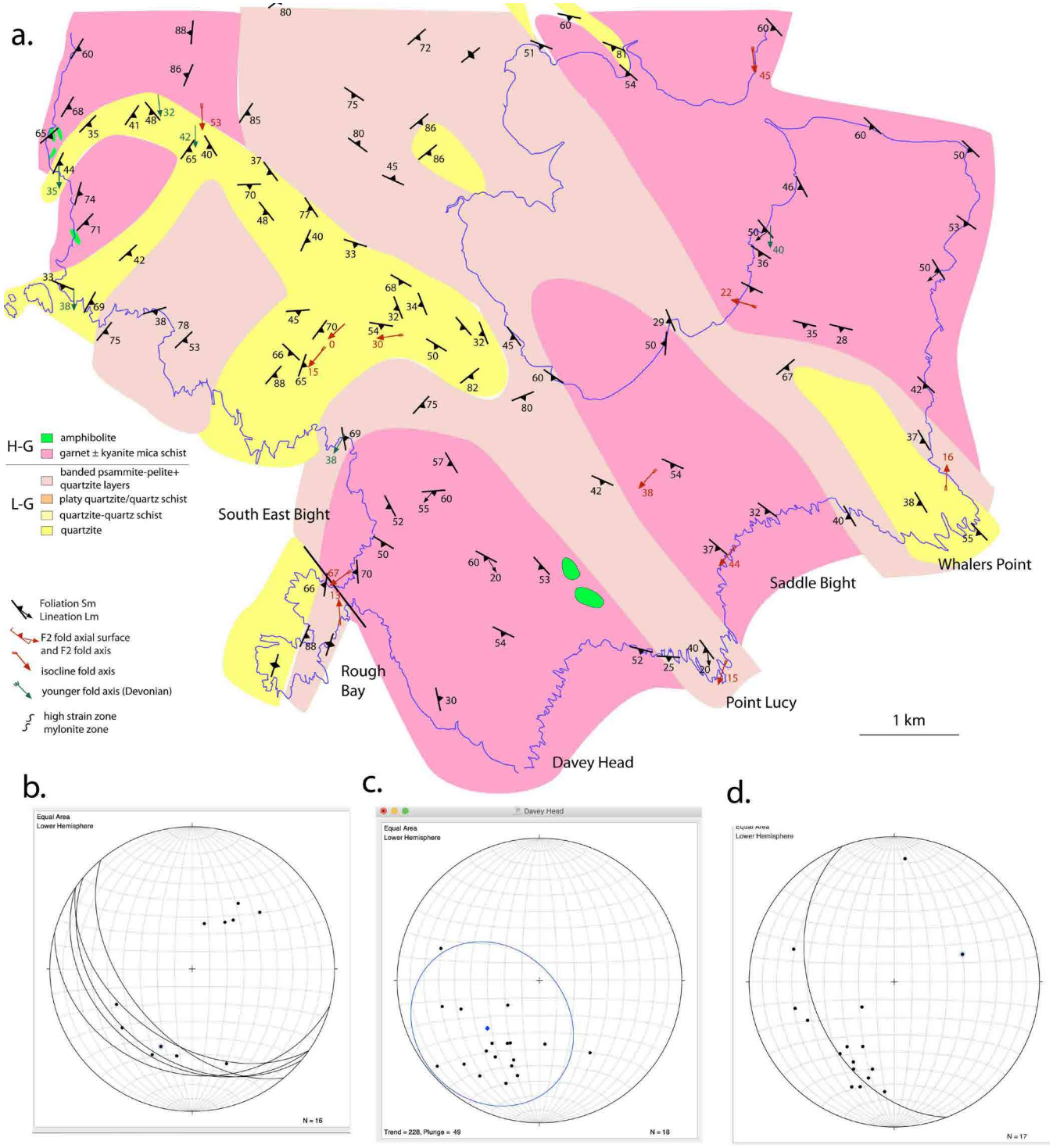


Figure 63. Davey Head structural geology. a) Structure map of the Davey Head area based on Williams (1978). b) Stereonet of Davey Head macrofolds with axial surface great circles, poles to axial surfaces and fold axes. c) Davey Head F1/F2 mesoscopic fold axes with weighted mean of 49/228. d) Saddle Bight F2 fold axes. All data was taken from Williams (1978) map.

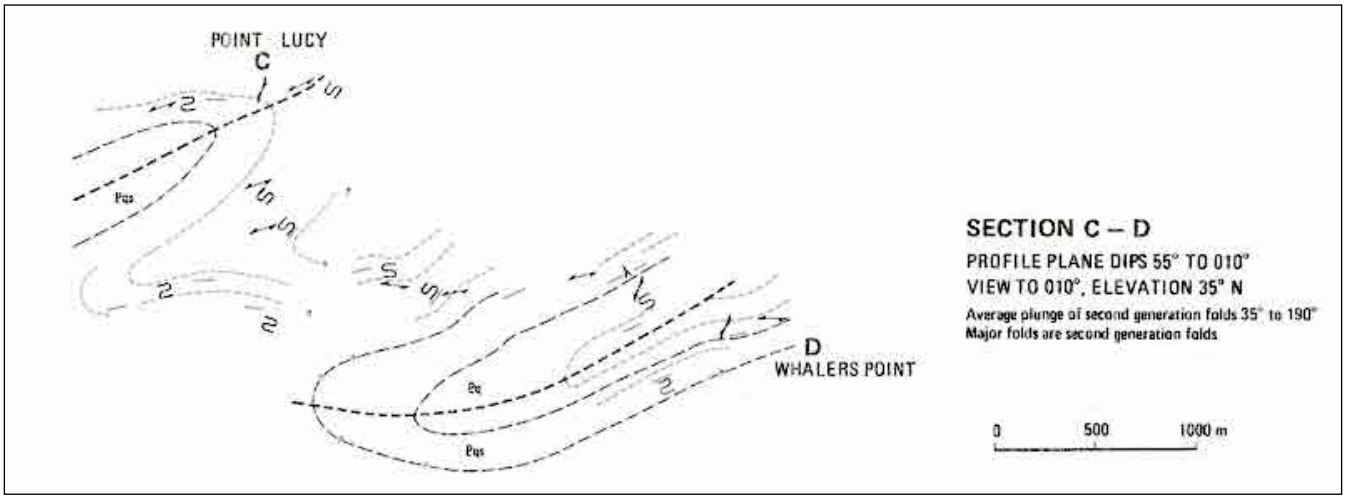


Figure 64. Profile section constructed by map projection onto a profile plane (with attitude 55°/010°) as map inset from Williams (1978).

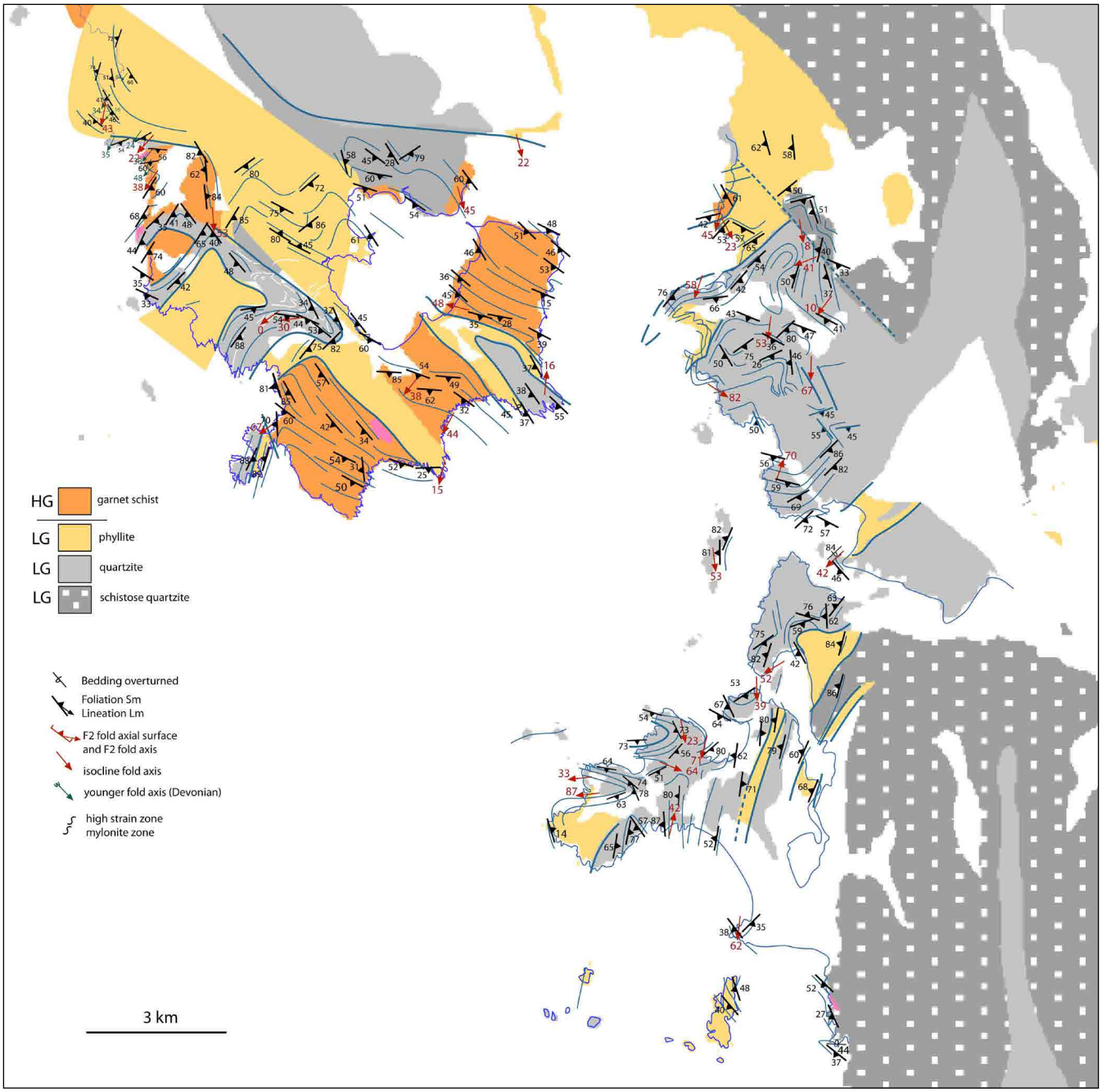


Figure 65. Structural map of the Port Davey area based on Williams (1978). Formlines in So/Sm are shown by thin blue lines. Base map is from Mineral Resources Tasmania 1:250000 digital atlas.

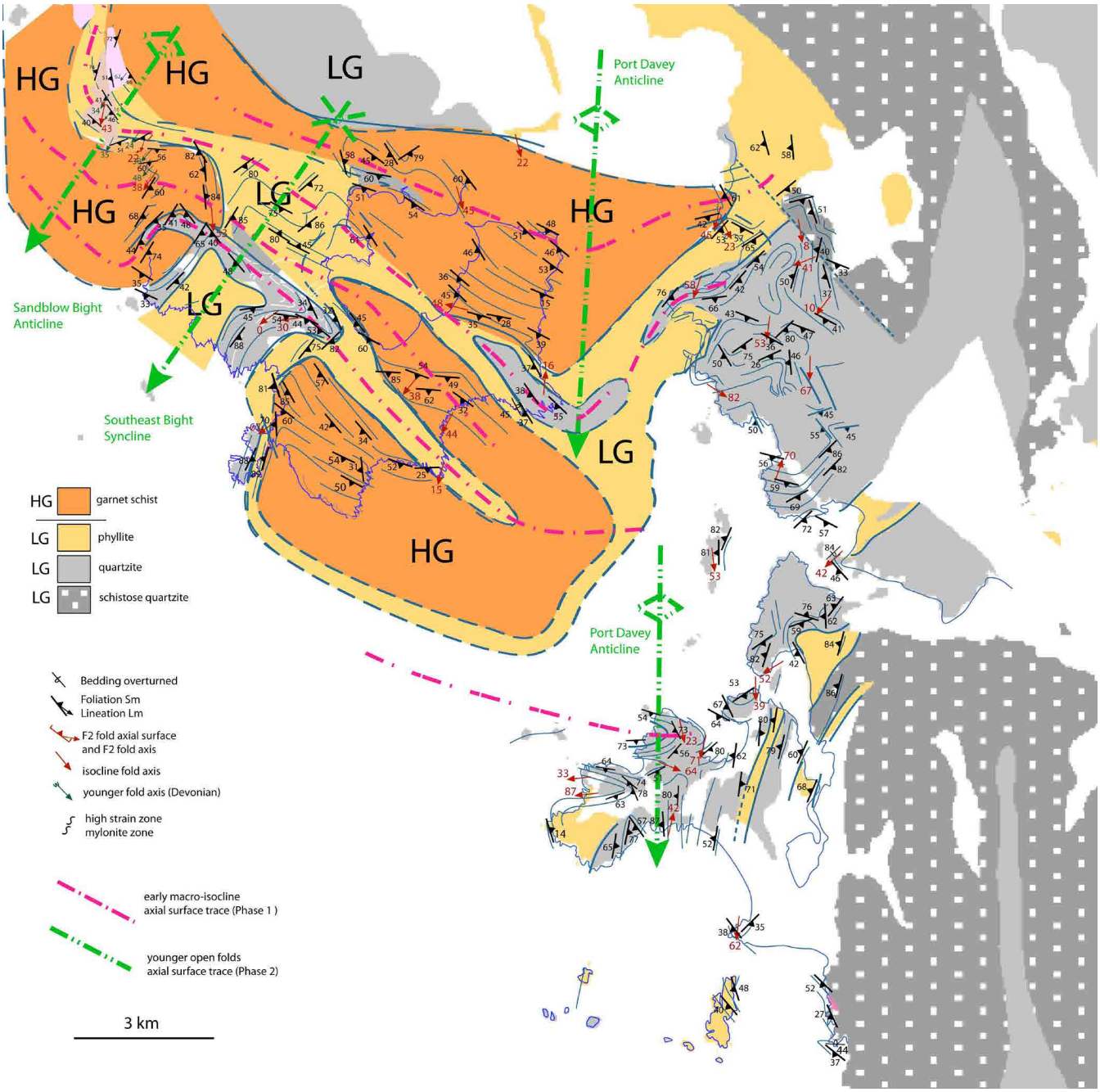


Figure 66. Port Davey interpretation map based on form-lines in So/Sm and the interpreted structural geometry (after Williams (1978)). The pink dot-dash lines are the interpreted early F1/F2 macro-fold axial surface traces. The green dash-dot lines are the axial surface traces of the younger Devonian northeast- and north-trending open folds (see Figure 65 and Mineral Resources Tasmania 1:250000 digital atlas).

The intensity of the early deformation in the Davey Head area quartzites is shown by flattened, metre-scale isoclines within transposed So/Sm (Figure 67), intensely flattened asymmetric isoclines within mylonitic zones (Figure 68) and internal boudins (Figure 69). Higher strain is also suggested by augen-shaped fold pods and closed-loop outcrop patterns typical of curved hinge-lines and sheath-folding (Figure 70).

The map pattern of litho-tectonic units (Figures 63 and 65) and an outcrop scale example (Figure 71) show a similarity to a "mushroom" or Ramsay (1967) Type 2 fold interference (Figures 72c, d and 73). In this scenario, northwest-trending, tight to isoclinal, recumbent macro-folds are refolded by upright, northeast-trending folds (Figure 66). Such geometry is consistent with the overall regional structural interpretation, but inspection

Figure 67. Intensely flattened isoclinal fold hinge within intensely foliated, transposed quartzite (Plate 4, Williams, 1982).

Figure 68. Strongly flattened isoclinal folds formed during the early deformation (Plate 6, Williams, 1982).

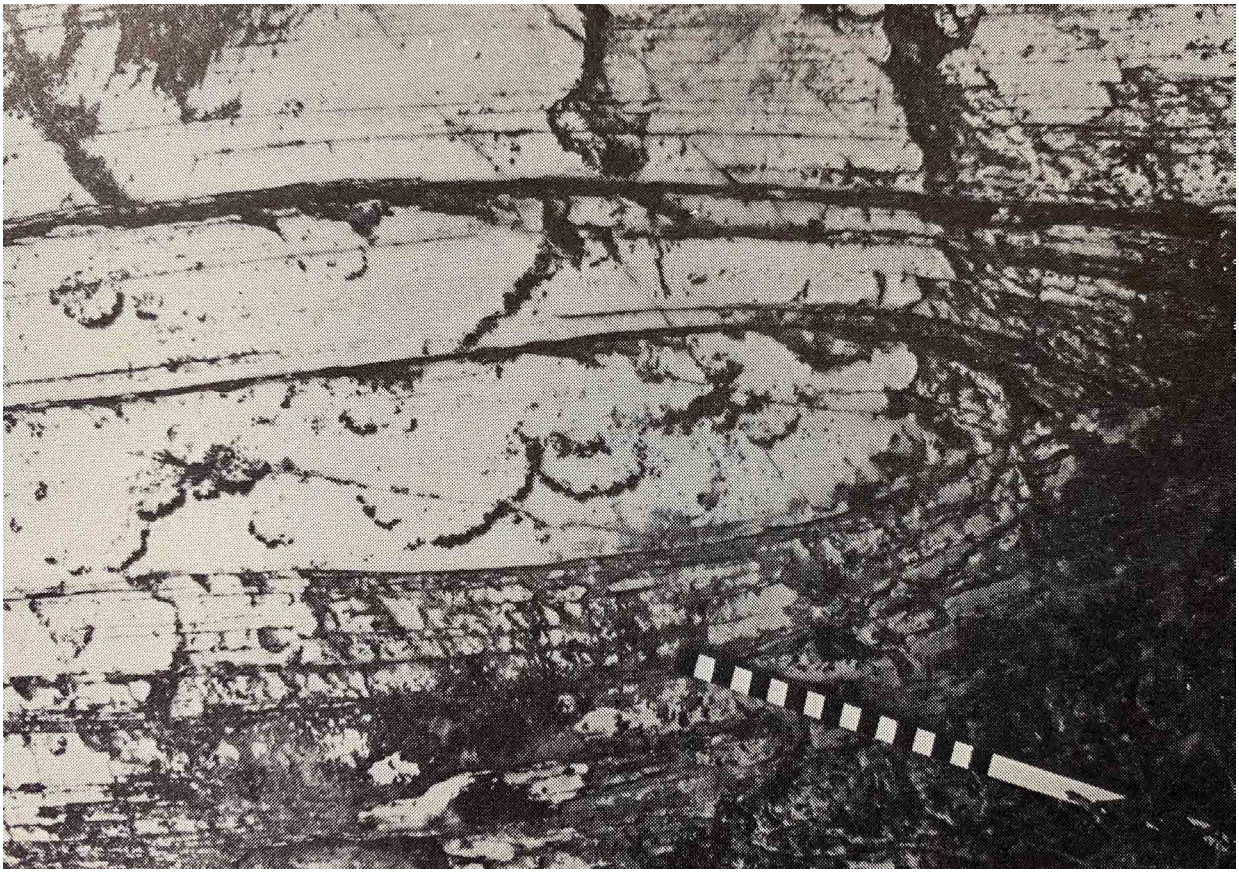

Figure 69. Internal boudinage within apparent thick-bedded quartzite. This is indicative of extreme flattening within the transposed and intensely foliated quartzite. (Plate 3, Williams, 1982).

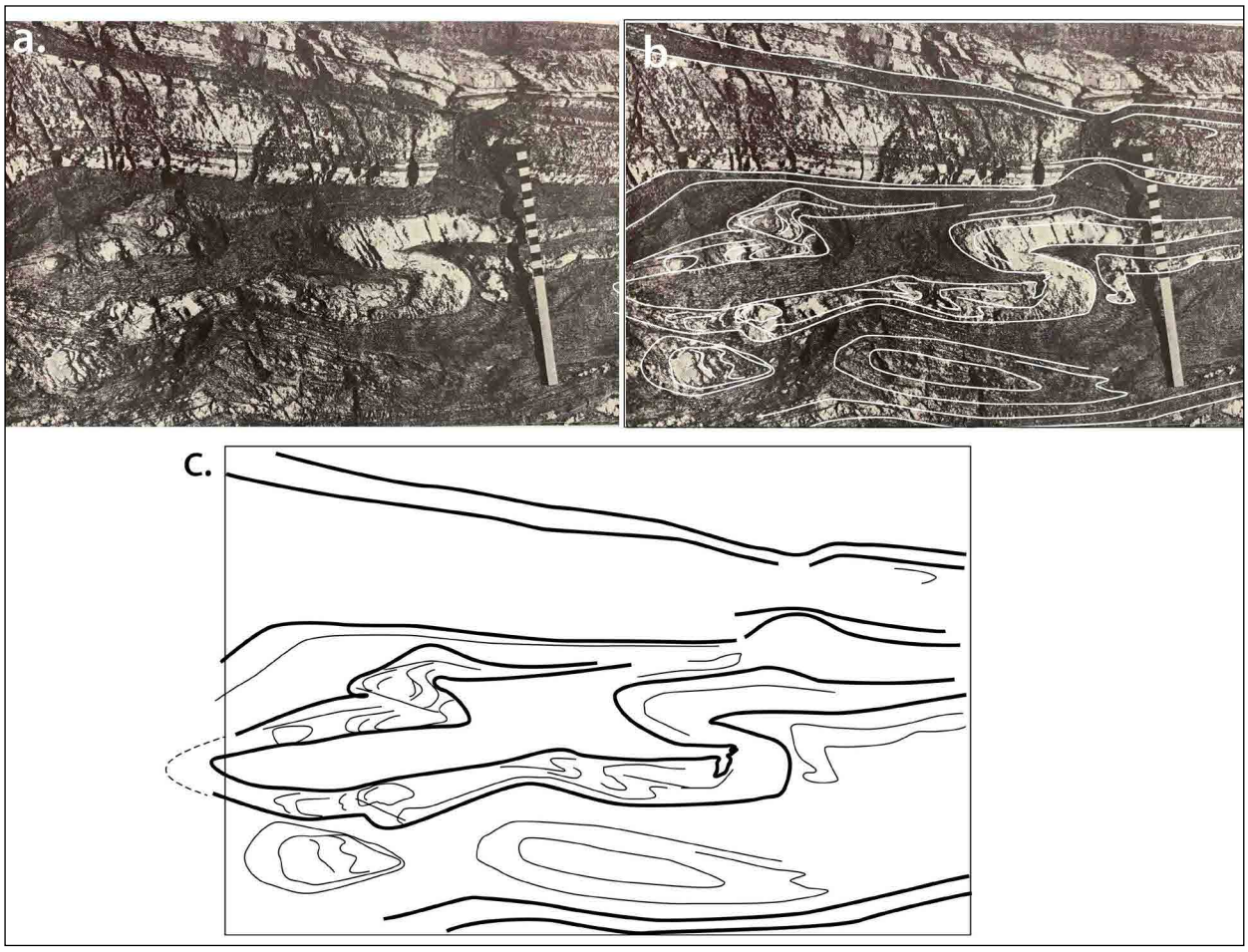


Figure 70. Thicker bedded quartzite with boudinage (upper layers) and isoclinal fold pair with apparent convergence of layers and closed-loop patterns indicative of curved hingelines. Outcrop photo northwest Saddle Bight (DN104506) (Plate 10, Williams, 1982). The boudin neck appears at high angles to the outcrop suggesting that the Lm/stretch is in the plane of the photograph.

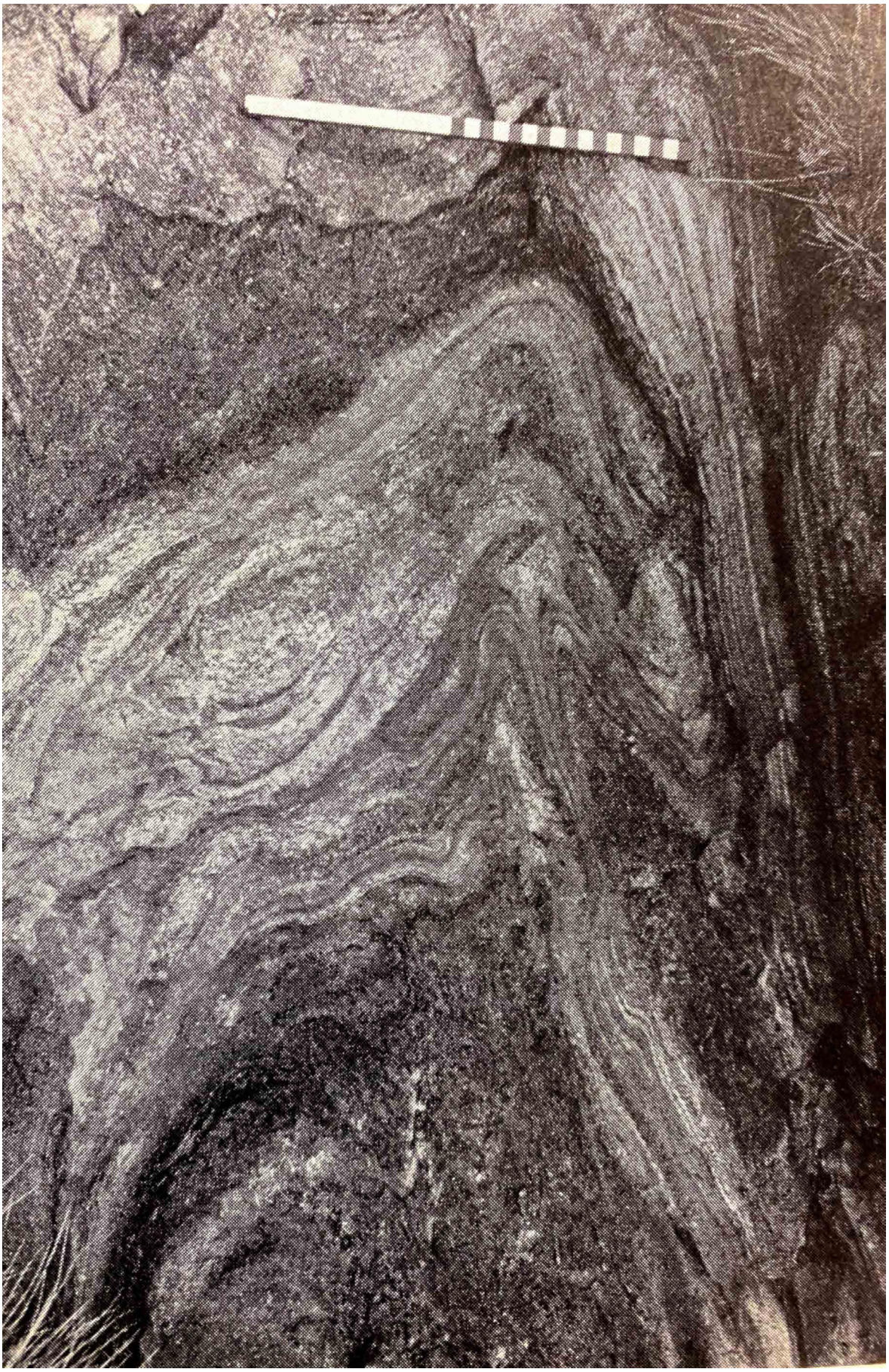

Figure 71. Small-scale example of the apparent "mushroom" style fold interference pattern in the Davey Head area (Plate 7 from Williams, 1982). An isoclinal recumbent fold set F1/F2 is refolded by an upright fold set with an axial surface at high angle (~90°) to the early axial surface traces. Note the original photo has been rotated through 90° to better reflect the inferred macro-relationships at Davey Heads.

of the meso-fold plunges and the So/Sm attitudes across the "mushroom" suggest a more complex pattern. The reclined nature of the Point Lucy and Whalers Point macro- isoclinal folds, the complicated Sm attitudes through the core of the "mushroom" as well as the presence of both north-south trending and the northeast-trending folds that refold the early macro-isoclinal folds (see Figure 63) require a more complex initial geometry of the early folds. Significant hinge-line curvature reflecting a sheath-like character of the Port Davey macro-folds may explain some of the geometrical complexities as well as the distinct reclined geometry more typical of a Ramsay Type 3 refold interference pattern (compare Figure 72a, b with Figure 72c, d).

A sheath-like geometry of the early F1/F2 macro-isoclines is suggested by the reclined geometry of the Whalers Point and Point Lucy folds (Figure 63b). Figure 74 shows the effects of Type 2 refolding on initial cylindrical folds versus non-cylindrical folds with curved hingelines and a marked sheath-like character. The diagram compares Ramsay Type 2 fold interference

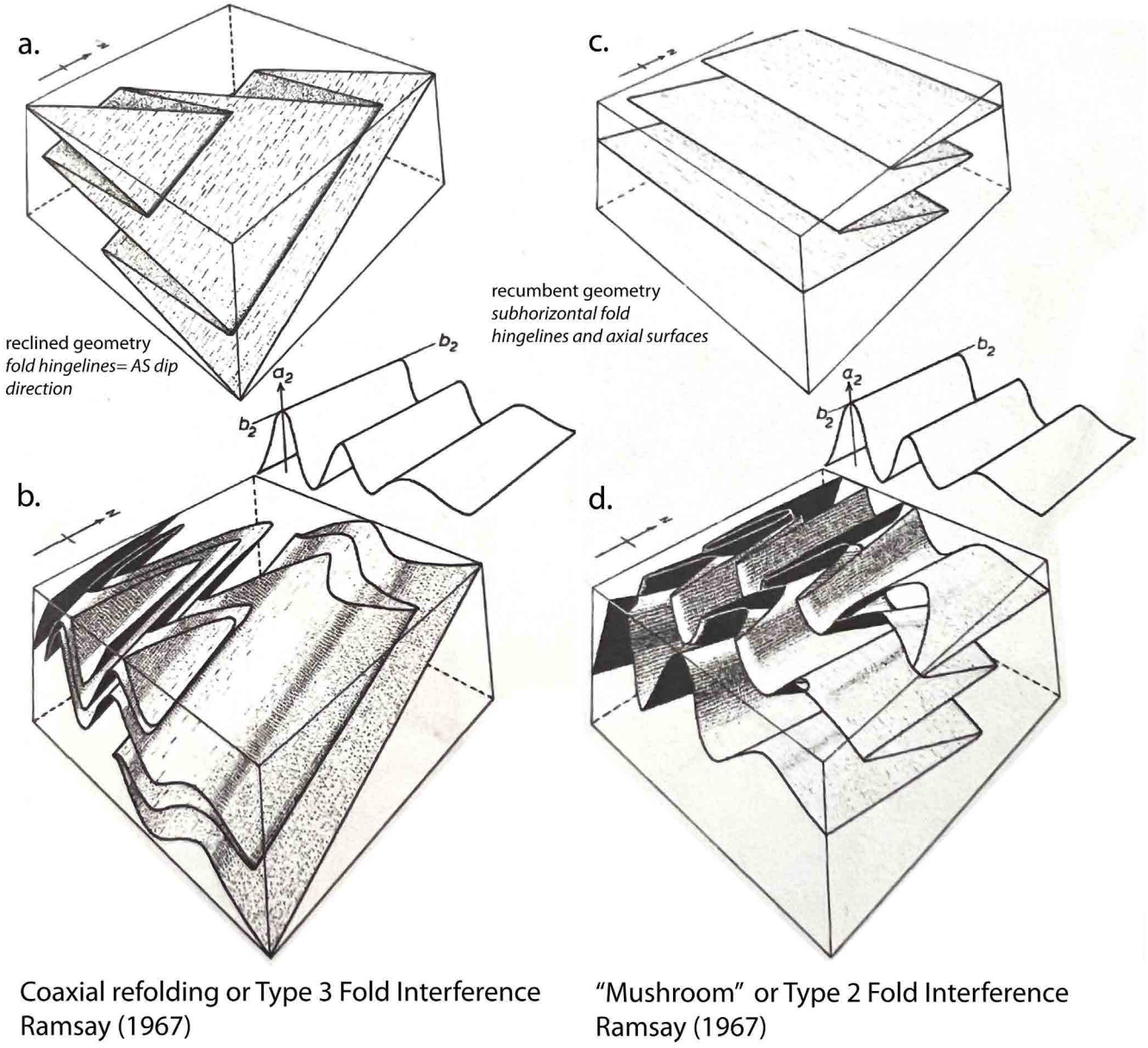


Figure 72. Ramsay fold interference diagrams (modified from Ramsay, 1967, figures 10-8 and 10-15). a) Initial reclined fold geometry. b) Type 2 coaxially refolded reclined folds from (a) due to upright refolding. c) Initial recumbent folds. d) Type 3 'mushroom" fold interference due to upright refolding.

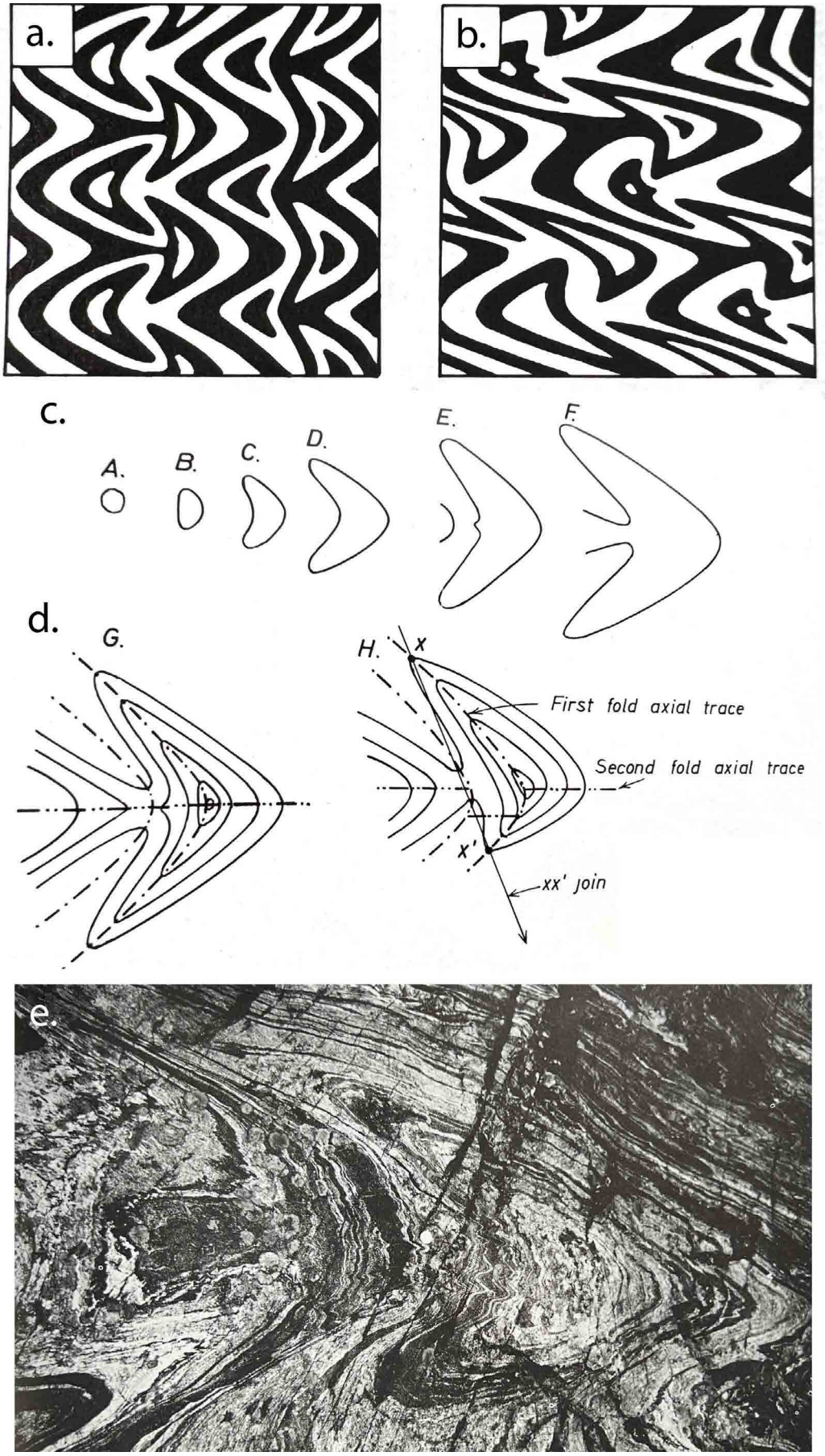


Figure 73. Type 2 fold interference patterns after Ramsay (1967). a) and b) Theoretical outcrop patterns where a) has perpendicular superposition of the two fold phases, and b) has oblique superposition of the two phases. (Ramsay & Huber, 1987, figure 22.16). c) Two dimensional forms of the Type 2 fold interference with A to F shapes derived from un-roofing different layers in a folded multilayer, d) more detailed formline shapes showing the axial surface trace relations between first and second phase folds with orthogonal fold superposition in (G) and oblique fold superposition in (H). The x-xx' join defines the axial surface strike of the first phase recumbent folds (figure 22.18 from Ramsay & Huber, 1987). e) Outcrop photograph of an asymmetric Type 2 interference pattern in hornblende-biotite gneisses from the Lepontine nappes of the Swiss Alps (figure 22.19B from Ramsay & Huber, 1987)

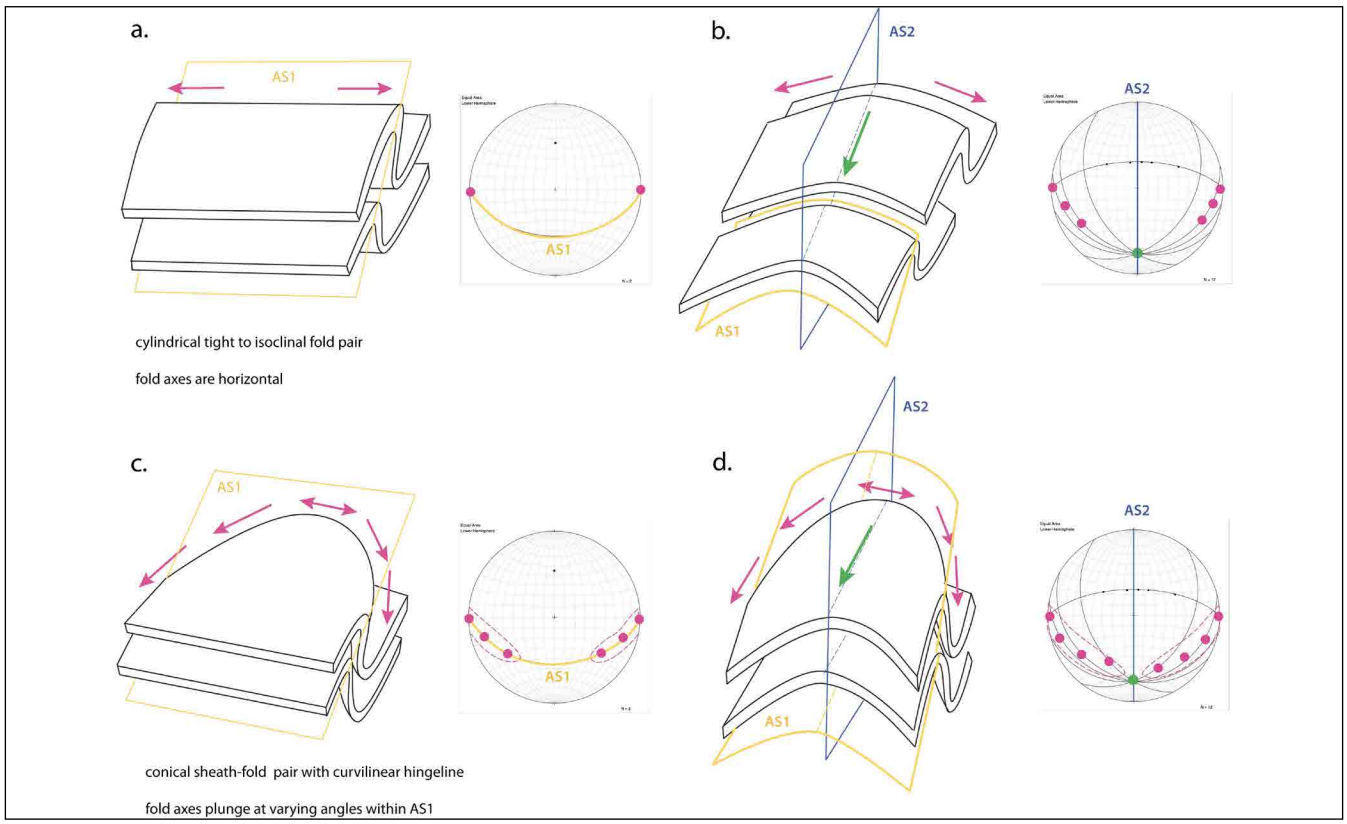


Figure 74. Diagramatic explanation for the reclined fold geometry of the Davey Head Point Lucy and Whalers Head macro-folds. a) Case 1: Initial cylindrical tight to isoclinal folds with stereonet representation of the axial surface (AS1 in orange) and the hingeline-fold axis (red dot). b) Refolded folds in (a) by a plunging upright anticline (AS2 in blue). Stereonet representation with vertical AS2 and great circles as folded segments of the early axial surface AS1. The refolded early hingeline-fold axis distribution is shown by the red dots. c) Case 2: Initial early folds with sheath-like form and curved hingelines. The red arrows denote the changing fold axis orientations around the curved hingeline with the accompanying stereonet representation of the fold axis spread within the AS1 axial surface. d) Refolded sheath folds in (c) with changing fold axis spread and stereonet representation.

(Figure 74a) but with superposition on a sheath-fold geometry (Figure 74c). Note the expected differences in the early meso-fold axis pattern with a greater fold axis spread towards the TD and/or stretching direction (stereonet green dot) and a resultant reclined geometry (compare 3D forms and stereonets in Figure 74b and 74d).

A reclined geometry is not expected from a Type 2 fold interference and is more typical of a Type 3 fold interference (Figure 72).

## 4.0 MACRO-STRUCTURE AND GEOMETRY OF THE SOUTHWEST COASTAL BELT

### 4.1 Map Patterns, Lithological Relationships and Regional Structural Implications

Previously the Southwest high-grade coastal belt was considered a collage of internally deformed slabs or fault-bounded slices where the contacts are high-strain mylonites with strong to intense L-S tectonite fabrics and shear bands (S-C' structures) (Meffre et al., 2000, 2001). In many cases, however, the contacts between the units have been reactivated by younger brittle, commonly dip-slip, normal faults.

Taken in isolation the map pattern does suggest a collage of units bounded by high strain zones, but 1) convergence of Sm and pinch out of units, 2) apparent repetition of a high-grade schist/ low-grade phyllite/ low-grade quartzite sequence (top-to-bottom stacking) and 3) changes in FA (fold axis) to Lm (mineral/ stretching lineation) must also be considered in any regional structural interpretation.

In the current re-assessment and analysis, emphasis was placed on the attitude relationships of the early F1/ F2 mesoscopic isoclinal folds, the apparent repetitions of as well as the pinch-outs in litho-tectonic units. A geometric model of an isoclinally folded, intercalated succession of high-grade schists, low-grade pelite and low-grade quartzite is discussed with high-strain zone

contacts between the different units. It is important to note that apart from reconstructed fold profiles at Point Lucy and Whalers Point (Williams, 1978), no large-scale fold hinges have been mapped and/or previously recognised throughout the southwest high-grade coastal belt. Regional scale isoclinal macro-folds are however, important elements of other parts of the Tyennan domain (Gray & Vicary, 2021a, b).

*4.1.1 Interpretation Methodology*

The approach adopted in this study and the evolution of the structural interpretation for the Southwest coastal high-grade belt is shown in the succession of diagrams (Figures 75 to 78). Initially a stitch map of the detailed maps presented in Section 4.1.2 was created (Figure 75), followed by establishing formlines in the foliation Sm attitude data to provide the general form of the regional structure (Figure 76). The formline interpretation was then combined with the distribution of litho-tectonic units on the lithology map (Figure 77) to create an isoclinal-fold interpretation map assuming litho-tectonic unit pinchouts were fold-hinge zones (Figure 77), not unlike those defined and established for the Franklin fold-nappe of the Central Tyennan (Gray & Vicary, 2021b). The axial surface traces of each of the macro-folds were then defined (Figure 78).

The aim was to utilise the detailed mapping by McNeill (1985) in the north and by Williams (1978) in the south at Port Davey to establish the structural geometry at each end of the belt. These geometries and incorporated lithologies were then projected southwards and northwards respectively using ListMap air photos and the compiled structural maps largely from data collected by Hall (2005, 2006 and 2008). Where possible structural data and the ListMap airphotos were used to provide more detailed maps of the high-grade to low-grade contacts.

*4.1.2 Southwest Coastal High-Grade Belt Regional Structural Interpretation*

Structure of the Southwest high-grade coastal belt can be considered in three parts, a Northern part from Top Rocks to Mulcahy Bay, a Southern part from Wreck Bay to Port Davey, and a Central part from Mulcahy Bay to Wreck Bay.

4.1.2.1 Northern Part

The Northern part of the coastal belt contains an inferred macro-fold hinge (Nye Bay fold-nappe) reflected by a narrowing and pinch-out of the high-grade schists at Elliott Point (Figures 38 and 44). The reclined, south-closing geometry of this macro-fold is suggested by the map pattern, changes in attitude of the early F1/F2 mesoscopic isoclines, and attitude changes of the lineation Lm from upper to lower fold limb (Figure 45 and 52). Thickening of the pelite (Ptp) southwards on both macro-fold limbs (Figures 38 and 56) suggests layer-thickening towards the fold hinge at Elliott Point with thinning or layer attenuation northwards along the limbs.

This macro-fold may represent the continuation of the south-closing Franklin fold-nappe from Mt McCall underneath the Cambro-Ordovician cover across the Elliot Range Anticline to Moores Lookout, to North Broken Hills and to Nye Bay an extent of some 50 km. Fold repetition of units gives a map width from limb to limb of ~12 km (Top Rocks to the Giblin River valley).

The northern part of the Southwest high-grade coastal belt is affected by north-south Devonian folding, including the south-plunging Lawson Range Anticline and the Giblin Syncline (Figures 38 and 39). These folds re-fold the early-formed fold-nappe (Figure 40).

4.1.2.2 The Southern Part

The Sandblow Bay to Davey Head region is dominated by a regional "mushroom" Ramsay (1967) Type 2 fold interference pattern (Figures 63, 65 and 66) with initial northwest-trending macro-isoclinal folds with sheath-like curved hingelines refolded by northeast-trending, southwest-plunging open folds including the Sandblow Bay Anticline and South East Bight Syncline and the north-trending, south plunging Port Davey Anticline (Figure 66).

4.1.2.3 The Central Part

The Central part is dominated by a series of interpolated alternating high-grade and low-grade bands, interpreted as in-folds of high-grade schists within the low-grade quartzite-phyllites. Pinch-outs of the schists are considered fold closures to give a stacked sequence of west-plunging, north- and south- closing isoclinal macro-folds (Figures 77 and 78). The alternating north- and south-closing hinges were extrapolated to the north from the macro-folds that are part of the Davey Head regional-scale fold interference (Williams & Corbett, 1977).

Formlines derived from foliation Sm attitude trends (Figure 76) were used to extrapolate contacts forming as structural interpretation map of the discontinuous coastal outcrops (Figure 77).

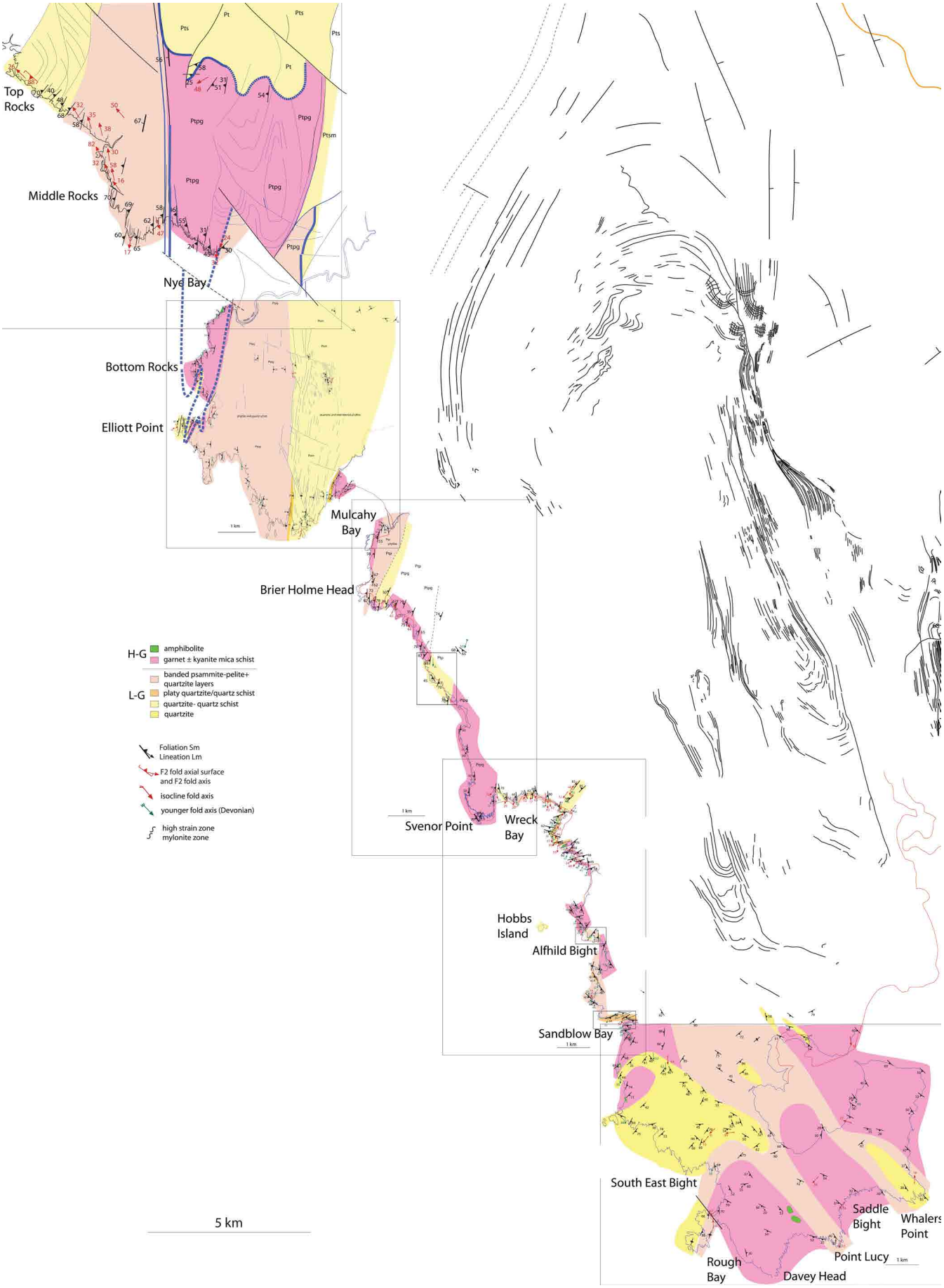


Figure 75. Structural and lithological map from Top Rocks to Davey Head based on stitching all the various detailed structure maps.

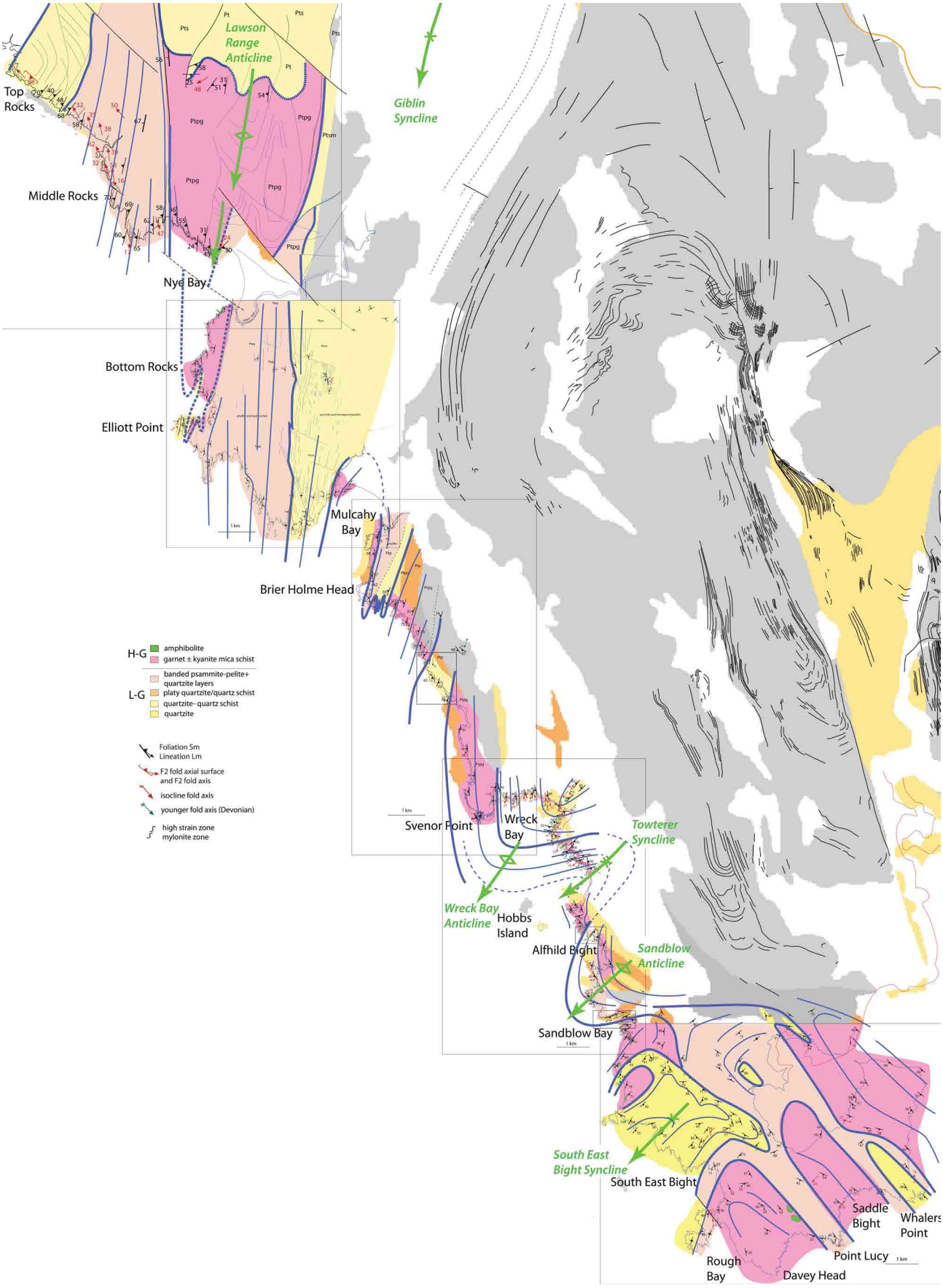


Figure 76. Structural interpretation map utilising Sm and So/Sm formlines to extrapolate the mapped distribution of lithologies and establish a macro-structural geometry.

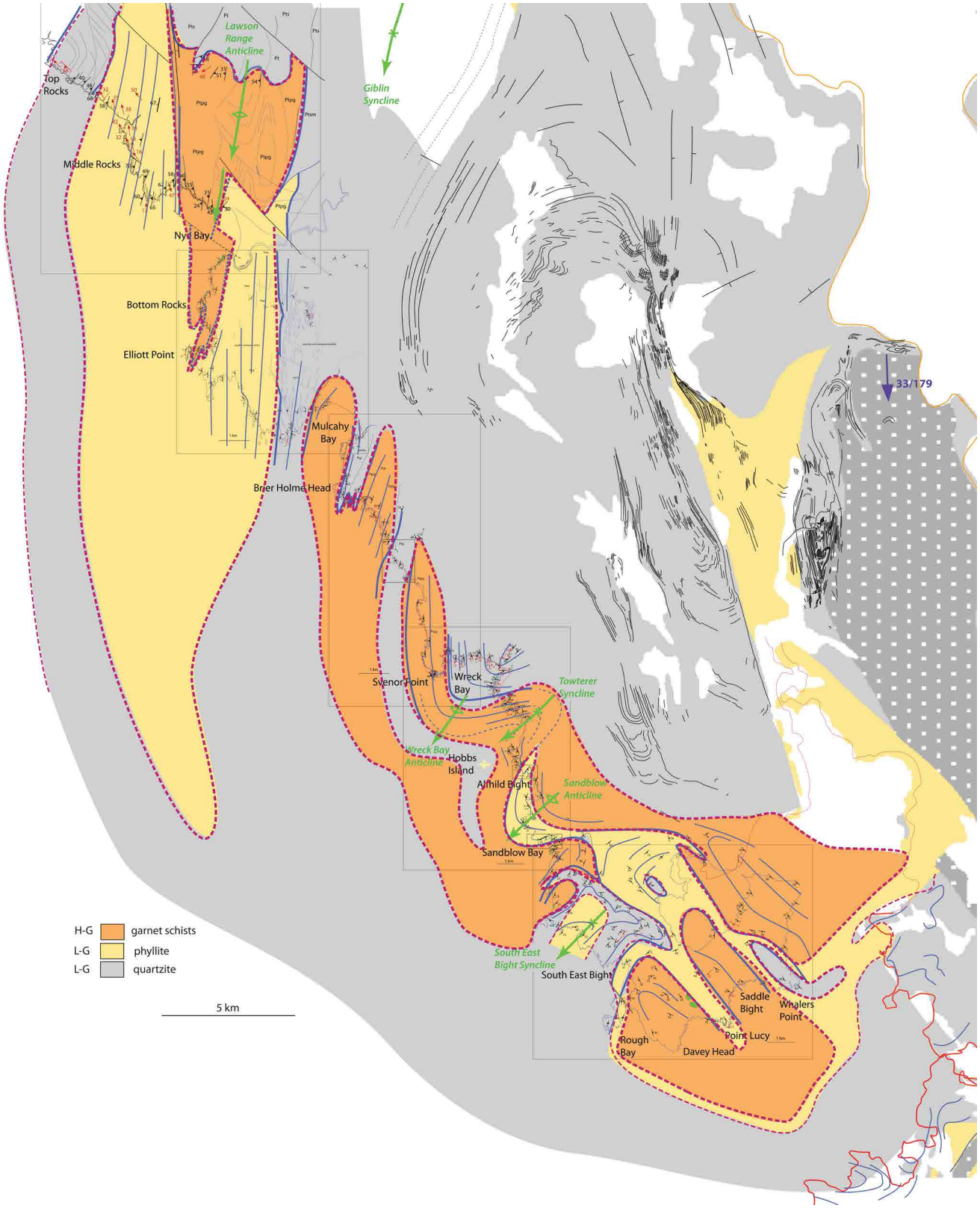


Figure 77. Simplified interpretation map showing a lithology overlay on the detailed map base of the High-Grade Coastal Belt.

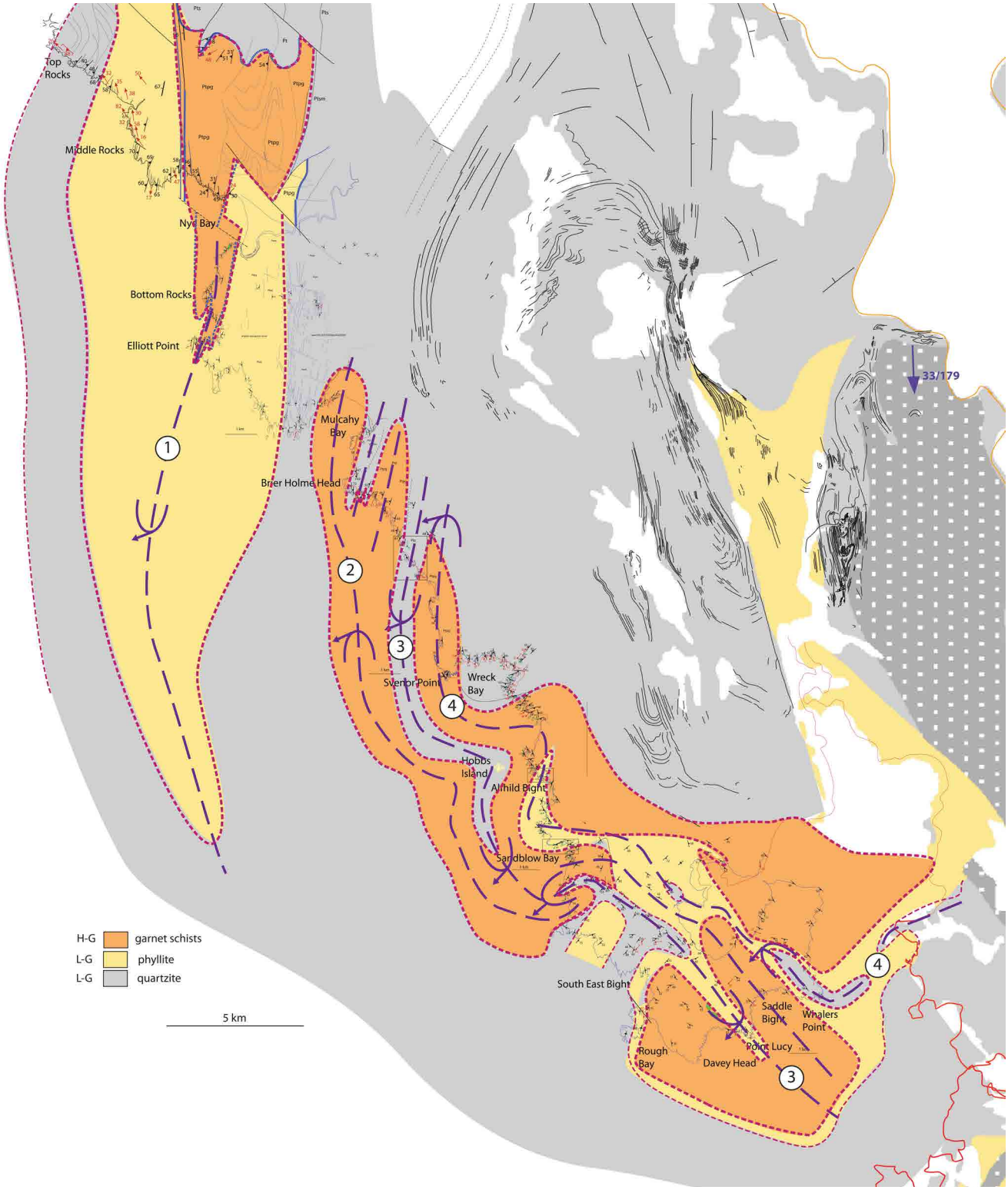


Figure 78. Axial trace map of inferred recumbent fold closures based on outcrop structural data and lithological distribution from Figures 75 and 76. Macro-folds include: 1) Nye Bay south-closing fold-nappe. 2) doubly-plunging, north-closing Mulcahy Bay fold. 3) south-closing in-fold in low-grade quartzite.4) north-closing Svenor Point fold cored by high-grade schist.

### 4.2 Early Fold Axis Orientation

Early fold axis (FA) variability is reflected in Figure 79. Measurements of isocline attitude have been taken from various sources largely field notes by MH Hall (Nye Bay to Towterer Beach), Ron Berry and Sebastian Meffre (Nye Bay to Mulcahy Bay), Andrew McNeill for Nye Bay. Other sources include measurements 1) from 1:25,000 Lewis, Elliott, Mulcahy and Propsting Map sheets, and 2) in stereonet form from Spry & Baker (1968), McLean & Bowen (1971), and Williams (1982).

The stereonets as insets show a changing early isocline fold axis distribution from Middle Rocks northwest of Nye Bay to Knapp Point at Port Davey (Figure 79). This fold axis distribution reflects the presence of a series of regional-scale macro-isoclinal folds (Figure 78) as well as the interference of the Devonian north-south open folds and southwest-northeast trending folds (Figure 80). There are narrow zones where the early fold axes

are directly south plunging including Nye Bay north, Mulcahy Bay north and Wreck Bay north. These alternate with zones/domains where the early fold axes have more variable southwest or northeast plunges. There is also a zone from Top Rocks to Middle Rocks where the early F2 folds are northwest plunging.

Quartzite of the Lawson Range north of Nye Bay shows the largest spread in F1/F2 fold axis orientation (~180°) within a moderately to gently S-dipping girdle reflecting the modal axial surface (or Sm) (Figure 79a and b). These folds have either reclined or inclined plunging geometry. Isoclines in the same quartzite in the Lawson Range Anticline hinge also show reclined geometry but with a lesser (~90°) fold axis spread within a S-dipping partial girdle (Figure79b). In the Giblin River area isocline axes show ~100° spread but within a gently north-northeast-dipping girdle (Figure79d).

In the low-grade pelitic rocks of Nye and Mulcahy Bays isoclines tend to be upright, north-south-trending with a bimodal fold axis pattern, where axes either plunge moderately or gently to the north or south (Figures 79g, h and i). In the Wreck Bay area the fold axis pattern approaches a unimodal cluster (Figures 79j and k), whereas at Port Davey there is a consistent southwest plunge defining a partial girdle with a 30°-60° spread in plunge direction (Figures 79m, n and o).

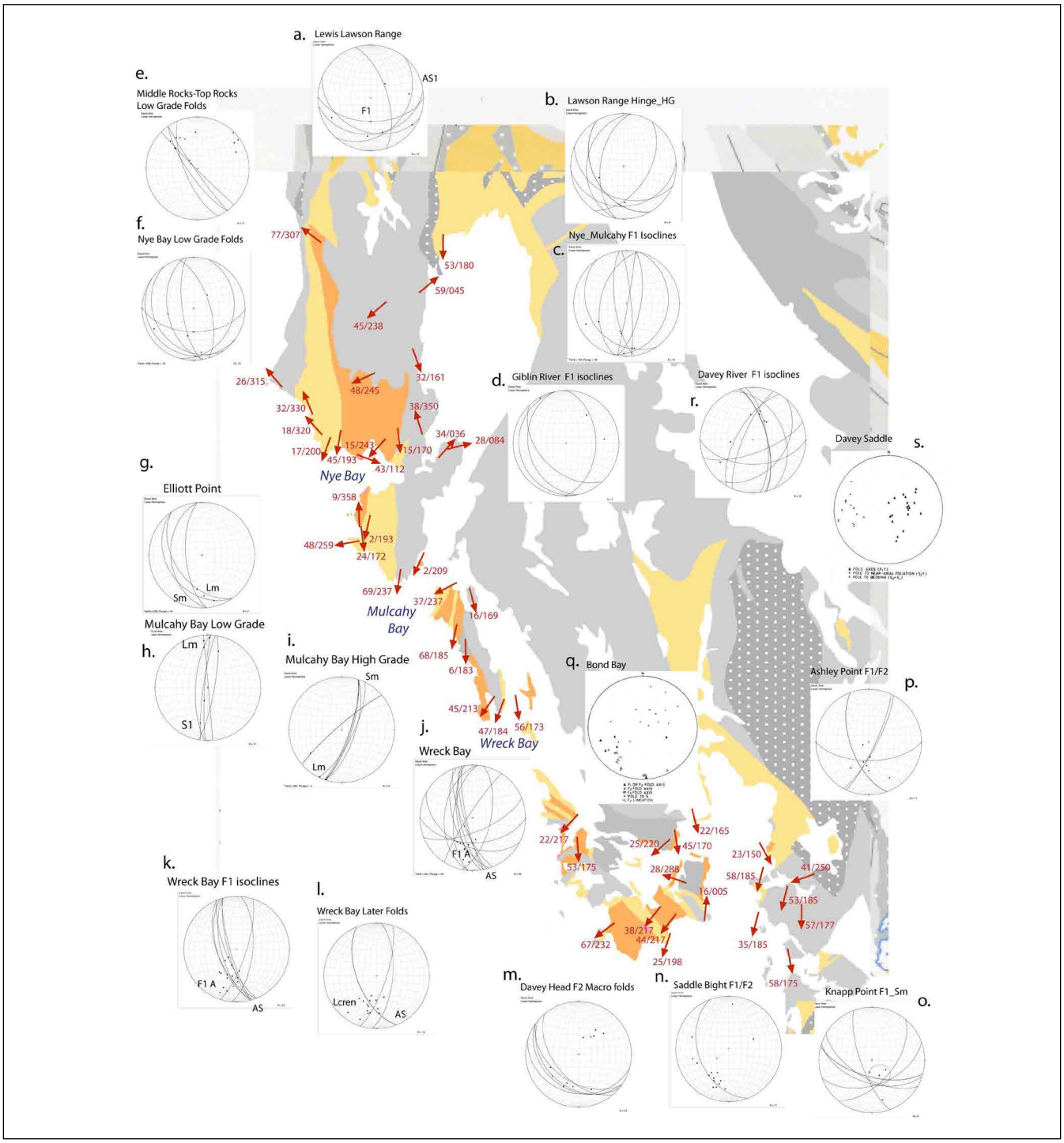


Figure 79. Early F1/F2 fold axis data map with the local stereonet determinations. Map base is a simplified lithotectonic map derived from the 1:250,000 Mineral Resources Tasmania digital atlas.

### 4.3 Early Fold Axis (FA) and Lineation (Lm) Relationships

Rotation sense, either clockwise or counter-clockwise, of the fold axis trend (FA) towards the lineation Lm trend changes from limb to limb for regional-scale inclined plunging to reclined macro-folds. Such changes in the fold axis FA^Lm rotation sense can be used to identify fold hinges in shear-related regional-scale folds (Alsop & Holdsworth, 1999). The approach was used to both establish and verify the positions of fold axial surface traces (AST) in the Central Tyennan domain (see Gray & Vicary, 2021b).

In the Southwest High-Grade Coastal Belt changes from clockwise to counter-clockwise sense occur at Nye Bay, Mulcahy Bay and Sandblow Bay (see positions marked by H in Figure 80) confirming the presence of the macro-folds hinges 2, 3 and 4 in Figure 78. Further south in the Port Davey area limited lineation Lm data precludes verification of the regional fold hinge-lines there.

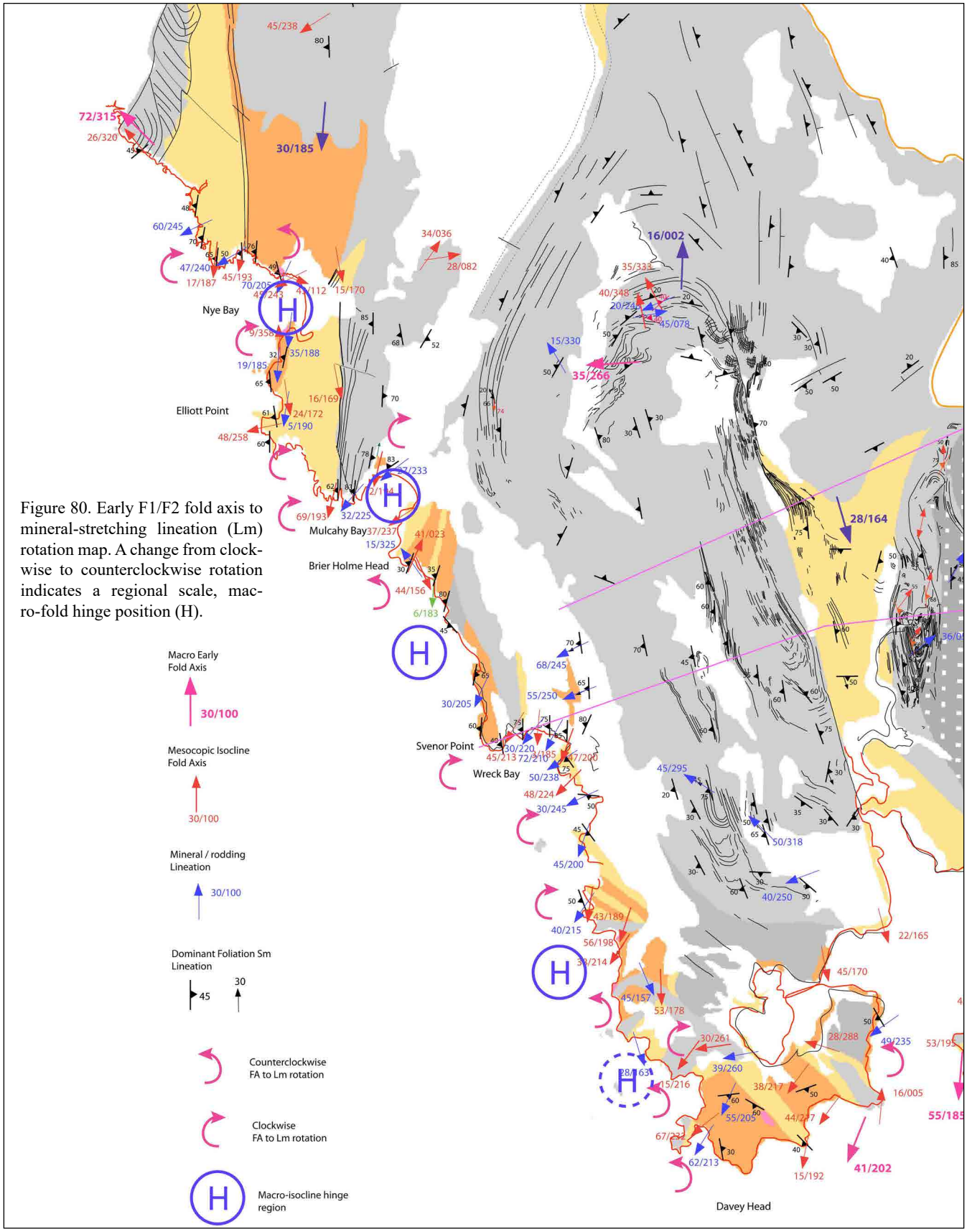


Figure 80. Early F1/F2 fold axis to mineral-stretching lineation (Lm) rotation map. A change from clockwise to counterclockwise rotation indicates a regional scale, macro-fold hinge position (H).

### 4.4 Younger Fold Axis (FA) Trends

Younger more open folds refold the early macro-isoclinal folds. As these folds also fold the Ordovician sandstone and conglomerate that sits unconformably on the older quartzite-pelite sequence they are considered mid-Devonian in age related to Tabberabberan deformation (Seymour, 2014).

The refolding can be seen in the form-line interpretation maps of the coastal belt (Figures 76 and 77). Fold plunges and fold axis trends are depicted as β intersections in stereonets of foliation Sm great circle traces (Figure 81). Much of the western part of the Southern Tyennan domain including the High-Grade Coastal Belt is refolded by north-south trending folds (Figure 81). The coastal belt from Wreck Bay to South East Bight are refolded by northeast-trending folds with southwest plunges (Figures 76 and 77).

The main younger folds that affect the coastal belt are listed below with their fold axis attitudes. These are:

| | |
|---|---|
| Lawson Range Anticline: | 25°/202° |
| Giblin Syncline: | 25°/178° |
| Wreck Bay Anticline: | 49°/217° |
| Towterer Syncline: | 49°/212° |
| Sandblow Bay Anticline: | 44°/207° |
| South East Bight Syncline: | 36°/217° |
| Port Davey Anticline: | 41°/215° |

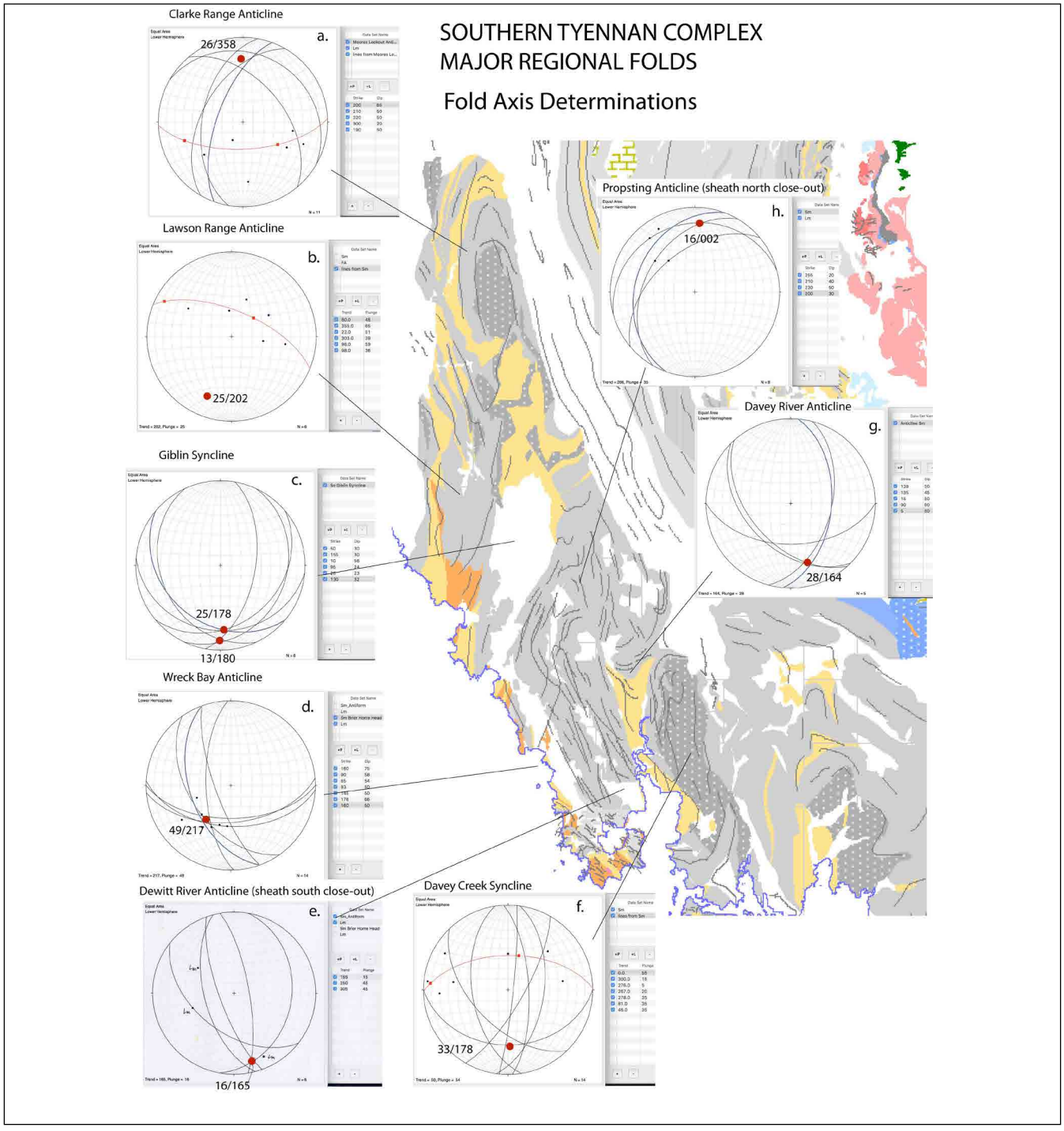


Figure 81: Stereonet fold axis determinations for the younger, Devonian major folds that impact the western part of the Southern Tyennan domain including the Southwest High-Grade Coastal belt.

## 4.5 Isoclinal Macro-folds and Fold-Nappes

*4.5.1 Final Geometry*

The interpreted Southwest High-grade Coastal belt structural geometry is dominated by a regional-scale isoclinal fold-nappe with reclined geometry, underlain by a series of second or third order regional-scale isoclinal folds that are part of a fold stack along the macro-fold lower limb (Figure 82). The Nye bay fold-nappe is a south-closing, west plunging macro-isoclinal fold that has an overturned western limb that extends from the northern part of Nye Bay to Top Rocks. The inferred closure, based on extrapolation of contacts southwards into the Southern Ocean assuming a flattened similar-fold form, gives length scales of ~30 km for the hinge within low-grade pelite and almost ~45km for the hinge in quartzite (Figure 80). Unfolding the inferred fold geometry requires a stacking sequence of high-grade schists underlain by low-grade phyllite, underlain by quartzite.

The lower limb transition to the underlying fold stack occurs across Mulcahy Bay with an inferred macro-fold hinge suggested by the change in FA^Lm rotation (Figure 80). Overall the sequence from Mulcahy Bay to Davey Head is a high-grade macro-fold pod with isoclinal infolds of low-grade phyllite and quartzite. The inferred closures in this coastal segment are indistinct as actual fold hinges and appear as attenuated pinch-outs of the various strongly to intensely foliated and transposed lithologies (Figures 77 and 78). Supporting the macro-fold pod interpretation are changes in FA^Lm rotation at Mulcahy Bay, Brier Holme Head-Svenor Point and Sandblow Bay (Figure 81). The lithological distribution in outcrop pattern (Figure 75) combined with the meso-isocline fold plunges (Figure 80), suggest the high-grade macro-fold is closed in the north and south defining a regional scale augen/pod (compare Figures 78 and 82).

The regional-scale augen consists of 3 macro-isoclines including an upper north-closing fold cored by high-grade schist, a middle south-closing fold in low-grade quartzite/ phyllite and a lower north-closing fold cored by high-grade schist (see hingelines 2, 3 and 4, Figure 78). This geometry is more complex in the South East Bight -Port Davey area with the development of second- or third-order macro-isoclines highlighted within the Type 2 fold interference pattern (Figure 78).

*4.5.2 Interface with the Structurally Lower Propsting-De Witt Mega-sheath Fold*

The interface of the isoclinally folded coastal high-grade belt with the quartzite of the Propsting-De Witt mega-fold is a disjunct "zone" concealed by younger Tertiary and Quaternary sediment of the Lower Hut Plains and extensive wind-blown dune systems south of Towterer Beach. The boundary was originally defined as a north-northwest-trending fault (Figure 2) that truncated structure of the coastal belt (Hall, 1966; MRT 1:250000 digital map).

There is clear disharmony between the coastal high-grade folded package and the underlying, homoclinal, west-dipping quartzites of the De Witt Range (Figures 76 and 77). Such disharmony may also relate to a hidden high-strain interface where the contacts and isoclinal macro-folds merge, or swing into parallelism, with the quartzites of the De Witt Range. Formlines from the ListMap airphoto stitches suggest that the uppermost part of the mega-sheath fold is a high-strain, mylonitic carapace (Figure 83).

The aeromagnetics provide another view of this undercover contact zone (see Section 4.5.3).

*4.5.3 Geophysical Considerations*

In general terms interpretation of the aeromagnetics suggests the quartzites have low magnetic susceptibility, the low-grade pelites (phyllites and quartz phyllites) have moderate to high magnetic susceptibility and the high-grade schists have moderate to low susceptibility (Fiure 84).

Magnetic high and lows along with their boundaries have been delineated by line traces that supposedly reflect elements of the west coast geology (Figure 85). Superposition of the ground-based structural/formline interpretation shows poor correspondence overall between the geophysical interpretation and the structural geology interpretation (Figures 85 and 86). This discordance perhaps suggests a more complex pattern to the distribution of magnetic mineral phases in the West Coast rock sequence.

The geophysics supports:

1. Discord or disharmony of the Southwest High-Grade Coastal belt with the underlying De Witt-Propsting mega-sheath fold.
2. Offshore onto the continental slope the linear magnetic highs appear to define a series of regional-scale, north-south trending, tight chevron folds with angular hinges (outlined by the black dashed lines in Figure 84). These folds however are discordant to the structural interpretation from the ground-based structural data (Figures 85 and 86).

The best fit is from the quartzites along the De Witt Range defining the western margin of the De Witt-Propsting mega sheath-fold, as well as the eastern boundary of the Southwest High-grade coastal belt. Intervening between the two magnetic highs is a broad poorly magnetic area (blue area in Figure 84) that coincides approximately with the Hut Plains.

Considerations for any geophysical interpretaion must include

1. All units are moderately to steeply west-dipping from Top Rocks to Port Davey
2. Fold forms are based on formline interpretation from the coastal strip mapping and therefore must constrain interpretation of the aeromagnetics.

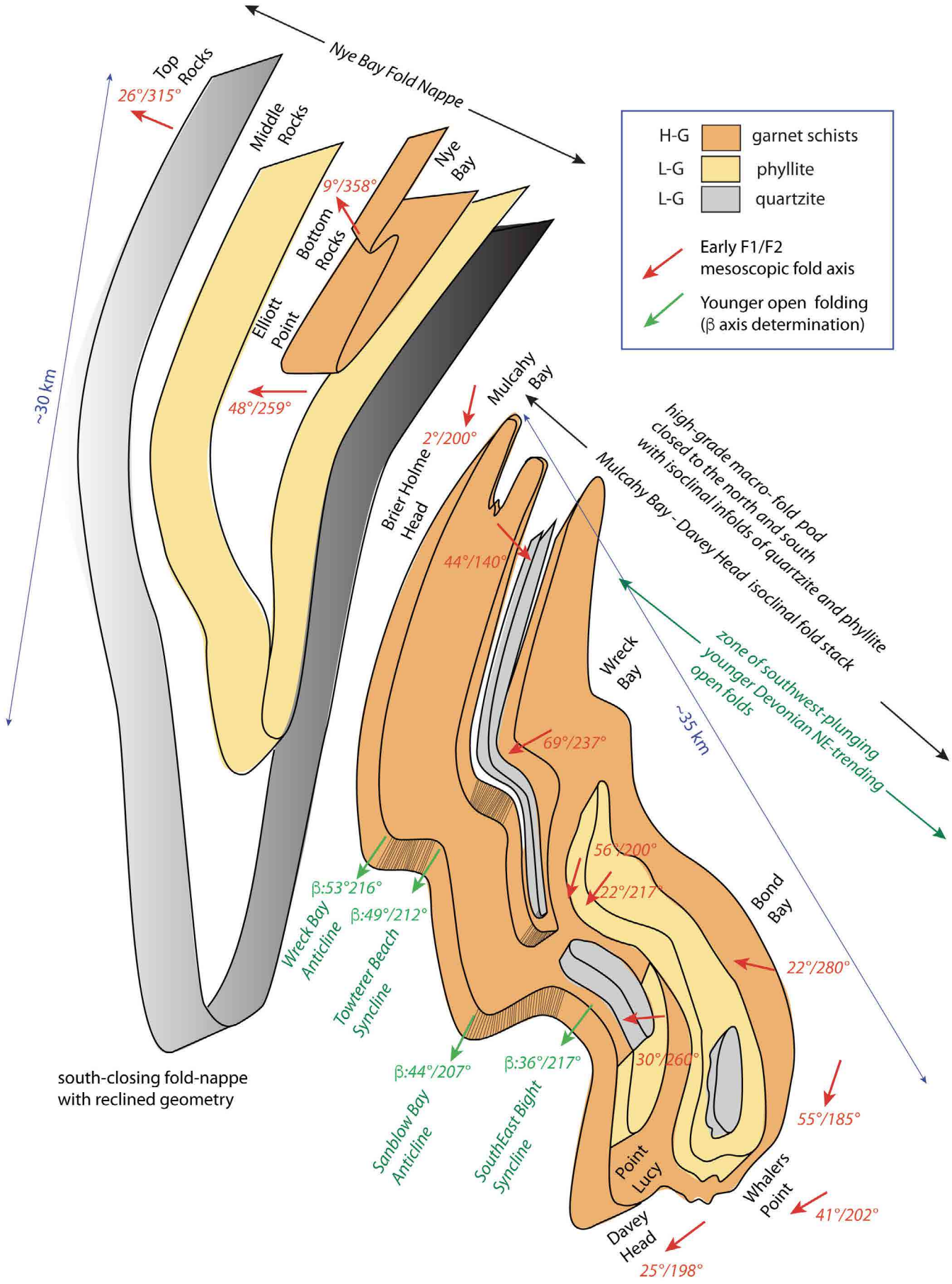


Figure 82. Interpreted 3D geometry of the Southwest high-grade coastal belt based on map views and fold axis data. Early F1/F2 meso-scale isocline axes are shown by red arrows with plunge/plunge direction in red text. The axes of the younger Devonian folds that refold the sequence are shown by greens arrows with plunge/plunge direction in green text. Approximate positions of geographic locations in the 3D model are shown in black text.

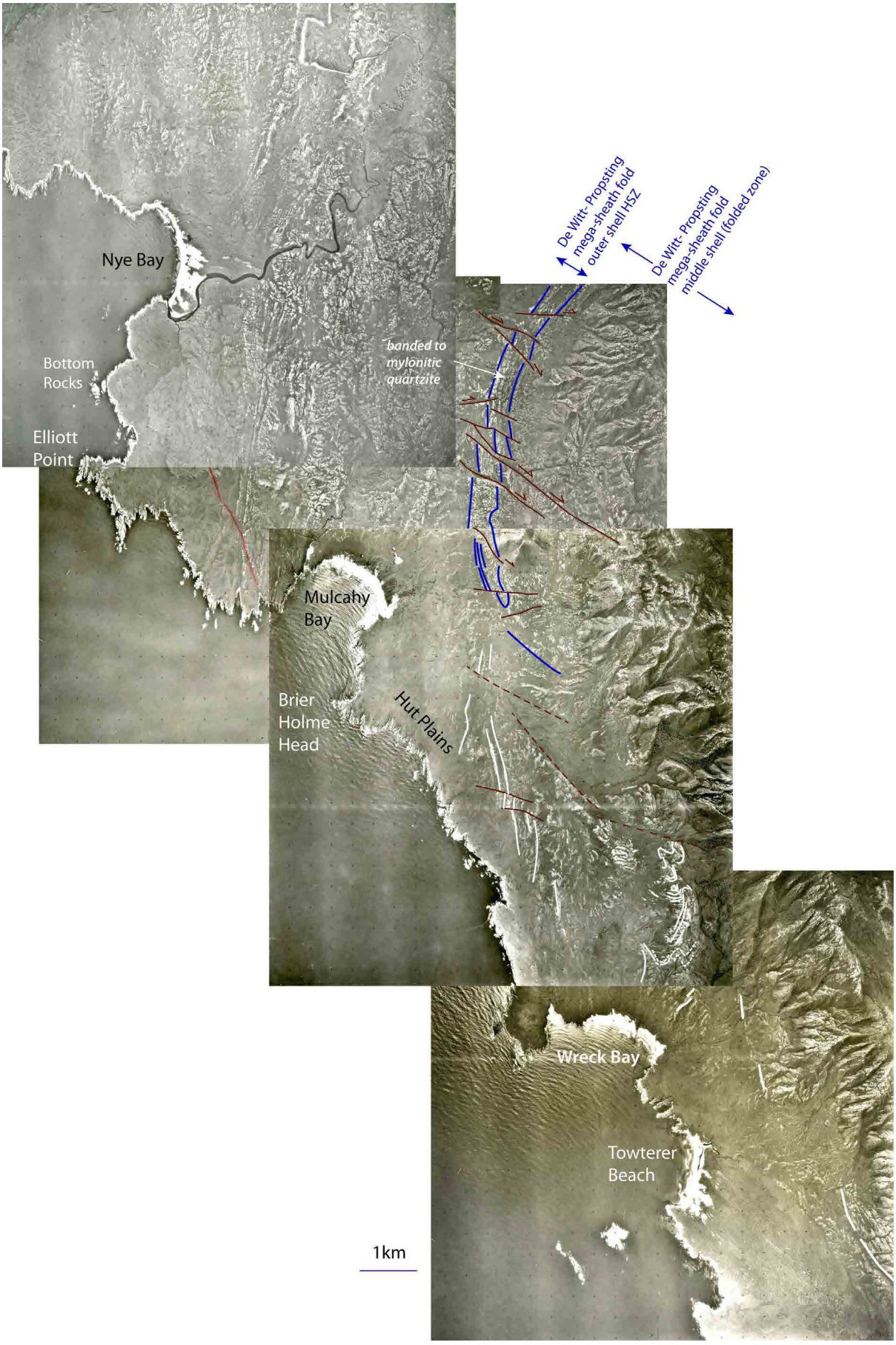


Figure 83. Air photo stitch of the West Coast High-Grade belt showing So/Sm form-line and fault interpretation of the coastal plains inland from the coastal outcrops and west of the De Witt Range (ridge along bottom right side of photo stitch).

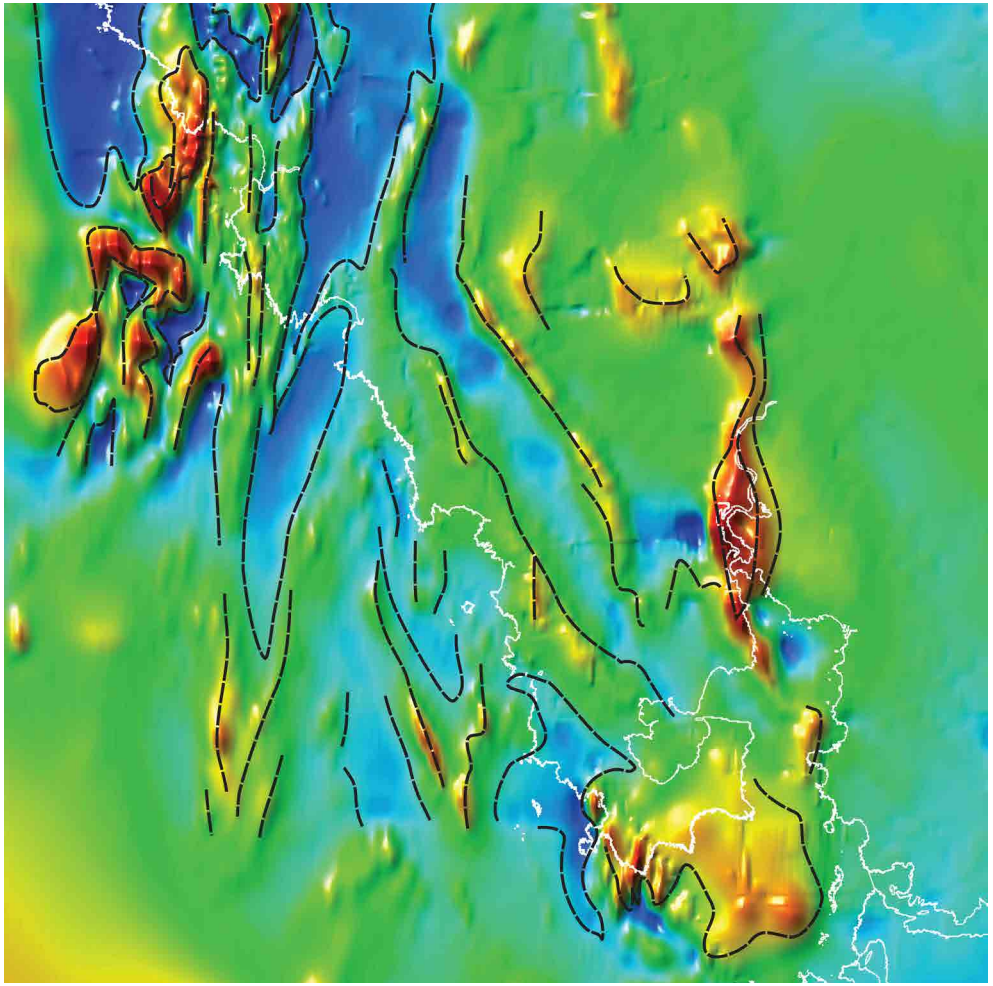

Figure 84. Total Magnetic Intensity image (400m line spacing) with black dashed lines as trend lines in the aeromagnetics.

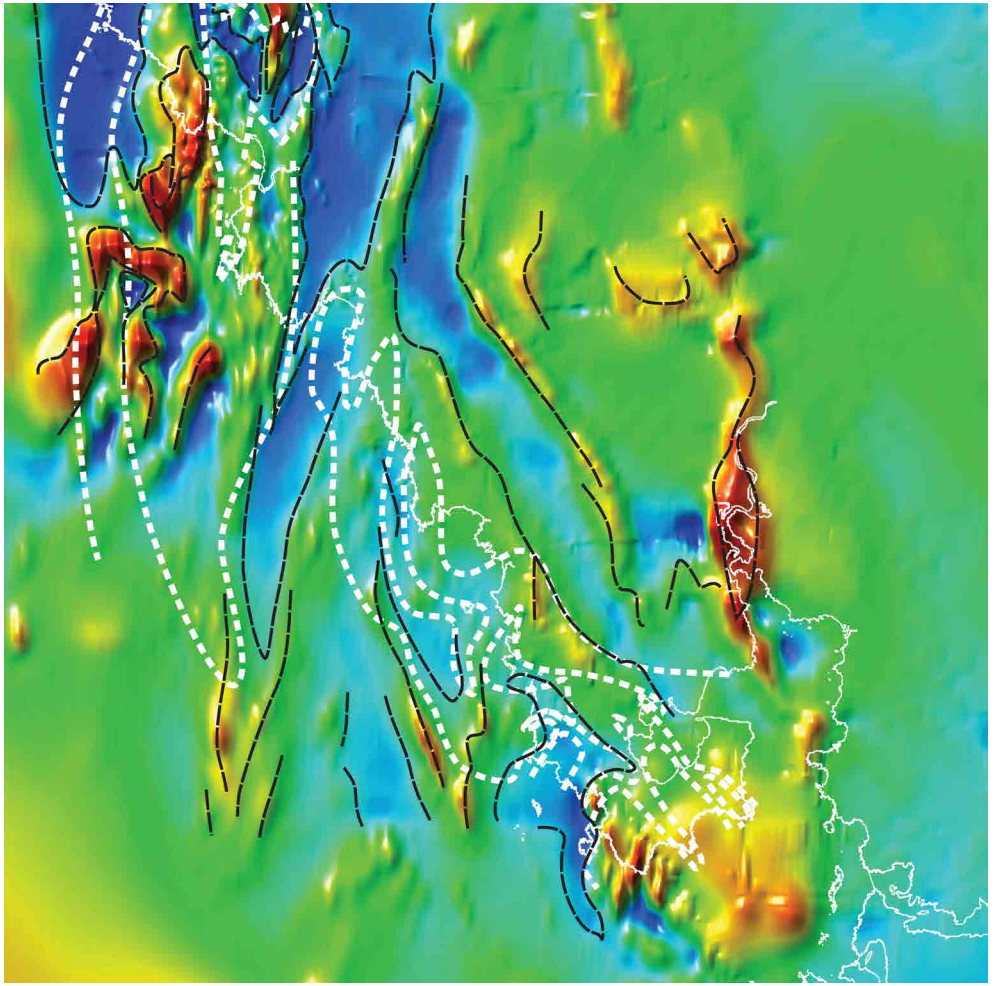

Figure 85. Total Magnetic Intensity image (400 m line spacing) with black dashed lines as trend lines in the aeromagnetics. The ground-based structural interpretation (refer Figures 75 and 76) is shown by the white dashed lines.

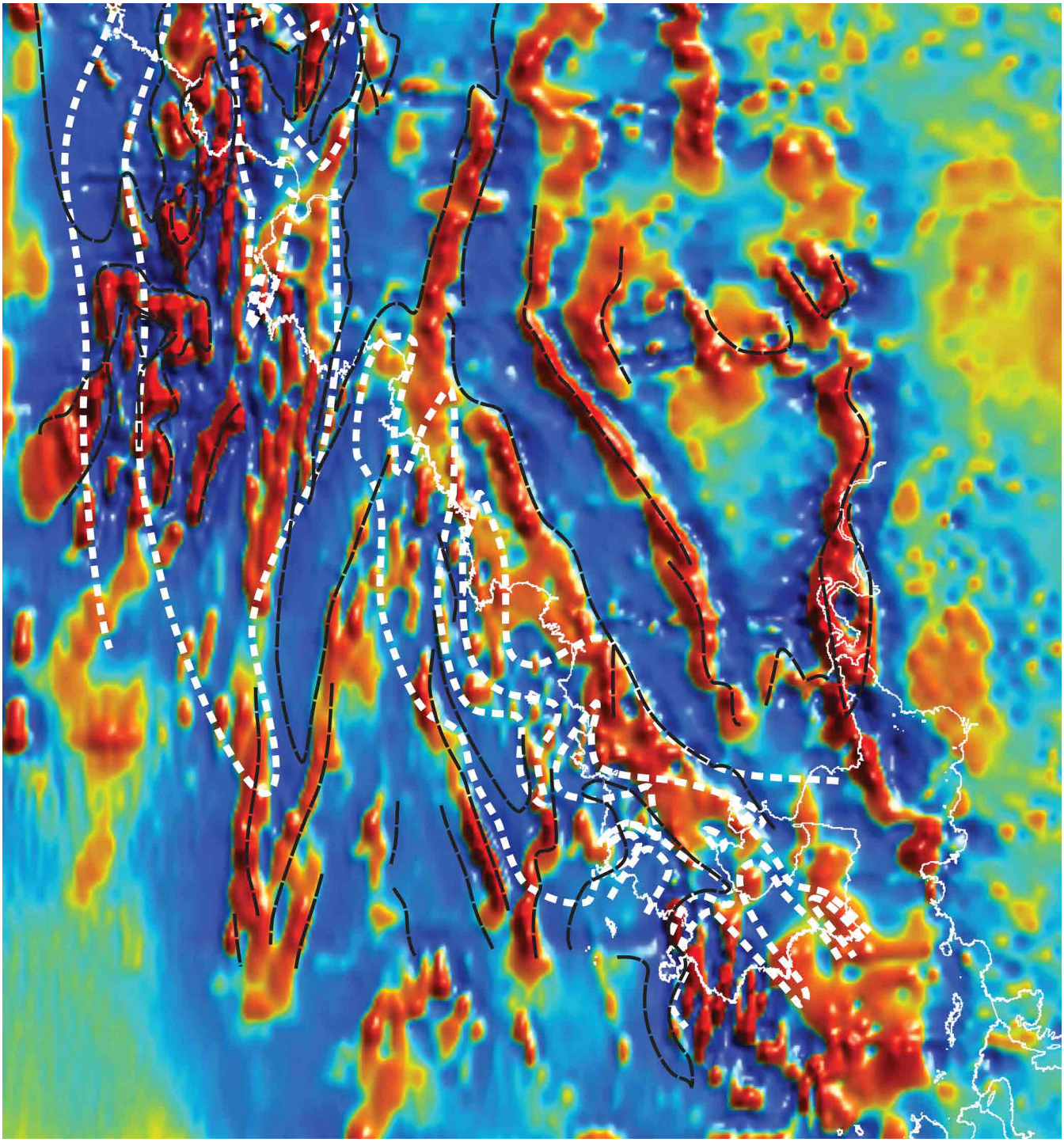

Figure 86. Reduced to Pole First Vertical Derivative aeromagnetic image with black dashed lines as trend lines in the aeromagnetics. The ground-based structural interpretation (refer Figures 75 and 76) is shown by the white dashed lines.

## 5.0 SHEAR SENSE INDICATORS AND TRANSPORT DIRECTION

To determine the transport direction (TD) attitudes of a foliation Sm with lineation Lm are required to define the movement plane, combined with shear sense indicators within that plane.

Indicators can include:

1. tails on porphyroblasts including garnet and albite in the high-grade schists.
2. tails on deformed quartz vein "fish".
3. shear bands (S-C' planes) (Figure 91).

Refer to Passchier & Trouw (1996) for more detailed treatment of shear sense indicators and determination.

Sm and Lm attitude data incorporating fabric shear sense "markers" are not common, with shear sense indicators most easily recognisable in the high-grade, porphyroblastic schists.

Shear sense data was utilised from field notes by Berry (1997) and Miller (2004). Data recorded by Berry (1997) included 1) Sm and Lm attitude data with fabric shear sense recorded when observed, and 2) shear band shear sense, but did not include shear band Sb attitude

data. Miller (2004) data included Sm, Lm and shear band attitudes with shear sense.

### 5.1 Movement Plane and Transport Direction

Determinations of movement planes (MP) and transport directions (TD) for the Southwest High-Grade Coastal Belt give a dominant northeast-southwest trend (Figure 87a, c, d, e and g), although east-northeast- south-southwest trends occur (Figure 87f, h).

Fold axis trends of the early isoclines across the Lawson Range (Figure 87b) show a directional grouping about the mean movement plane (MP) trend in (Figure 87a), but with some axis plunge directions at high angles to the mean MP. This is characteristic of fold hingeline rotation in a shear-related deformation environment, where some earlier-formed hingelines have rotated towards the bulk stretch direction and later-formed folds have initiated at high angles to the regional stretch and have not suffered significant shear strain.

Most of the restorations depicted in Figure 87 involved determination of the movement plane containing the perpendicular to Sm and the lineation (see Section 5.3.1). Knowledge of the transport direction within the movement plane requires fabric shear sense information. In the Southwest High-Grade Coastal Belt sinistral tails on porphyroblasts viewed in the Lm-movement plane give a north-over-south transport (Meffre et al., 2001).

### 5.2 Shear Sense Pattern

Fabric shear sense and shear band S-C' data show an apparent domainal pattern within the high-grade schists of the Southwest High-Grade Coastal Belt (Figure 88). Overall the fabric shear sense data show a sinistral shear sense within the Lm-movement plane, but some dextral tails have been recorded between the Giblin River mouth and Elliott Point. The significance of these is not known at this point although observations in the incorrect plane may give a "false" or incorrect sense (Figure 89). This clearly requires field checking.

Figure 88 is really a plot of the distribution of S-C' shear bands with colour-coding of those with sinistral sense (in blue) and those with dextral sense (in red). This distribution, based on recording of S-C' shear bands when observed by Berry (1997) and Miller (2004), suggests localised domains of shear band development within the high-grade schist lithology. These domains appear to coincide with the attenuated pinch-outs defined as macro-fold hinges in Figures 76 and 77 as shown in Figure 90. Based on the observed sinistral fabric shear sense (Meffre et al., 2001), the sinistral S-C' shear bands should be considered synthetic (same sense as the overall shear within the main shear zone), whereas the dextral would therefore be considered antithetic (opposite sense to the shear sense within the main shear zone).

The presence of both synthetic and antithetic shear bands (Figures 90 and 91) is suggestive of regions that have undergone non-plane shear strain, such that components of orthogonal shortening occur within the zone of shearing. Equal development of antithetic and synthetic shear bands indicates a non-rotational pure shear deformation environment (Passchier and Trouw, 1996, fig 5.17b). The significance and Sm^Sb relationships of the west coast shear band data is further investigated and discussed in Section 5.3.2.

### 5.3 Restoration of Shear Indicators

The methodology of restoration of both Lm/Sm and Sb data is discussed and various examples presented utilising different approaches depending on the availability of data. The issue of recognition of synthetic versus antithetic shear bands (S-C') is also discussed with significant implications for the shear sense and transport direction (TD). The shear sense and therefore transport direction determined from restored Lm/Sm data versus restored Sb data is also presented and discussed.

#### *5.3.1. Lineation Lm with shear sense*

Restoration of Lm means removal of any younger deformation effects by 1) removing the plunge of younger (regional) folds from foliation Sm and shear band Sb attitude measurements, and 2) returning the So/Sm or Sm to the horizontal with the movement plane constructed by a great circle fit of the restored pole to Sm and restored Lm. To rotate planar elements the poles of the planes are used. All rotations are along small circles that run east-west on the stereonet.

An example of restoration is provided from the unconformity area at the south end of Mulcahy from Berry (1997) structural data. The aim was to restore the unconformity to the horizontal by 1) removal of the Devonian fold plunge, 2) rotation of the bedding defining the unconformity to the horizontal and 3) at the same time rotating the Cambrian foliation/lineation in the Mesoproterozoic high-grade schist quartzites below. The resultant determination is the pre-Late Cambrian attitude of the foliation Sm and lineation Lm.

Three different scenarios are used as examples to determine the Cambrian transport direction responsible for the deformation. Each is an example constrained by the available structural data. The minimum required data are the attitudes of the Cambrian foliation Sm and lineation Lm and the local/regional Devonian fold axis. Figure 92 shows in stereonet form the resultant TD depending on the approach used from 1) restoration of Sm and Lm by removal of the Devonian fold-plunge and rotation of the unconformity to the horizontal (Figure 92c), 2) restoration of Sm and Lm by removal of the Devonian fold-plunge without restoration of the unconformity to the horizontal, but returning the foliation Sm to the horizontal (Figure 92d), and 3) restoration of Sm and Lm without the Devonian fold plunge removal but with rotation of the unconformity to the horizontal (Figure 92e).

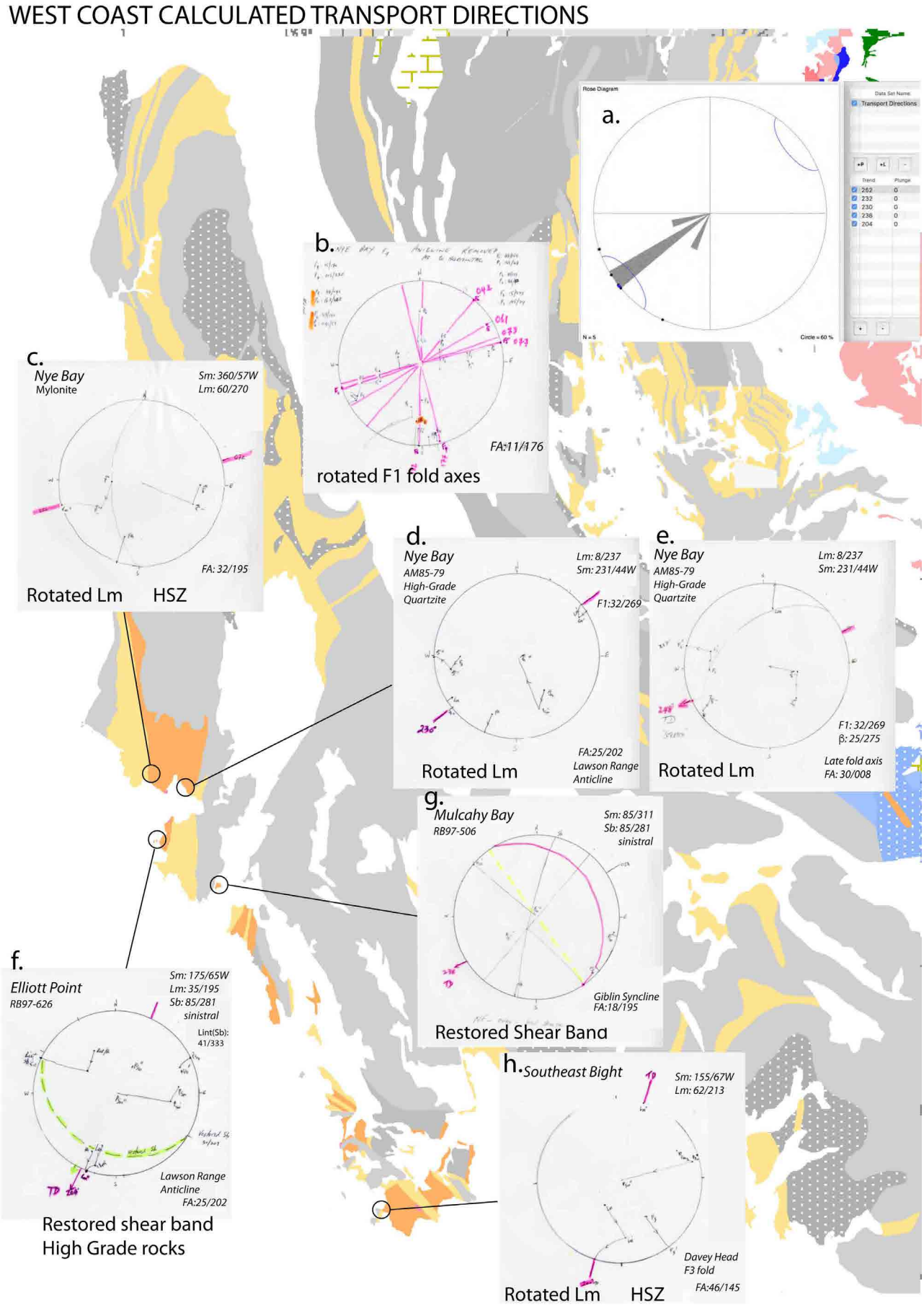


Figure 87. Calculated west coast movement planes (MP) and transport directions (TD) with stereonet insets showing the Lm, Sm and Sb data used (top right of each stereonet), the restoration rotations by removal of the regional younger fold plunge (listed bottom right of each stereonet) and the determined MP or TD (pink direction lines). a) Polar histogram plot of the determined movement planes from the included stereonets. The 60% cone of confidence small circle is shown. b) fold axis plunge-directions of the early isoclines from across the Lawson Range. c), d) and e) are restorations and movement plane determinations for the Nye Bay area. f) and g) are shear band restorations for the Elliott Point and Mulcahy Bay areas respectively. h) Movement plane determination from South East Bight high-strain zone.

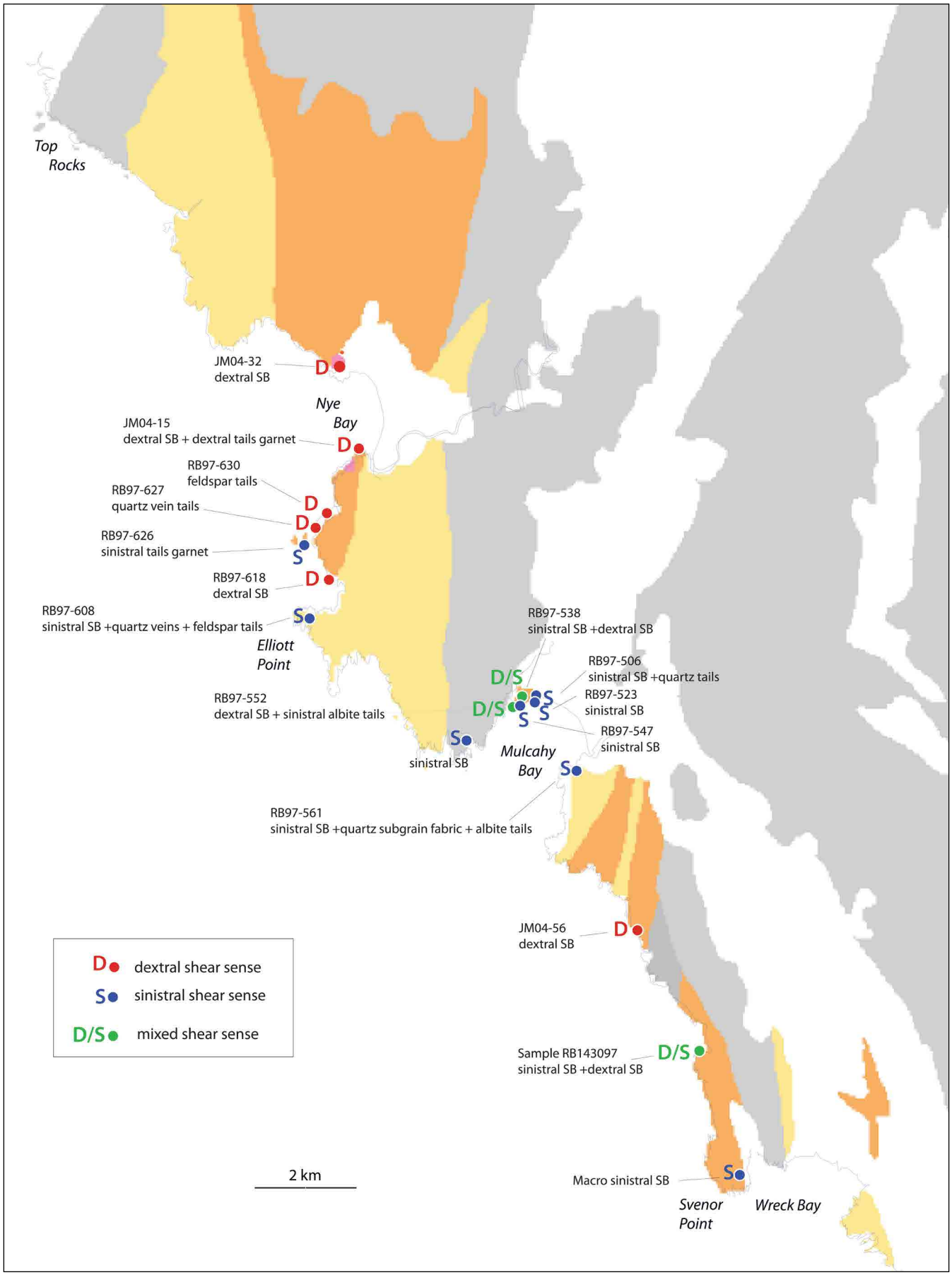


Figure 88. Shear sense indicator map summarising all the available shear sense data with dextral data occurrences in red, sinistral occurrences in blue and mixed shear sense occurrences in green (commonly sinistral fabric indicators with dextral shear bands).

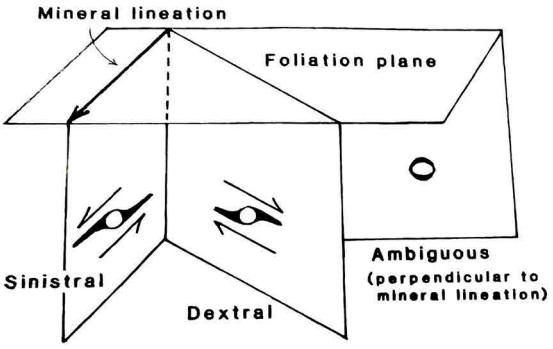


Figure 89 (left). Diagram showing apparent shear sense variation depending on the direction of viewing of the plane of the exposure (figure 11-31d from Marshak and Mitra, 1988). The shear sense should always be determined in outcrop views parallel to the movement plane (i.e. the plane orthogonal to the foliation containing the mineral lineation Lm).

Figure 90 (below). Shear sense distribution map with the superposition of the isocline macro-fold axial surface traces (AST) from Figures 76 and 77.

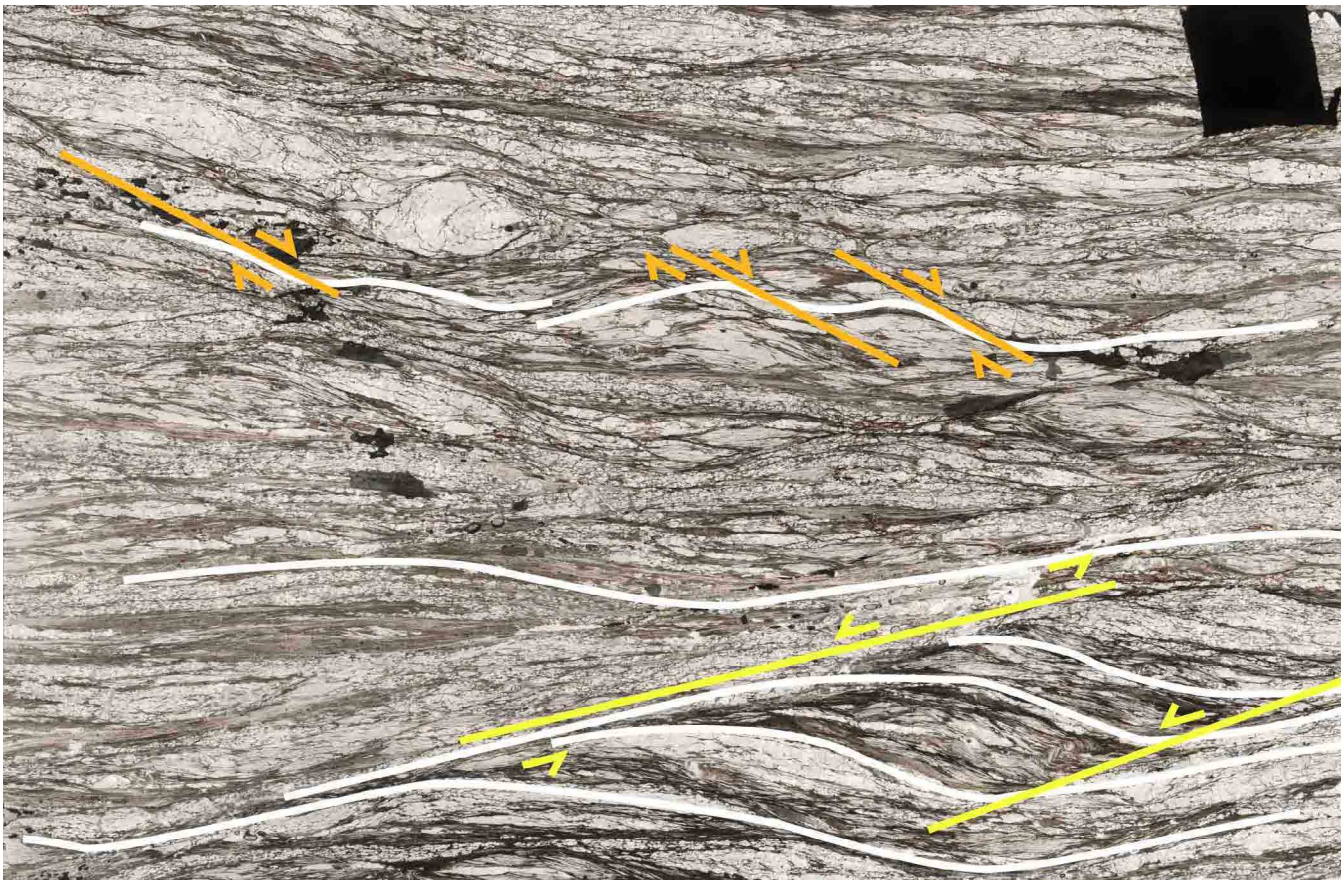

Figure 91. Dextral (orange) and sinistral (yellow) shear bands (S-C') within intensely deformed, high-grade schist at the north end of Mulcahy Bay. Smaller wavelength dextral shear bands at the top of photo are transitional into a zone of larger wavelength sinistral shear bands in the lower part of the photo. Sample is RB97-506. (Photo credit: Ron Berry).

In most cases in the Tyennan there is no preservation of the Cambro-Ordovician unconformity, such that approach (1) cannot be undertaken. In some instances knowledge of the younger Devonian folding is also not known, so approach (3) is required. Generally approach (2) has been used for most of the Tyennan domain, including the Southern Tyennan and the Central Tyennan (Gray & Vicary, 2021b).

*5.3.2. Shear band (S-C' planes)*

Examples of shear band restoration are presented from Elliott Point (locality RB97-626) to show the differences between determined transport directions from restored and non-restored shear bands (Figure 93). In Figure 93a the movement plane has been derived by using Lint (the intersection point between the shear band Sb and the foliation Sm) as the pole to the movement plane (red great circle, Figure 93a). This gives a calculated TD of 238° that approximately matches the field measured stretching plane (blue great circle, Figure 93a) with a strike of 250°. Removal of the younger regional fold plunge and then restoring Sm to the horizontal using small circle rotations in Figure 93b gives a restored shear band of 50/206° with a TD towards 206°. The example shows a resultant ~30° angular difference between the restored and non-restored data.

The angular difference in dip between the dominant foliation and the restored shear band is therefore 50° (Figure 93b). Based on fabric shear sense (see Section 5.2.1 above) the sinistral shear band would be classed as synthetic (i.e. same shear sense as the zone of shearing) with a resultant TD of 206°, but the angular separation of Sm^Sb is much higher than that expected for a synthetic set (nominally with a 20-30° Sm^Sb).

Examples of TD determined from localities with measurements of Sm, Lm and dextral shear bands (Figure 94), data collected by Miller (2004), show discordance or angular separation between the TD determined from the Lm/Sm movement plane (i.e. the plane containing the normal to Sm and the lineation) versus TD determined from restored shear bands (i.e. direction orthogonal to shear band strike with sense in the direction of dip) by removing the regional fold plunge and then rotating the foliation Sm to the horizontal along with all other data points.

From the original, non-restored data Figure 94a and Figure 94c show significant disparity between movement planes derived from the Sm pole-Lm plane fit (dashed green great circles: green MP) to that from Lint as pole to the movement plane (pink MP) at the two localities.

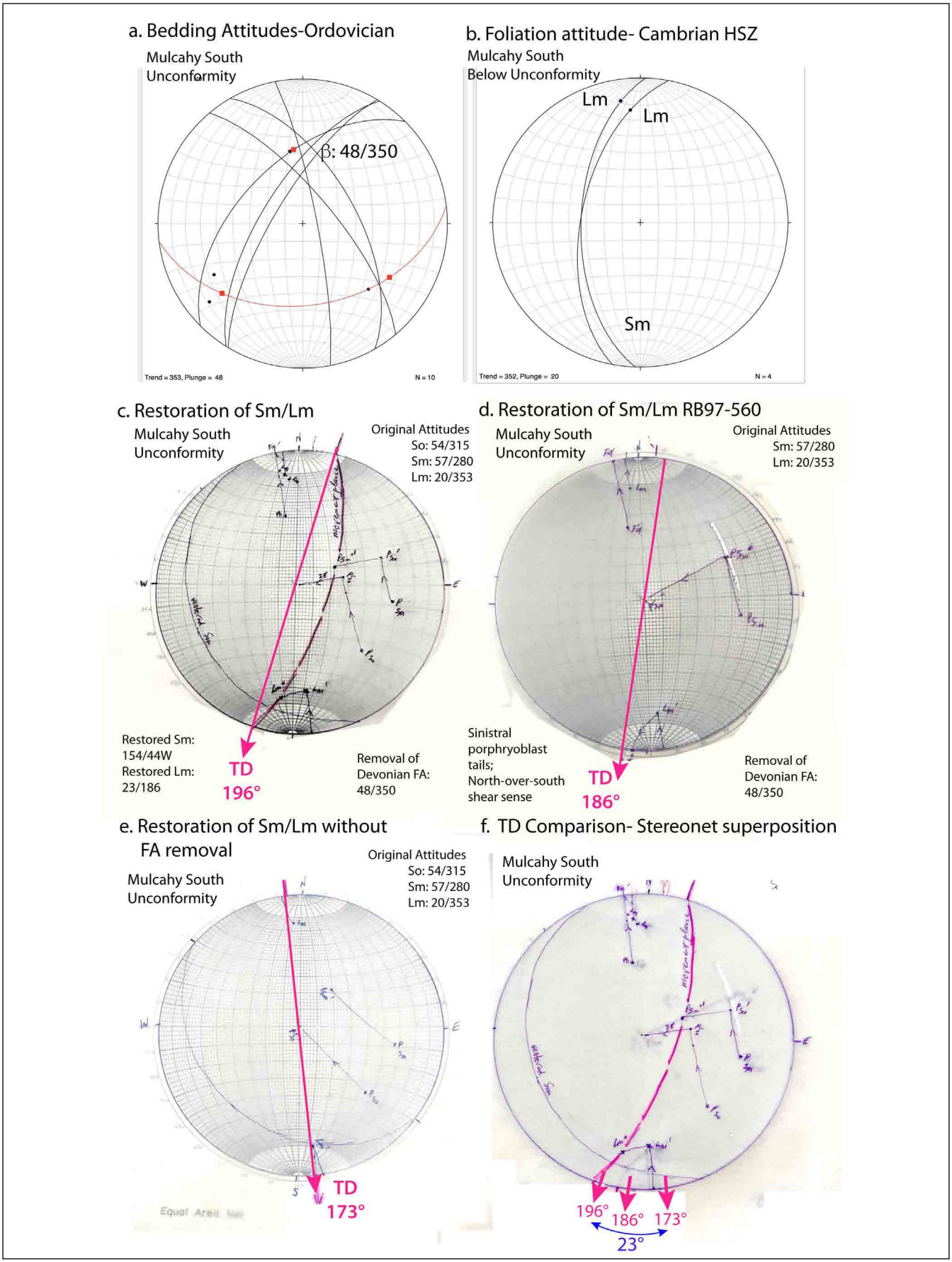


Figure 92. Restoration of structural relationships at the Ordovician unconformity, south end of Mulcahy Bay with (a) and (b) as stereonet plots of the structural data used for the restoration and (c), (d) and (e) various restoration example approaches. TD: determined transport direction.

a) Stereonet plot with Devonian fold axis (ß intersection) determined from folded bedding plotted as great circles above the unconformity. b) Stereonet plot with high-grade mylonitic foliation Sm and associated lineation Lm in quartzite/schist below the unconformity. c) Stereonet showing restoration of Sm and Lm by removal of the Devonian fold-plunge and rotation of the unconformity to the horizontal. d) Stereonet showing restoration of Sm and Lm by removal of the Devonian fold-plunge without restoration of the unconformity to the horizontal, but returning the foliation Sm to the horizontal. e) Stereonet showing restoration of Sm and Lm without the Devonian fold plunge removal but with rotation of the unconformity to the horizontal. f) Superposition of stereonets from (c), (d) and (e) to give a combined plot showing a 23° spread in the calculated transport directions (TD).

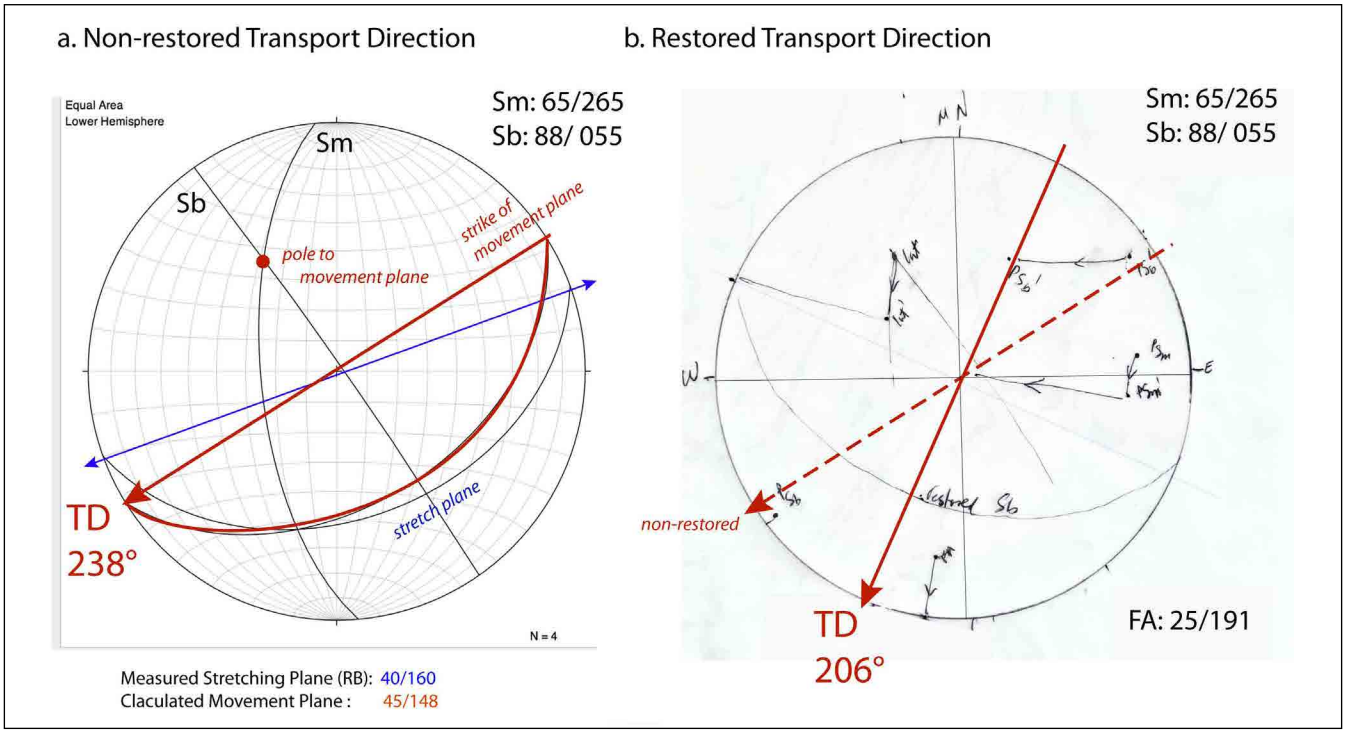


Figure 93. Comparison of Transport Directions (TD) calculated from shear bands between a) non-restored data with respect to the local fold axis, and b) restored data through removal of the local fold axis. Data from Elliott Point locality RB97-626 (Berry, 1997).

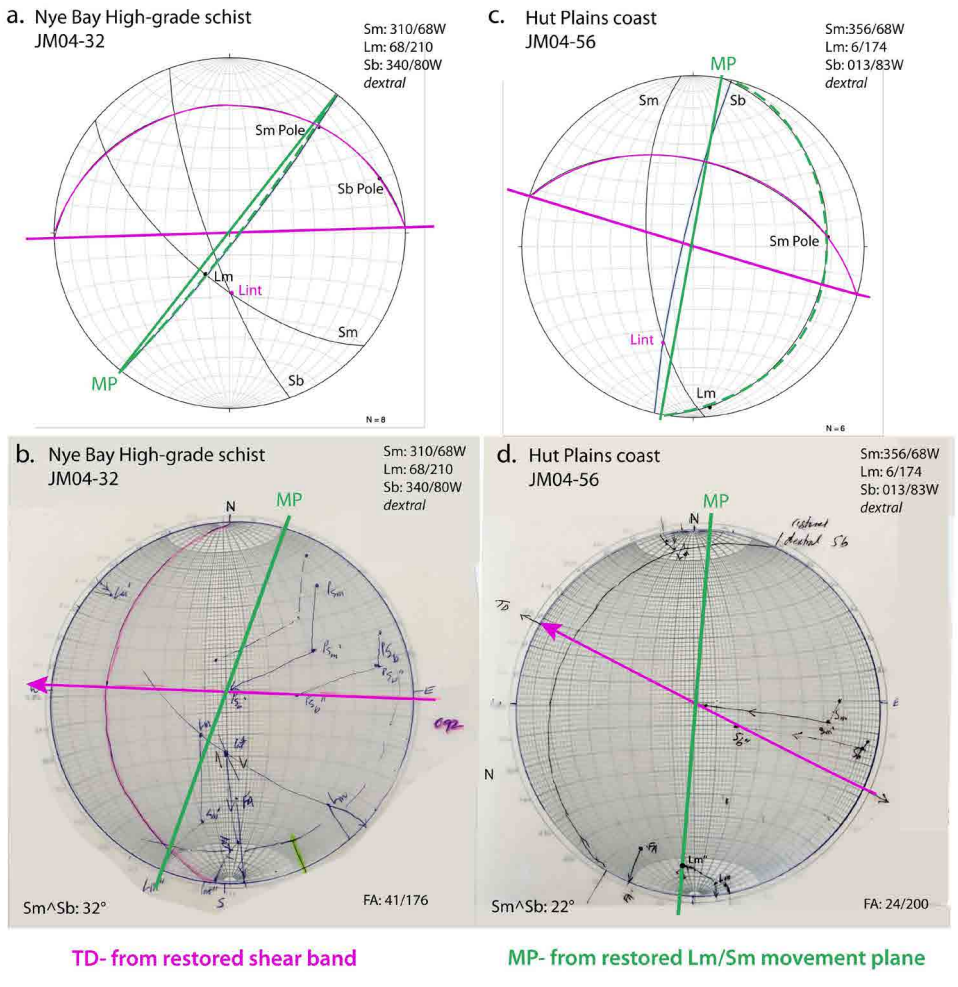


Figure 94. Examples of restoration of combined Lm/Sm and dextral shear band data collected by Miller (2004) at Nye Bay and Hut Plains coast. a) and b) are stereonet plots of the non-restored data but showing movements planes derived from Sm pole-Lm plane fits (green great circles; green MP) and from the shear bands (pink great circles: pink MP). c) and d) are show restored data on plots with the respective different movement planes shown. The green great circles (green MP) from restored Sm pole-Lm plane fits and the pink great circles (pink MP) from the restored shear bands.

They give ~50° and 90° angular differences. Restored data, restored by removal of the younger Devonian regional fold axis from the two localities (Figures 94b and d), gives angular discordances of ~75° and ~70° between the movement planes.

The restored shear band planes have Sm^Sb angular differences of 20° and 30° more typical of synthetic shear band sets.

In summary, the Southwest High-Grade Coastal Belt shows:

1. An overall southwest-northeast trending movement plane with sinistral fabric shear sense giving TD towards the southwest (Figure 87a).
2. Domains of both sinistral and dextral shear bands (Figure 88) that appear to match macro-isocline hinge zones as inferred from So/Sm formlines coupled with lithology pinchouts, suggesting a greater flattening component within the attenuated fold noses (Figure 90).
3. Different movement plane TD for Sm/Lm with fabric-shear sense, sinistral shear bands and dextral shear bands (Figures 92 and 94).
4. Almost 90° discordance between TD determined from Sm/Lm with fabric shear sense and that from dextral shear bands (Figure 94) suggesting marked displacement direction differences and significant time separation between the early Sm/Lm development and the late stage shear bands that develop during shear zone strain hardening.
5. Restored sinistral shear bands give a more south-southwest TD (Figures 87f and 93b) versus a more east-west movement plane for restored dextral shear bands (Figures 94b, d).
6. Angular separations Sm^Sb of 20°-30° for both restored dextral shear bands (Figure 94) and restored sinistral shear bands (Figures 87f and 87g), but also 50°-60° for another case of a restored sinistral shear band (Figure 93b).

These data provide an apparent complexity not observed at other locations in the Tyennan domain. This may be due to the greater and more continuous exposure along the coastal belt through the high-grade sequence compared to the inland exposures of the Tyennan region (cf. Gray and Vicary, 2021a, b; Gray and Vicary, 2022a).

More combined Sm, and Lm data with shear sense along with shear band data are clearly needed across the Tyennan domain to resolve this apparent complexity.

## 6.0 CONCLUSIONS

1. Previous interpretations of the Southwest High-Grade Coastal Belt did not consider or recognise the presence of isoclinal macro-folds (Meffre et al., 2000, 2001), but compare Williams (1978). Based on detailed coastal mapping emphasis was placed on the sequence as a series of potentially stacked, fault-bound slices of both high-grade and low-grade rocks.
2. Based on repeated litho-tectonic units, limited younging data and relations between lineation Lm and mesoscopic isocline fold axes this study argues that the Southwest High-Grade Coastal Belt is dominated at the highest structural level by a regional-scale isoclinal fold-nappe with reclined geometry (Nye Bay fold-nappe). This is underlain by a series of second or third order regional-scale isoclinal folds that are part of a fold stack along the macro-fold lower limb.
3. The fold stack extending from Mulcahy Bay to Port Davey has the form of a closed macro-fold pod or augen in high-grade schist with isoclinal in-folds of low-grade phyllite and quartzite. The inferred closures in this coastal segment appear as attenuated pinch-outs of the various strongly to intensely foliated and transposed lithologies.
4. Contacts between the high-grade/ low-grade lithological assemblages are mylonite zones of variable width with L-S tectonite fabrics and shallowly plunging mineral lineations. Many of the contacts have been reactivated with younger brittle deformation showing cataclasite development and down-dip lineations with normal sense movement (cf. Meffre et al., 2001). In the structural geometry presented here these contacts have also been folded along with the adjacent litho-tectonic units and potentially reactivated at this time.
5. Determinations of movement planes (MP) and transport directions (TD) for the Southwest High-Grade Coastal Belt suggest a complex movement history, but give a dominant northeast-southwest trend with TD towards ~250°, although dextral shear bands suggest a TD towards 270°-300°.

## 7.0 ACKNOWLEDGEMENTS


- Mineral Resources Tasmania (Andrew McNeill) for providing support through the 2016-2020 Geoscience Initiative.
- Mike Hall, Ron Berry, Sebastien Meffre, John Miller, Peter Williams and Paul Lennox for southwest coastal mapping and structural data collection. This compilation would not have been possible without their fieldwork.
- Ron Berry for providing copies of his 1997 field mapping sheets, detailed field notes and field notebook.
- Access to map sheets and/or field notebook copies of Hall, Miller, Williams and Lennox was through Mineral Resources Tasmania and Parks and Wildlife Service (PWS).
- Jo-Anne Bowerman for scanning photographic slides from Andrew McNeill's BSc (Hons) study.
- Chris Large for editing and formatting this Mineral Resources Tasmania Geological Survey Paper.
- Parks and Wildlife Service (PWS) for allowing helicopter access and landing in the World Heritage Area as well as permits for measurement, sampling and photograph collection.
- Jason Bradbury DPIPWE for assistance with WHA and PWS permits for scientific research.
- Rodney Smith from Rotorlift for helicopter transport into the Tasmanian southwest.
- Rick Allmendinger and Nestor Cardozzo for use of OSX Stereonet.

## 8.0 REFERENCES


Alsop, G.I. and Holdsworth, R.E., 1999. Vergence and facing patterns in large scale sheath folds. *Journal of Structural Geology*, 21, 1335-1349.

Berry, R.F., 1997. Unpublished Field Notes.

Berry, R.F., Chmielowski, R.M., Steele, D.A. and Meffre, S., 2007. Chemical U-Th-Pb monazite dating of the Cambrian Tyennan Orogeny, Tasmania. *Australian Journal of Earth Sciences*, 54, 757-771.

Chmielowski, R.M., 2009. *The Cambrian metamorphic history of Tasmania*. PhD Thesis, University of Tasmania.

Chmielowski, R.M. and Berry, R.F., 2012. The Cambrian Metamorphic History of Tasmania: The Pelites. *Australian Journal of Earth Sciences*, 59, 1007-1019.

Ellis, D.J. and Green, D.H., 1979. An experimental study of the effect of Ca upon garnet-clinopyroxene Fe-Mg exchange equilibria. *Contributions to Mineralogy and Petrology*, 7, 13-22.

Gray, D.R. and Vicary, M. J., 2021a. Structural Geology of Frenchmans Cap, Central Tyennan Domain, Tasmania. Mineral Resources Tasmania, *Geological Survey Paper,* 6, 44p.

Gray, D.R. and Vicary, M. J., 2021b. Structural Geology of the Central Tyennan Region, Tasmania. Mineral Resources Tasmania, *Geological Survey Paper,* 7, 69p.

Gray, D.R. and Vicary, M. J., 2022a. Structural Geology of the Arthur Range, Central Tyennan Domain, Tasmania. Mineral Resources Tasmania, *Geological Survey Paper,* 8, 79p.

Gray, D.R. and Vicary, M. J., 2022b. Structural Geology of the Southern Tyennan Domain, Tasmania. Mineral Resources Tasmania, *Geological Survey Paper* in preparation.

Hall, W.D.M. 1966. Interim Geological Report on the South West Portion of Exploration Licence 13/65, South West Tasmania. November 1965-May 1966. Unpublished report Broken Hill Proprietary Company Ltd. TCR 66_0424.

Hall, M., 2005. Unpublished field maps and notes (Top rocks – Nye Bay - Mulcahy Bay - Wreck Bay - Towterer Beach Area, 2004-05)

Hall, M., 2006. Unpublished field maps and notes (Gilbin River – Lawson Range area)

Hall, M. 2008. Unpublished field maps in the Wreck Bay to Davey Head area

Hall, M. and Vicary, M., (Compiler), 2010a. Digital Geological Atlas 1:25000 Scale Series. Sheet 3822. *Mulcahy*. Mineral Resources Tasmania.

Hall, M. and Vicary, M., (Compiler), 2010b. Digital Geological Atlas 1:25000 Scale Series. Sheet 3823. Elliott. Mineral Resources Tasmania.

Hall, M. and Vicary, M. (Compiler), 2010c. Digital Geological Atlas 1:25000 Scale Series. Sheet 4023. *Propsting*. Mineral Resources Tasmania.

Hall, M. and Vicary, M., (Compiler), 2010d. Digital Geological Atlas 1:25000 Scale Series. Sheet 4024. *Rookery*. Mineral Resources Tasmania.

Hall, W.D.M.; McIntyre, M.I.; Corbett, E.B.; McGregor, P.W.; Fenton, G.R.; Arndt, C.D.; Bumstead, E.D.; 1969. Report on Field Work in Exploration Licence 13/65, South-West Tasmania During 1967-68 Field Season. TCR 69_0555.

Holland, T.J.B., 1980. The reaction albite=jadeite + quartz determined experimentally in thge range 600-1200°C. *American Mineralogist*, 65, 129-134.

Mclean, C.J. and Bowen, E.A., 1971. Structure of the Precambrian rocks of the Davey River area, south western Tasmania. *Papers and Proceedings of the Royal Society of Tasmania*, 105, 97-104.

McNeill, A.W., 1985. *The structure and petrology of the Nye Bay area, south west Tasmania*. B.Sc (Hons) Thesis, University of Tasmania: Hobart.

Marshak, S. and Mitra, G., 1988. *Basic Methods of Structural Geology*. Prentice Hall, New Jersey. 446p.

Meffre, S., Berry, R. F. and Hall, M., 2000. Cambrian metamorphic complexes in Tasmania: tectonic implications. *Australian Journal of Earth Sciences,* 47, 971 – 985.

Meffre, S., Berry, R.F., Hall, M. and McNeill, A., 2001. The Structural Style of Cambrian Metamorphic Complexes in Tasmania: SW Tasmanian examples. *Geological Society of Australia Abstracts*, 64, 118-120.

Miller, J.M., 2004. Unpublished Field Notes.

Mulder, J.A., 2013. *The structure and metamorphism of the Cox Bight-Red Point area, South West Tasmania.* B.Sc (Hons) Thesis, University of Tasmania: Hobart.

Mulder, J.A., Berry, R.F. and Scott, R.J., 2015. The structure and metamorphism of the Red Point Metamorphic Complex- a newly discovered high-pressure metamorphic complex from the south coast of Tasmania. *Australian Journal of Earth Sciences*, 62, 969-983.

Passchier, C.W. and Trouw, R.A.J., 1996. *Micro-Tectonics*. Springer-Verlag, Berlin. 289p.

Quinquis, H., Audrun, Cl., Brun, J.P. and Cobbold, P.R., 1978. Intense progressive shear in Isle de Groix blueschists and compatibility with subduction or obduction. *Nature*, 273, 43-45.

Ramsay, J.G., 1967. *The Folding and Fracturing of Rocks*. McGraw Hill.

Ramsay, J.G. and Huber, M.I, 1987. *The Techniques of Modern Structural Geology*. Volume 2: Folds and Fractures. Academic Press. London. 700p.

Seymour, D.B., 2014. Chapter 6.1 Middle Devonian Deformation. In Corbett, K.D., Quilty, P.G & Calver, C.R. (Editors), Geological Evolution of Tasmania pp 273-296. Geological *Society of Tasmania Special Publication*, 24, Geological Society of Australia (Tasmania Division).

Spry, A.H. and Baker, W.E., 1965. The Precambrian Rocks of Tasmania, PartVII. Notes on the petrology of some rocks from the Port Davey-Bathurst Harbour area. *Papers and Proceedings of the Royal Society of Tasmania*, 99, 17-26.

Turner, N., 1989. Precambrian. In: Burret, C.F. and Martin, E.L. eds, Geology and Mineral Resources of Tasmania. *Geological Society of Australia Special Publication*, 15, 5-46.

Turner, F.J. and Weiss, L.E., 1963. *Structural Analysis of Metamorphic Tectonites*. McGraw Hill, New York. 545p.

Williams, P.R. 1976. Unpublished field notebooks. Davey Head 1 and 2. (F_PRW_18 and F_PRW_19). Mineral Resources Tasmania

Williams, P.R., 1978. Digital Geological Atlas 1:50000 Series. Sheet 8011S. *Davey*. Mineral Resources Tasmania.

Williams, P.R., 1982. Geological Atlas 1:50000 Series. Sheet 91 (8011S) Davey. *Explanatory Report Geological Survey Tasmania*.

Williams, P.R. and Corbett, E.B., 1977. *Port Davey. Tasmania*. Tasmanian. Department of Mines Geological Atlas 1:250,000 Series, Sheet SK 55-7.

# APPENDIX 1

FIELD NOTES - STRUCTURAL DATA - FIELD MAP

File Download

# APPENDIX 2

INTERPRETATION MAPS

File Download

Tasmanian
Government

**Mineral Resources Tasmania**
PO Box 56 Rosny Park
Tasmania Australia 7018
Ph: +61 3 6165 4800

info@mrt.tas.gov.au www.mrt.tas.gov.au